THE DESORPTION KINETICS OF METHANE FROM NONAQUEOUS FLUIDS FOR ENHANCED WELL CONTROL

A Thesis

Submitted to the Graduate Faculty of the
Louisiana State University and
Agricultural and Mechanical College
in partial fulfillment of the
requirements for the degree of
Master of Science

in

The Craft & Hawkins Department of Petroleum Engineering

by
James Lee Nielsen Jr.
B.S., Duquesne University, 2016
May 2020

To my father and mother, Jim and Stephanie Nielsen, and to my grandfather Joseph B. Zuzik who all inspired me to go into the sciences and to never stop furthering my education.

ACKNOWLEDGMENTS

I would like to extend my sincere gratitude to the faculty members on my thesis committee, Dr. Yuanhang Chen, Dr. Louis Thibodeaux, Dr. Wesley Williams, and Dr. Mayank Tyagi. They have all been extraordinarily helpful and supportive during this process and I am eternally grateful.

A special thank you especially to my advisor and committee chair Dr. Yuanhang Chen for his continued support through difficult times and guidance throughout my graduate school studies. To all my fellow graduate students and close friends who I have worked with and who have helped me during my time here at Louisiana State University. And finally, to my mother and father who have been so supportive of me and my decision to further my education and work towards a graduate degree in Petroleum Engineering.

TABLE OF CONTENTS

LIST OF TABLES

LIST OF FIGURES

NOMENCLATURE

a, b, c	Correlation parameters
C_H	Solubility of a gas at a fixed temperature and pressure (M)
c_b	Concentration of component b
D_{CO2}	Diffusivity (m^2/s)
d_b	Bubble diameter (m)
$F_{emulsifier}$	Fraction of emulsifier in a blended fluid
F_{oil}	Fraction of oil in a blended fluid
F_{water}	Fraction of oil in a blended fluid
ΔF_c	Bubble free energy (kJ/mol)
j	Desorption Flux $\left(\frac{mol}{m^2 * s}\right)$
k_H	Henry's Constant (M/atm)
K	Mass transfer coefficient (1/s)
$K_L a$	Volumetric mass transfer coefficient (1/s)
K_D	Desorption specific mass transfer coefficient (1/s)
K_g	Mass transfer coefficient of the gas phase (1/s)
K_L	Mass transfer of the liquid phase (1/s)
L	Mass flow rate (kg/s) / cross sectional area (m^2)
l	Current gas loading at a specific pressure
l_{max}	Maximum gas loading at a specific pressure
l_0	Initial gas loading at a specific pressure
m	mass (g)
P	Pressure (psig)
P_1	Pressure in test section 1 at a specific time (psia)

P_{gas}	Partial pressure of a gas (psia)
$P_{solution}$	Vapor pressure of the solution (psia)
$P^{0}_{solvent}$	Vapor pressure of the solvent (psia)
Q_G	Gas side volumetric flow rate (m^3/s)
R	Gas constant, 0.08205 $\left(\frac{L*atm}{K*mol}\right)$
R_s	Total solubility of a fluid (M)
$R_{s,oil}$	Solubility of the oil phase (M)
$R_{s,water}$	Solubility of the water phase (M)
$R_{s,emulsifier}$	Solubility of the emulsifier (M)
t	Time (s)
T	Temperature (K)
u_G	Superficial gas velocity (m/s)
V	Volume (L)
V_1	Total Volume of gas that comes out from solution at any time t, converted to conditions in flow meter at T = 0 °C and P = atm
V_I	Total volume of gas come out from solution at t, at pressure condition of test section I and at room temperature (L)
V_{II}	Total volume of gas come out from solution at t, at pressure condition of test section I and at room temperature (L)
V_B	Total volume of gas come out from solution at t, at pressure condition of test section I and at room temperature
$V`_B$	Original total volume of blanket gas in test section II at P_1 (L)
V_T	Total volume of gas that comes out of the system (L)
$X_{solvent}$	Mole fraction of the solvent

SI Metric Conversion Factors

psi	× 6.895	=	kPa
ppg	× 1.19826*E−01	=	g/cm³
lbm	× 4.53592*E−01	=	kg
ft	× 3.048* E−01	=	m

Greek Symbols

ε	Gas holdup
ρ	Parameter in the modified Debye-Huckel expression
ρ_L	Liquid density (kg/m^3)
ρ_L	Molal liquid density (mol/m^3)
v	Kinematic viscosity (m^2/s)
μ	Viscosity of the liquid (Pa s)
μ_{CO_2}	Standard chemical potential of CO_2 in the liquid phase (J/mol)
σ	Surface tension of the liquid (kg/m s^2)

ABSTRACT

The mass transfer of a dissolved gas evolving to return to the gaseous phase from a liquid is governed by many parameters. This process affects the development of an oil and gas well due to the possibility of gas contamination occurring from either an influx entering the wellbore, or drilling through gas-bearing formations. Once this dissolved hydrocarbon gas circulates up the wellbore, it will begin to evolve from solution and poses a potential risk to drilling equipment, the environment, and personnel at a drilling rig. Being able to predict the behavior of gas desorption based on a known set of variables for a specific fluid/gas combination is critical. In this study, we investigated how changing the starting saturation pressure and fluid type have on the mass transfer coefficient for nonaqueous-based fluids commonly used in drilling operations.

The work in this thesis summarizes multiple investigations of these variables which affect the desorption kinetics and relate them to processes involved with well control operations. By designing and utilizing a custom apparatus, we have studied the desorption behavior of two different types of fluids in their pure form and each as an emulsion with water. During our preliminary testing and experimental development, it was determined that the starting pressure that the fluid had been saturated with methane at and the rate at which we allowed the fluid to desorb, through a pressure drop, had the most significant effect on the mass transfer coefficients of desorption. We observed strong relationships between the starting saturation pressure and oil/water ratio in emulsion fluids for the calculated mass transfer coefficients. These observations allow us to predict the coefficient at expanded pressures and different oil/water ratios. This study will lead to the development of more accurate models that will better predict the behavior of gas desorption from nonaqueous fluids for enhancing well control operations.

CHAPTER 1. INTRODUCTION

Mass transfer exists in many forms and plays a vital role in an uncountable number of processes that govern both the natural world and our industrial society. From the smallest movement of the sodium and potassium ion pumps within our cells to the movement of hydrogen and helium within the largest stars of our universe, the concept of mass transfer can describe them all. In the most basic and simple definition, the idea of mass transfer is the change in the position of a substance from one point to another. This does not include any chemical changes to a substance, after a translational shift has occurred, but can include a physical change in terms of phase changes like those from a gas to liquid, liquid to solid, and any combination of those mentioned. In most engineering problems and phenomena, mass transfer involves this phase change of a substance or material. In petroleum engineering, mass transfer exists in many aspects. For this thesis, we will be investigating gas-liquid mass transfer when studying the desorption of a gas that has been previously absorbed into a nonaqueous drilling fluid.

1.1. Sources of Gas Entry to a Wellbore

When developing an oil or gas well, there are generally two types of gas entry into the wellbore, drilled-gas and active gas flow, as a gas kick.[1] During drilling operations, the drill bit will pass through many rock formations as it is directed towards a hydrocarbon-bearing rock formation. These rock formations all have varying degrees of natural permeability and porosity that are inherent to the rock formation.[2] Within the rock's pore space, fluids and gasses can exist. Usually, the pore space is filled with water, but often the rock formations will have gas naturally trapped within its pore space.[2] While drilling through a gas-bearing rock formation, the gas within the pore space will most often be natural gas or hydrogen sulfide gas, generated from nearby source rock formations.[3] Penetrating formations bearing gas while drilling will naturally release minute

quantities of the gas into the wellbore. At high pressures, the relatively minute initial volume of trapped gas that is freed from the rock will coalesce and can grow exponentially as the gas circulates up the wellbore to the surface. The growth in gas volume is due to a pressure drop, and if the bubbles coalesce it will lead to a surge in drilling fluids before the gas escapes the well. All of which lead to possible risks to equipment and personnel at the surface.[4] A mud-gas separator at the surface is employed to help clean the drilling fluids to safely remove uncoalesced small quantities of gas. However, the separator may be overloaded when a large gas influx is taken downhole.

When a well is drilled, drilling fluid is used to fill the wellbore to provide hydrostatic pressure preventing the flow of formation fluids and gasses from entering the wellbore from the near-wellbore area.[5] When there is an imbalance in the hydrostatic pressure between the drilling fluid and the formation being drilled, an influx may be taken, or a hydraulic fracture induced to the formation. The hydrostatic pressure must be maintained within a specific operating window for the well as dictated by the natural pore pressure of the formation being drilled, along with the fracture pressure of the formation. This is illustrated in Figure 1.1 which shows the relative range of equivalent circulating density of the drilling fluid of a well based on this pressure window for a given depth. When the hydrostatic pressure of the drilling fluid goes below the natural pore pressure of the rock formation, there is a potential for an influx of pore fluid and/or gas to enter the wellbore.[4,6] While drilling through formations that have high pore pressure and large amounts of gas trapped in the pore space, a gas influx, or gas kick, can rush into the wellbore when the hydrostatic pressure from the drilling fluid is not properly maintained.[5] When a gas influx enters the wellbore, it produces a much more severe and significant problem at the surface than the previously described gas that enters due to the drilled gas from the formation.

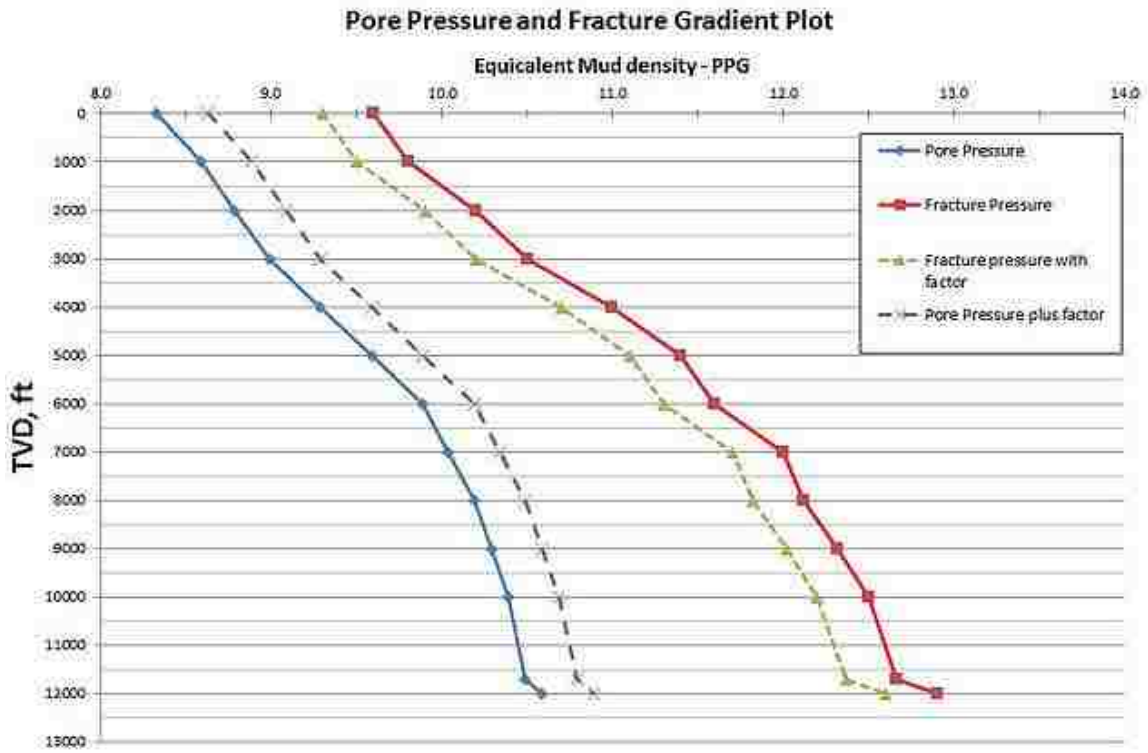

Figure 1.1. Pore and fracture pressure window for a well. Common practice safety range for the equivalent mud density exists between the pair of dotted lines to account for a safety factor for each pore pressure and fracture pressure lines. Equivalent mud density is measured in pounds per gallon.[4]

1.2. Behavior of an Influx in Drilling Fluids

Once a gas influx enters the wellbore, two possible scenarios exist which are dependent on the type of drilling fluid and the entering gas. When natural gas enters a wellbore occupied by aqueous-based drilling fluids, the influx will stay suspended in the gaseous state, with very little absorption into the fluid, as it circulates up the wellbore.[4] However, when the drilling fluid is a nonaqueous-based drilling fluid, the natural gas will begin to dissolve into the drilling fluid and, depending on the hydrostatic pressure within the fluid column, the entire volume of the gas influx may be absorbed by the drilling fluid.[4] When this occurs, the dissolved gas will remain within the drilling fluid until the hydrostatic pressure above the gas-cut fluid reduces to shift the equilibrium of gas solubility to favor the natural gas returning to the gaseous state.[1,4]

During normal drilling operations, drilling fluid is constantly circulating within the well to remove drill cuttings. As the gas-cut fluid circulates up a wellbore, the hydrostatic pressure can reduce quickly, and consequently shift the equilibrium point to induce the evolution of natural gas from the drilling fluid. The amount of gas that will evolve is proportional to the shift in the equilibrium point which is dependent on the change in pressure. The rate at which the gas will evolve is partially dependent on the change in pressure alongside a series of other variables which we discuss in the following chapters. With a large shift in the equilibrium point, rapid evolution of gas may occur and make the fluid appear as if it is boiling. Every fluid and gas combination has known well control procedures for recognizing their presence and successfully controlling each. Figure 1.2 illustrates the difference between a gas influx entering a wellbore containing an aqueous fluid and a nonaqueous fluid.

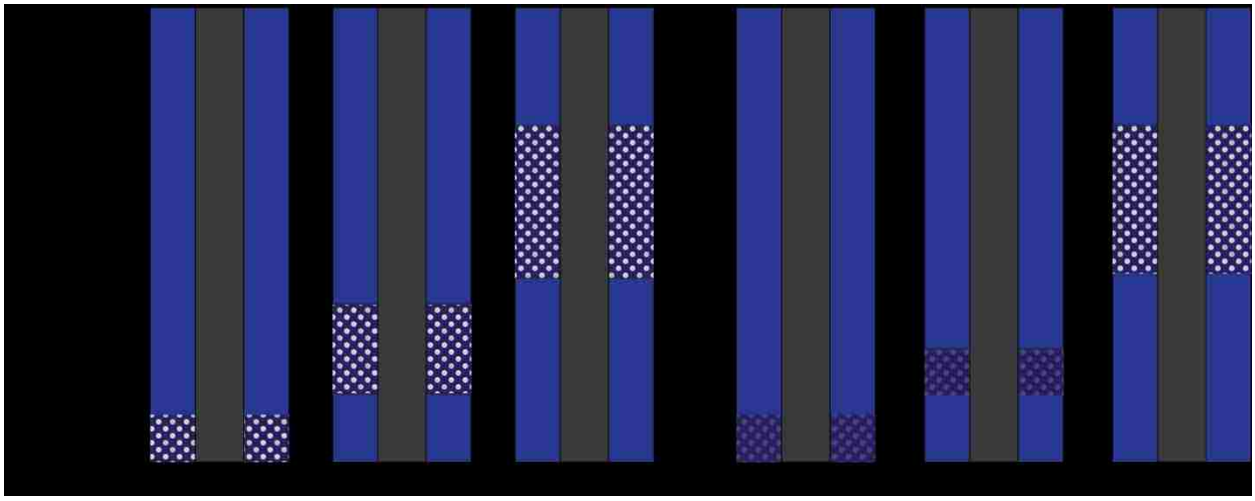

Figure 1.2. Illustration of the commonly assumed gas kick behavior in both aqueous-based (A, B, C) and nonaqueous-based drilling fluids (D, E, F) indicating how natural gas in aqueous-based fluids will remain in the gaseous state (white circles), whereas natural gas will initially absorb into the nonaqueous fluid (grey circles) before rapidly evolving to return to the gaseous state as the hydrostatic pressure reduces while the fluid circulates up the wellbore.

1.3. Use of Nonaqueous Drilling Fluids

Nonaqueous drilling fluids are more expensive than aqueous-based fluids, however, they are often used in difficult drilling situations where their technical advantages are required.[6] Nonaqueous fluids are used frequently to perform operations such as drilling through troublesome, hydratable shales; drill deep, hot wells where aqueous-based fluids may be unstable; drill salt, anhydrite, gypsum, and mixed salt zones; drill and core hydrocarbon-bearing formations near the bottom of wells; and increase lubricity to decrease torque and drag when drilling a directional well.[10] Burke and Veil (1996) conducted a study that investigated the costs of using aqueous and nonaqueous-based fluids while constructing comparable wells during offshore drilling operations. Drilling times were reduced by 50 to 60 percent, and costs were generally cut in half for wells using nonaqueous-based fluids.[11] In these cases, the nonaqueous fluid drill cuttings were discharged to the ocean. If the cuttings cannot be discharged, often due to environmental regulations, the added cost to transport the cuttings to the shore for land-based disposal may make the use of nonaqueous fluids cost-prohibitive.

Diesel is the most common nonaqueous-based drilling fluid used when constructing a well.[6] However, in recent years, the use of synthetic drilling fluids are becoming more common due to enhanced fluid properties, formation compatibility, and safer environmental impacts in the event of a spill or accident.[6-8] Nonaqueous synthetic drilling fluids are often used during offshore drilling operations because of their decreased environmental impact and local regulations which stipulate their use.[6] Commonly used synthetic fluids include linear alpha olefins (LAO's) internal olefins (IO's) and esters.[6]

1.4. Well-Control Applications

The use of nonaqueous drilling fluids significantly increases the risk to worker and equipment safety when considering gas influx scenarios. Many suggest that the easiest way to prevent this gas absorption scenario is to only use aqueous-based drilling fluids.[6,10] Although this does prevent the problem from occurring, many current and future offshore well development operations would be entirely impossible without the use of nonaqueous-based fluids.

When a gas influx has been detected, there are two generally accepted methods that are employed to control and safely handle the influx: the driller's method, and the weight-and-wait method.[12] The driller's method relies on two complete and separate circulations of drilling fluid in the well to kill an influx.[13] After suspending drilling operations, the first circulation using the present drilling fluid removes the influx completely from the wellbore, then, a kill-weight drilling fluid that balances the new formation pore pressure is circulated through the well. The weight-and-wait method only relies on one complete circulation where the kill-weight mud is immediately circulated after detecting the kick to prevent further gas influx into the well.[13]

In recent years, there has been the advent of new drilling techniques and technology to supplement the drilling process to allow for easier and faster navigation of the mud weight window and reduce the risk of influxes into the well. One of the primary technologies now used is known as Managed Pressure Drilling (MPD). MPD utilizes multiple pieces of equipment installed at the surface to be used alongside operational protocol to provide greater and immediate control of the equivalent circulating density (ECD) of the fluid within the well without requiring any additional weighting agents to be added to the fluid.[14]

1.5. Managed Pressure Drilling

MPD techniques are very useful and applicable during well control operations during an influx because of their ability to quickly change the ECD of a fluid within a well.[14] In a gas influx scenario within a nonaqueous drilling fluid, the ECD of the fluid can be increased to help control the desorption of the gas influx from the fluid and not require the blowout preventer to be closed.[14,15] By using a variable choke at the surface to regulate the flow rate of the returning drilling fluid, personnel can immediately increase the pressure within the well. Using a backpressure pump during MPD operations will also allow for pressure control within the well. In addition to the equipment that MPD operations bring, the use of operational matrices illustrating the corrective methods to be employed, depending on situation-specific parameters and accurate analysis of the influx, are also used on a case-by-case basis. These matrices allow for faster decisions to be made to either allow drilling operations to continue with a given set of adjustments or to cease circulation and to shut-in the well. By utilizing the procedures for the MPD equipment indicated by the matrices, it is possible to re-dissolve the gas into the drilling fluid to prevent a surge of drilling fluids above the evolved gas layer.[15] If the gas-cut fluid can be safely removed from the wellbore without significant evolution of the gas, the risk to workers and equipment is greatly reduced.[14] It is therefore extremely important to be able to predict the behavior of the influx based on the conditions within the well to control the evolution of gas from the nonaqueous-based drilling fluids.

1.6. Riser Gas Migration

One of the most important well control scenarios is in the event of riser gas migration. Riser gas migration is when an influx of gas, either still dissolved in solution or existing as free gas, has entered the riser during offshore drilling operations.[16-18] When the gas has entered the riser, it has

already circulated above the subsea blowout preventer and can no longer be easily controlled. The riser is often a very thin-walled, large-diameter casing string that is primarily used to isolate the drilling fluids circulating through the well from the surrounding seawater.[6,16,17] Risers are not designed to withstand high internal pressures and are subject to bursting if there is a significant pressure within the riser compared to the hydrostatic pressure of the ocean water. When gas enters the riser, it can potentially lead to bursting or explosive unloading of the riser. MPD techniques can help control riser gas migration but our control over this well control scenario is limited by our knowledge about the behavior of natural gas evolving from nonaqueous-based fluids. By investigating and improving our understanding about the many properties that govern the behavior of the evolving gas, the techniques utilized when controlling riser gas migration can be greatly enhanced.[14,15]

1.7. Objectives of This Thesis

Due to the nature of gas being able to dissolve in a nonaqueous-based drilling fluid, it is imperative to better understand the kinetics of gas desorption. A greater understanding will allow us to improve current well control practices by more accurately predicting the behavior of a dissolved gas influx. In this study, we will be investigating the mass transfer of natural gas, represented by methane, evolving out of multiple nonaqueous base drilling fluids at various pressures to observe the effects that the starting saturation pressure and fluid type have on the mass transfer coefficients for each combination. Being able to measure and predict the mass transfer coefficient for a gas evolving from a nonaqueous-based drilling fluid will allow models to better represent the behavior of a gas influx and allow personnel to begin corrective well control measures.

In this study, we will be developing an experimental apparatus that will be used to conduct experiments using two different nonaqueous base fluids. Each will be tested in this study across a range of pressures and oil/water emulsion ratios to measure the mass transfer coefficient. These observations can then be used to extrapolate the rate of mass transfer for gas desorption at significantly higher pressures. The first fluid tested will be standard petroleum-based No. 2 diesel fuel. The second is an internal olefin synthetic base fluid. Each base fluid will be subjected to a series of individual emulsion (oil in water) mixtures produced from diesel and internal olefin synthetic fluids at varying oil/water (O/W) ratios.

CHAPTER 2. LITERATURE REVIEW

2.1. Gas Solubility

The kinetics governing gas-liquid mass transfer follow a series of properties that can be used to describe how a gas evolves from a fluid. The solubility of a gas within a fluid is one of the most important properties. The concentration at saturation is strictly governed by the partial pressures of the substance and the temperatures at which it is being dissolved.[19] The primary equation that expresses the relationship between gas solubility and pressure is known as Henry's Law, seen below in Equation 1.1. where P_{gas} is the partial pressure of the gas, k_H is Henry's law constant, and C_H is the solubility of a gas at a fixed temperature in a particular solvent.[20,21]

$$C_H = k_H P_{gas} \quad [1.1]$$

The relationship in Henry's law can be expressed using Le Chatelier's principle.[16] This principle stipulates that if you disturb a system that is at equilibrium, the system will adjust itself to the changes made and arrive at a new equilibrium. In the context of this study, the increase or decrease in pressure will shift the equilibrium of dissolved gas due to a change in solubility of the gas within a specific fluid. Figure 2.1 illustrates this phenomenon such that when the pressure of a gas-liquid system is increased, the solubility of the gas increases, therefore the concentration of gas within the liquid will also increase due to a shift in the equilibrium. It has been well documented that the temperature of the fluid will also affect this relationship such that the higher the temperature, the lower the solubility of dissolved gas, and vice versa.[16,19] We will not be investigating the effects of temperature in this study.

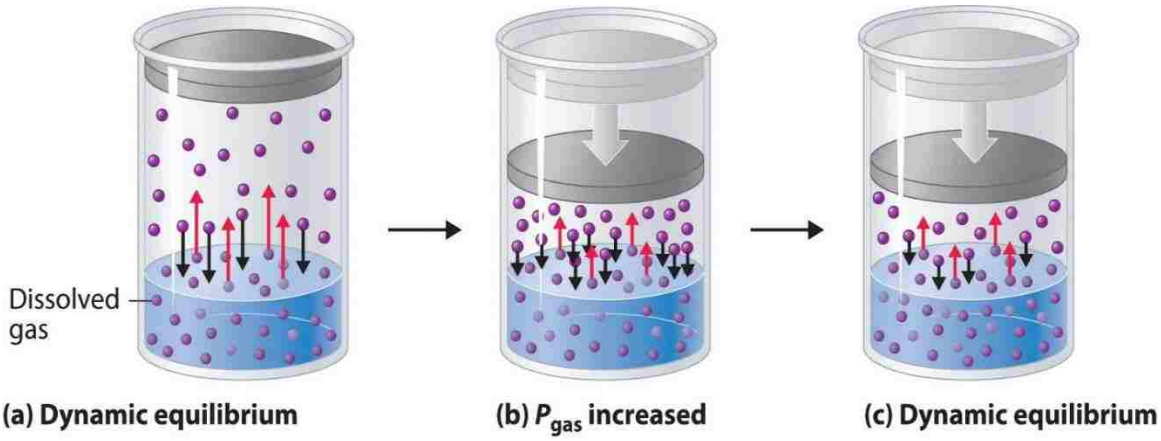

Figure 2.1. Illustration representing Henry's Law showing how the concentration of dissolved gas at any dynamic equilibrium will increase as the pressure above the fluid increases.[16]

When each of these processes come together, they present a picture that defines the solubility of a gas within a liquid species. Many experiments and studies have been performed relating these physical external conditions to the solubility of a gas by measuring a change in concentration within the fluid. These processes can be further investigated to identify the rate of change in the concentration of the gas in the liquid. Studying the rate of change in concentration is to study the mass transfer of gas dissolving into or evolving out of a fluid and a new series of equations based on the theory of Henry's law is used. In the scope of research for this thesis, we will be focusing our investigation on the rate at which the concentration of a dissolved gas will change due to a change in the pressure exerted on a fluid. The rate of gas-liquid mass transfer can be experimentally calculated for two different mechanisms: increasing the concentration of gas in a fluid towards saturation for the process of gas absorption or decreasing the concentration away from saturation for the process of gas desorption. The second process of gas desorption, which this study is focused on, is a very important subject for many industries, with major implications when constructing an oil and gas well.

2.2. Kinetics of Gas-Liquid Mass Transfer

Any gas-liquid contact will produce an interface where mass transfer can occur. The driving force of this mass transfer is primarily due to the partial pressures of gas on both sides of the interface which is controlled by the concentration difference within the gaseous phase and liquid phase. When the concentration of a gaseous species within a liquid is zero or close to zero, it will begin to immediately dissolve into solution and will form a concentration gradient in the liquid at the gas-liquid interface. As more of the gaseous species dissolve into the liquid phase, the gas will begin to distribute homogeneously throughout the solution. The primary driving force of this phenomenon is diffusion.[22] As the gas is dissolving into solution, a portion of the gas will also evolve from the solution, albeit initially at a much slower rate than the absorption of the gas into the fluid.[23] The difference in the rate between gas absorption and desorption will eventually reduce to zero over an extended period of time as the concentration of gas increases in the fluid until the aforementioned equilibrium point is reached.[23,24] This phenomenon of the changing gas absorption and desorption rates is illustrated in Figure 2.2.

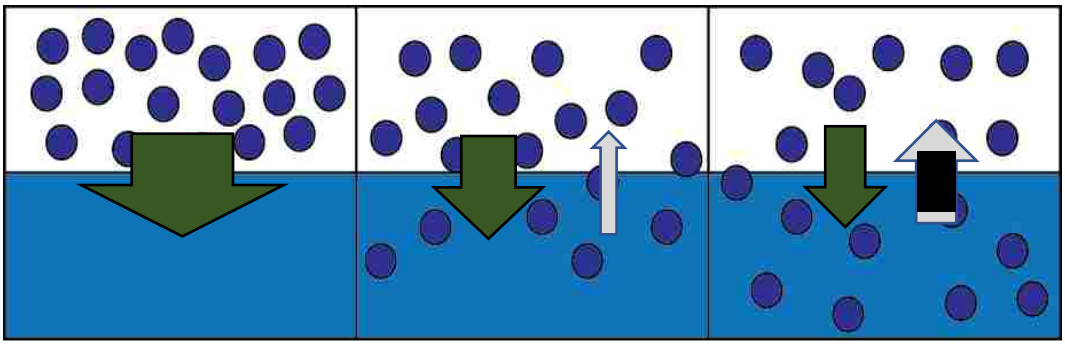

[redacted]

At the surface, it would appear that the concentration difference and diffusive gradient are the only parameters that govern this phenomenon. However, the mass transfer of a gaseous species from one phase into or out of a liquid species is governed by a complex and wide array of processes which include: intermolecular forces, mixing conditions, both bulk and interfacial rheology, chemical reactions, the surface area of contact, temperature, and pressure.[25] With this number of processes all working hand-in-hand governing gas-liquid interactions, it becomes difficult to isolate and measure the relative impact of each variable in this phenomenon.

2.3. Mechanism of Bubble Growth in Gas-Saturated and Super Saturated Fluids

To further complicate the desorption phenomena of gas-liquid mass transfer, multiple desorption mechanisms exist and are governed by the same processes, but to different magnitudes. Under a mild shift in properties such as temperature and pressure, the rate of diffusion can increase so significantly that the dissolved gas can violently evolve from solution due to a phase shift within the fluid to form bubbles.[26] The mechanisms for bubble propagation and growth have been studied extensively over many decades. Through all of the research that has been conducted to study this phenomenon of rapid phase change, two predominant theories are widely accepted that govern the formation of bubbles within gas saturated fluids: Classical Nucleation Theory, and Harvey Nuclei.[27] Both theories stipulate that a rapid phase change within the fluid, to result in mass transfer from the dissolved state within a liquid to the gaseous state, will only occur in solutions which have been saturated or supersaturated, unless agitated through vibrations or turbulence.[31,32] Classical Nucleation Theory stipulates that bubbles form from an initial bubble size of zero whereas Harvey Nuclei assumes that there are locations where free gas exists, trapped on a surface in contact with the supersaturated fluid that allows for a nucleation point for the free gas to grow before releasing from the point as a free moving bubble.[27-30] For our study and within the topic of

well control scenarios, the theory of bubble propagation proposed by Harvey Nuclei does not apply as well as Classical Nucleation Theory.

Classical Nucleation Theory argues that random statistical fluctuations of dissolved gas molecules are responsible for the formation of a gas nucleus that will shrink if it is smaller than a critical size or grow spontaneously into a bubble if it is larger than this critical size. The critical size is defined by the surface tension of the solvent and dissolved gaseous solute species.[31] Figure 2.3 illustrates the change in free energy that controls the critical radius of the bubble which dictates the possible future growth of the bubble.

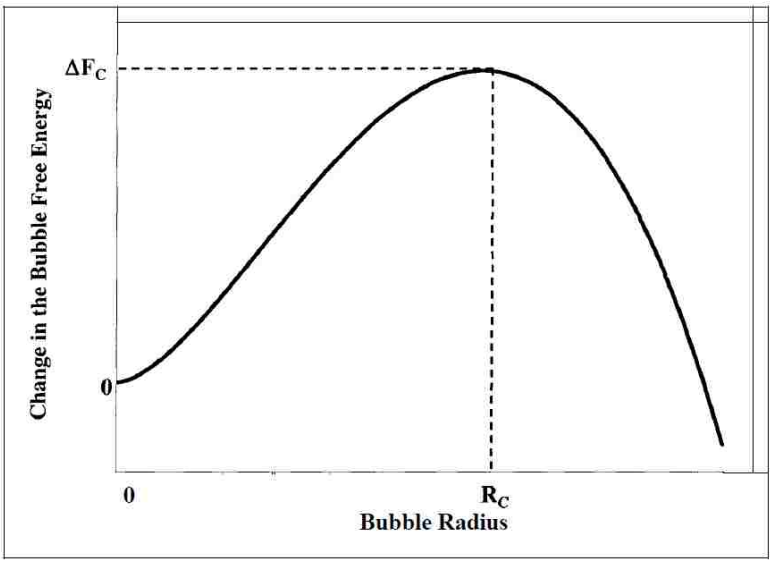

Figure 2.3. Change in free energy for a gas bubble as a function of the bubble radius for homogeneous nucleation.[26]

The change in the bubble's free energy, ΔF_C, can be shifted significantly when the pressure and temperature of a fluid with dissolved gas is increased or decreased therefore making the gas more or less likely to form bubbles spontaneously.[32] Significant experimental research verifying the critical size of bubbles in gas-liquid solutions was performed by Tucker and Ward (1975).[33] By using pressures as low as 150 mmHg, critical bubble sizes for oxygen bubbles in water were

manipulated in the range of 25 to 150 pm. Tucker and Ward were able to experimentally prove that bubbles smaller than the critical size would shrink, while bubbles larger than the critical size would continue to grow spontaneously.[33] In our study, we will be forcing a decrease in the methane bubble's free energy by inducing a rapid pressure change within our experimental apparatus. We will not be measuring the change in the bubble's free energy due to the change in pressure during this study. However, it should be noted that this mechanism and type of measurement may be usable in future studies by way of relating bubble growth to the mass transfer coefficient in desorption related mass transfer experiments.

In terms of the surface area of contact, Wilt (1986) and Eddington and Kenning (1979) investigated the effect of contact angle on bubble nucleation. Wilt concluded that homogenous nucleation and heterogeneous nucleation at smooth planar surfaces or surfaces with conical or spherical projections will not occur.[34] Contact angles of 94-130° were found to induce nucleation.[34] Eddington and Kenning observed that progressively increased contact angles resulted in higher nucleation site densities, as would be expected from heterogeneous nucleation theory at a smooth planar interface. It was not clear whether the bubble formation was due to true heterogeneous nucleation or if it originated from pre-existing gas nuclei.[35]

A study conducted by Jackson (1994) investigated how bubble formation was affected by turbulence and friction within a cell.[36] His research showed how the presence of impurities, friction, and turbulence within a fluid significantly decreased the saturation requirement that was necessary to achieve bubble formation. In our experimental study, a very rapid decrease in pressure will induce significant bubble propagation and growth which increases the turbulence of the fluid. The degree to which the turbulence will be affected is uncontrollable within our apparatus unless a method becomes available to relate the available measurable variables to the turbulence.

This cumulative research on bubble growth is significant for our study because it identifies additional elements that we cannot control during each desorption test. As the first bubbles begin to evolve from solution, due to a pressure change and resulting change in the free energy of the bubble's formation, the turbulence within the fluid from the rising bubbles will influence further gas desorption from the changing surface area. The test apparatus also has an unmeasurable number of nucleation points which present a factor that cannot be absolved because the apparatus is not constructed using a smooth material. This may affect results when comparing data after conducting the same test and following the same procedure on a different apparatus like the high-pressure apparatus, which we will describe in Chapter 3.5.

2.4. Experimental Studies of Mass Transfer Kinetics

Mass transfer effectiveness is usually expressed by means of the volumetric mass-transfer coefficient, $K_L a$, where the effects of the previously mentioned variables are reflected in the value of the general mass-transfer coefficient, K. The only variables which do not influence the coefficient, K, are the concentration gradients and the interfacial area of contact.[22]

While the interfacial area of contact is controlled by the hydrodynamic and interfacial forces that are influenced by the disturbance of the fluid, the value of the mass-transfer coefficient is dependent on the continuous phase in terms of the size of the bubbles, the mobility of the interface, slip velocity and the physical properties of the system.[37] Unfortunately, where this phenomenon is primarily studied within the realm of chemical engineering for reactor design, the complex conditions encountered in most of the reactors and situations which have been investigated have led to the development of a large number of varying equipment, and system-specific mass transfer correlations, which apply only to very narrow and particular conditions.[38,39] In turn, many

investigations only studying the effect of pressure on the mass transfer have been done using CO_2 for both the absorption and desorption processes in water.

Multiple studies were conducted by Watten, Pfeiffer, and Colt,[40-42] investigating liquid-gas mass transfer using CO_2 in water as a representative model of the phenomena. In each of these studies, the analysis of desorption has been performed by investigating the rate at which CO_2 evolves from the water. Many studies focused on the rate of mass transfer where air was used as a stripping gas to actively induce CO_2 evolution from a saturated aqueous solution. Others relied on a pressure differential to induce passive desorption.[43] Gas stripping is a process where a gas, which has a low solubility with a solvent, is injected to induce the evolution of a different species of soluble dissolved gas from the solvent.[44] In this thesis, we will only be focusing on passive desorption using a pressure differential to cause a shift in the equilibrium point of methane in a nonaqueous fluid to induce the evolution of dissolved gas.

Many studies focus on both absorption and desorption kinetics because they follow the same pathways of investigating mass transfer.[45] For the purpose of this thesis and this literature review, we will only focus on the concepts of desorption with a brief introduction and mention of absorption in order to list the foundational principles that govern this type of mass transfer. Most methods of measuring the mass transfer during each process of absorption and desorption involve calculating the change in concentration of a gas from a selected fluid. The methods described in many of these studies helped us develop a foundation for our own study by measuring the volume or mass of dissolved methane within our column of nonaqueous fluids. These studies heavily influenced our design and progressional development of the experimental apparatus used in this study and the other mass transfer studies performed in our research group.

2.5. Differences in the Absorption and Desorption Kinetics of Mass Transfer

There have been many studies performed analyzing the differences in the rates of mass transfer for both the absorption and desorption process. However, the literature that exists does not firmly conclude that both processes share the same rate of mass transfer or if one is higher than the other.[45] Several authors have stated that the volumetric mass-transfer coefficients for the absorption and desorption processes of CO_2 to and from water are equivalent since both processes are considered as purely "physical" as opposed to "chemical" processes, such as the absorption and desorption of CO_2 to and from diethylamine (DEA) where both processes for CO_2 and water is accompanied by a chemical reaction.[25,46,47] Other studies show that there are in fact differences between the rates of absorption and desorption.[48] In addition to this, multiple studies contradict each other stating that in some instances, the mass transfer coefficients for absorption show a higher rate whereas others show that the desorption rates are higher while using the same gas-liquid combination.[49] For our own study, we will not be investigating the absorption phenomena. However, it must be noted that for future studies related to our own work, there is currently no conclusive consensus in the literature on how the rates of absorption and desorption relate to each other.

2.6. Mass Transfer Desorption Studies

To better understand how to develop our experimental apparatus and conduct our experiments, we looked to recent desorption studies to identify variables involved in the desorption phenomena that could be reasonably investigated. The active desorption of CO_2 from tap water in counter-current packed towers, using air as the stripping gas, was investigated by several authors. Sherwood et al.[50], Sherwood and Holloway[51], Rixon[52], and MW Kellogg[53] found that K_La was independent of the gas flow rate per area and increased with the increase in the liquid flow rate per area. However, Cooper et al.[54] reported that K_La varied with both liquid flow rate per area that for

a specific area, the increase in K_La tended to decrease at the higher values of the liquid flow rate per area. The study performed by MW. Kellogg, for the desorption of CO_2 from seawater, observed that the K_La values for seawater were somewhat higher than those recorded for tap water.[53]

Weiland and Thuy[26] conducted an experiment using supersaturated distilled water solutions and gas streams of CO_2, air, and/or nitrogen by using a column and agitated pressurized vessels. They identified two types of desorption phenomena: quiescent desorption, which occurs when the CO_2 saturation level is modest to low, and bubble desorption, which occurs at high or supersaturation levels. K_La was found to be higher for bubble desorption and tended to increase with the increase in the liquid stirring speed, the diameter of the liquid stirrer and temperature. These two desorption mechanisms will be further described in subsection 2.5 of this chapter. Hikita and Konishi correlated the experimental results into two separate equations to represent the volumetric mass transfer in the two distinct regions and then extended their earlier work to investigate the effect of several electrolytes with varying concentrations (sodium chloride, sodium sulfate, sodium bicarbonate, and barium chloride) on K_La.[55] The presence of electrolytes enhanced the K_La values when compared to distilled water, and the factor by which the K_La increased by the presence of electrolytes was a function of the ionic strength of the solution. Identifying that there are two processes, quiescent and bubble desorption, that exist due to changing concentration will be a very important consideration when analyzing the data from our experimentally determined results.

Another study using CO_2 conducted by Szekely and Fang investigated vacuum degassing and how bubble growth was affected and accelerated the mass transfer of CO_2 evolution from molten steel.[56] It was assumed that the bubbles were in dynamic equilibrium with their surroundings, more specifically: a) Inertial effects were neglected, the pressure within the bubbles was assumed to be

the same as the pressure in the liquid at the surface of the bubbles, furthermore, b) It was also assumed that the bubbles would move with their terminal rising velocity corresponding to their instantaneous size. With regard to assumption a), it has been shown, both through theoretical arguments and by direct experimentation, that at rapid growth rates the need to accelerate the fluid surrounding the bubble will require a pressure gradient and a pressure differential between the gas and the liquid. Their study showed that as a bubble begins to form and grow due to a pressure gradient, in the case of the study the gradient was provided via a vacuum to degas the fluid, the bubble will begin to increase in size and cause a phase shift for more dissolved gas and increase the rate of mass transfer.

2.6.1. Bubble and Quiescent Desorption

As previously mentioned, it was identified in a paper authored by Weiland, Thuy, and Liveris that there are two identifiable mechanisms or phenomena that exist when a dissolved gas is evolving from solution.[26] Each process was found to be directly linked to the current partial pressures of the gas in solution and if the sample of fluid was oversaturated with gas. When the gas concentration is high, near saturation, or oversaturated, one dominant process governing gas desorption was observed and consequently named bubble desorption. As the concentration of dissolved gas decreased, there would be a shift to a diffusive governed desorption process that was named quiescent desorption. The experiments conducted to identify these two types of desorption were done using CO_2 and water and found the shift in the two types of desorption through analyzing the rate of mass transfer in comparison to a pressure-reduction ratio.

The model which was used to determine the mass transfer coefficient was defined by the following Equation 2.1:

$$K_L a = \frac{R}{V}(C - C^*) \quad [2.1]$$

Where $K_L a$ is the mass transfer coefficient, R is the rate of desorption, V is the liquid volume and C and C^* is the concentration of CO_2 and concentration at equilibrium, respectively.

Weiland and Thuy were able to generate Figure 2.4, below, when comparing the mass transfer coefficient $K_L a$ to a pressure-reduction ratio of three separate experiments. This pressure reduction ratio was found through Equation 2.2 below.

$$r_P = \frac{P_{CO_2} + P_{H_2O}}{P_T} \quad [2.2]$$

During each experiment, the pressure within the testing apparatus was allowed to rapidly decrease. As the test vessel pressure dropped to ambient conditions, CO_2 evolved from the water because it was oversaturated with gas. Gas desorption continued until the concentration of CO_2 decreased to the equilibrium point for the solubility of CO_2 in water at atmospheric pressure. During the time period that the fluid is oversaturated and rapidly evolving, the partial pressure of CO_2 is significantly higher than the system pressure allowing for a pressure reduction ratio to be above 1.0.

Weiland's paper stipulates that if mass transfer takes place through a simple diffusion mechanism, the mass transfer coefficients defined by Equation 2.1 above should be independent of the driving force $C - C^*$. Henry's law defines concentration as a linear relation to the partial pressures of a solute and solvent species, therefore, we expect independence of the mass transfer coefficient from the pressure reduction ratio, as well. The change in mechanism from bubble desorption to quiescent desorption is noted in Figure 2.3 when the mass transfer coefficient $K_L a$ shifts from a constant value during quiescent desorption at a lower pressure-reduction ratio to a rapid increase in $K_L a$ during bubble desorption at a larger pressure-reduction ratio. This paper, by

Weiland, gives a significant degree of insight into the type of desorption phenomena we expect to see in our study. During the experimental phase of our experiment, which will be further described in Chapters 3 and 4, we predict to see a sudden change or turning point in the mass transfer coefficient, once a significant quantity of methane has evolved early in the experimental trial, when the rate of mass transfer significantly slows. At this point, we will assume that the mechanism of bubble desorption has shifted to that of, diffusive dominated, quiescent desorption. In this study, we are focusing on the mass transfer during bubble desorption due to its implications on well control outlined in Chapter 1.5 that a rapid onset of gas evolution will cause.

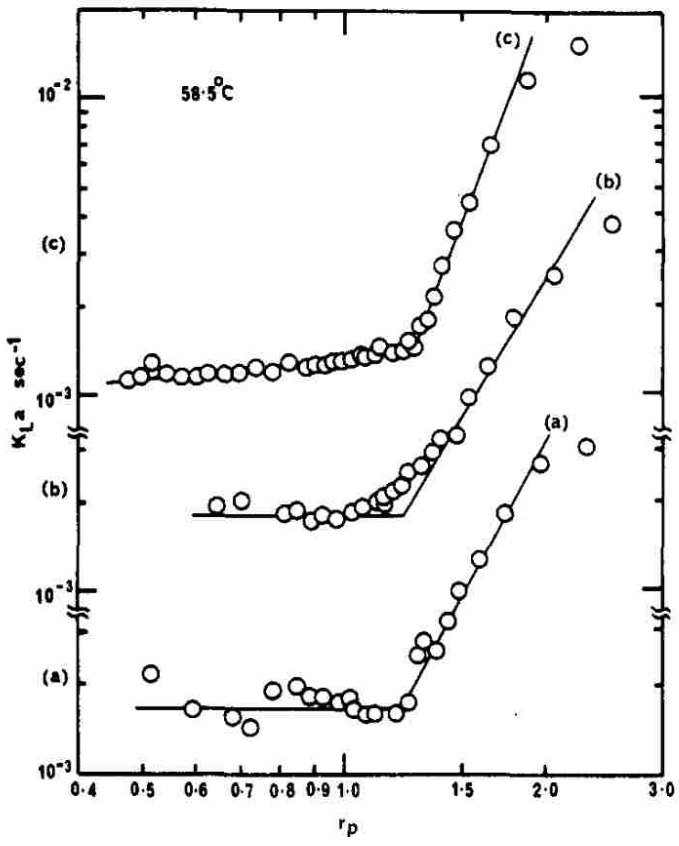

Figure 2.4. Variation of mass transfer coefficients in relation to pressure reduction ratio of three experiments conducted by Weiland et al., (1977).[26]

2.7. Desorption During a Gas Influx

When constructing an oil and gas well, being able to measure and predict the desorption of a gas from a nonaqueous fluid during an influx is of great significance. In recent years, it has become of the utmost importance due to more high-pressure and high-temperature wells being constructed and therefore a greater chance of encountering high pressure formations and gas entering the well. At the surface, a gas influx is indicated by multiple parameters: a reduction in the bottom-hole pressure, an increase in flow rate, drill-string weight change, pit volume increase, and many others. Once an influx is detected, the well will require well control techniques to be employed to manage the influx. Failure to implement well control practices could lead to confusion, misapplied techniques and potential disasters such as a blowout. In extreme cases when a subsea blowout occurs, additional wells may be required and drilled in order to flood the high-pressure formation causing the influx, before the blowout can be controlled and stopped.[4,5,57] When this uncontrolled discharge from the wellbore is directed into a weaker subsurface formation, it can be difficult to manage. Subsurface control can sometimes be regained only by sealing off and abandoning lower portions of the well.[4,5]

It is difficult, even with state-of-the-art computer models and software to predict the behavior of a gas kick (influx of gas into a well) in a well. Many well control computer models are greatly oversimplified and often do not accurately predict well behavior, due to the lack of considerations of factors that are complicated and not well understood to this date.[4] One of the greatest problems is the inability to accurately model flow behavior when a gas kick is taken while drilling with a nonaqueous drilling Fluids, oil-based drilling fluids and synthetic-based drilling fluids.[4,58,59]

2.8. Importance of Drilling Fluids During a Gas Influx

When a gas influx is taken within a nonaqueous drilling fluid, the influx can become completely dissolved within the solution and the resulting pit gain will appear to be very small or unnoticeable.[60] The resulting influx will not begin to appear again until the kick circulates high enough in the well to allow the hydrostatic pressure above it to be reduced enough so that gas can begin to evolve from the fluid.[17,61] When the gas begins to evolve from solution while inside the riser during offshore drilling, there are few methods to slow the evolution of the gas.[20,21,62] This may lead to explosive unloading of the riser and significant and hazardous conditions for workers and equipment at the surface.

The behavior of a kick varies greatly between wells and is significantly affected by the type of drilling fluid used in the well.[13-15,17] Drilling fluids or drilling muds are an essential component of the rotary drilling process used to drill for oil and gas on land and in offshore environments. The most important functions of drilling fluids are to transport cuttings to the surface; to balance subsurface and formation pressures preventing a blowout; and to cool, lubricate, and support part of the weight of the drill bit and drill pipe.[10] During drilling, the drilling fluid is pumped from the mud tanks down the hollow drill pipe and through nozzles in the drill bit. The flowing mud sweeps the crushed rock cuttings from beneath the bit and carries them back up the annular space between the drill pipe and the borehole or casing to the surface. Drill cuttings are particles of crushed rock produced by the grinding action of the drill bit as it penetrates the earth. When drilling through formations with a significant amount of gas trapped in the pore space, the cuttings from drilling the wellbore can allow a significant amount of gas to enter the wellbore and dissolve into the drilling fluid.

For a given drilling-fluid volume, the relative volumes of base oil, brine, and emulsifier in the drilling fluid can be determined from a standard retort analysis.[63] The solubility of a gas in a nonaqueous drilling fluid can be estimated by the following equation[64]:

$$R_{sm} = R_{s,oil}\,F_{oil} + R_{s,water}\,F_{water} + R_{s,emulsifier}F_{emulsifier} \quad [2.3]$$

The general equation for the solubility of a gas in oil and emulsifier, which was introduced by O'Brian et al. (1988)[65] is as follows:

$$R_{s,mud} = \left(\frac{p}{aT^b}\right)^n \quad [2.4]$$

Where R_s is the solubility, and a, b and n are coefficients which depend on the type of gas and liquid, gas specific gravity and temperature.

The most commonly used nonaqueous-based fluid is diesel where it is mainly used for onshore drilling operations. Other types of base fluids exist that are considered synthetics oils. These synthetic oils are mostly used for offshore drilling applications because of increased environmental regulations in the event of a spill.[10] The most commonly used synthetic oil is internal olefins (IO's) and internal olefin esters (IOE's), another lesser-used base fluid is linear alpha olefins (LAO's).[10] In nonaqueous-based fluids, the continuous phase is a liquid hydrocarbon mixture or another insoluble organic chemical. Nonaqueous-based drilling fluids are more expensive than aqueous-based fluids; however, they are often used in difficult drilling situations where their technical advantages are required.[10,14,15,57] Nonaqueous-based fluids are used frequently to perform operations such as drill troublesome, hydratable shales; drill deep, hot wells where aqeous-based fluids might become unstable; drill salt, anhydrite, gypsum, and mixed salt zones; drill and core hydrocarbon-bearing formations near the bottom of wells; increase lubricity to decrease torque and drag when drilling a directional well.[10,14]

With all the advantages of nonaqueous-based drilling fluids, the primary drawback is their ability to hide a gas kick.[10] When a gas kick or influx is taken within the wellbore, there are two commonly assumed gas behaviors that are experienced depending on the type of drilling fluid in the well. In aqueous-based drilling fluids, the gas kick or influx is not very soluble in the fluid and therefore a large pit gain will be experienced at the surface due to the influx.

One of the most expensive and potentially dangerous problems while drilling is the control of high-pressure formation fluids encountered while drilling for hydrocarbon reservoirs. Dynamic well control models have been used for many decades to be better prepared for different possible well control scenarios before drilling a new well.[59,62,64,65] Such calculations have many purposes, including calculation of kick tolerance to make sure physical limits are respected, and support of very realistic training of drilling crews.

Research has demonstrated the importance of advanced PVT properties of oil-based drilling fluids and hydrocarbons flowing in from reservoirs.[4,5,60] For example, laboratory experiments have demonstrated that transition to supercritical phase (or dense phase) may occur at as low as 4-500 bar pressure[66], and different base oils showed transition pressures that were around 100 bar different.[12,67] Furthermore, it has been shown that even state-of-art PVT software requires the use of non-trivial tuning procedures to match measured results.[68]

Other laboratory experiments have initiated the study of time delays in gas absorption and desorption, here referred to as kinetics. It is understood that these effects will influence well control responses significantly in some cases, however further experiments are required to determine model parameters.[67]

2.9. Factors Affecting Riser Gas Migration

Riser gas migration is of particular concern in deep offshore wells, in which a large amount of gas can be dissolved in nonaqueous drilling fluids due to the high pressure and temperature conditions of these wells. If the gas-cut fluid or free gas influx migrates beyond the BOP, there is no longer a controllable barrier above the influx.[20,21,62,70] Table 2.1 shows how significant the volume of riser gas is at various depths when using aqueous-based fluids. Some of the factors which will affect riser gas migration include Fluid Rheology, Gas Bubble Size, Liquid-Gas Solubility.

Table 2.1. Potential gas volume suspended in deep-water risers for water-based fluids.[70]

Riser Depth	Riser Volume	Potential Suspended Gas Volume		
		1%	2%	5%
Ft	bbl	bbls	bbls	bbls
500	184.7	1.8	3.7	9.2
1000	369.4	3.7	7.4	18.5
1500	554.1	5.5	11.1	27.7
2000	738.8	7.4	14.8	36.9
2500	923.5	9.2	18.5	46.2
3000	1108.2	11.1	22.2	55.4
3500	1292.9	12.9	25.9	64.6
4000	1477.6	14.8	29.6	73.9
4500	1662.3	16.6	33.2	83.1
5000	1847.0	18.5	36.9	92.4
5500	2031.7	20.3	40.6	101.6
6000	2216.4	22.2	44.3	110.8
6500	2401.1	24.0	48.0	120.1
7000	2585.8	25.9	51.7	129.3
7500	2770.5	27.7	55.4	138.5

2.9.1. Effect of Rheology on Gas Desorption

The rheology of a drilling fluid will significantly impact the rate at which a gas influx will migrate through the fluid. Blended drilling fluids are by nature non-Newtonian and exhibit pseudoplastic behaviors.[12] Two rheological models work well when characterizing a fluid: Bingham Plastic and the Power Law model. Each differ from Newtonian fluids by not having shear

rates proportional to the shear stress which is exhibited on a fluid.[71] The most significant property that the rheology of the fluid will affect, is the velocity of the influx within the drilling fluid.

An essential factor in the development of a gas kick is the rate at which free gas rises up the wellbore and the dynamic behavior of gas expansion in marine risers. Johnson et al. (1993)[72] was one of the first groups to conduct an experimental analysis of gas migration velocity during kicks. They concluded that gas in moderate concentrations (more than 10%), migrates quickly, typically at a range of 100 ft/min (i.e., 1.66 ft/sec). They showed that the yield stress of the drilling fluid which primarily assists in holding drill cuttings could also suspend gas bubbles.[72,73] Therefore, a migrating influx will leave a trail of suspended gas in the fluid that remains in suspension until the gas-cut fluid is circulated out of the well. In deep wells or wells with large annular geometries, the volume of gas suspended can become very significant in relation to the total influx volume. In some cases, the entire influx may become suspended.[72-75]

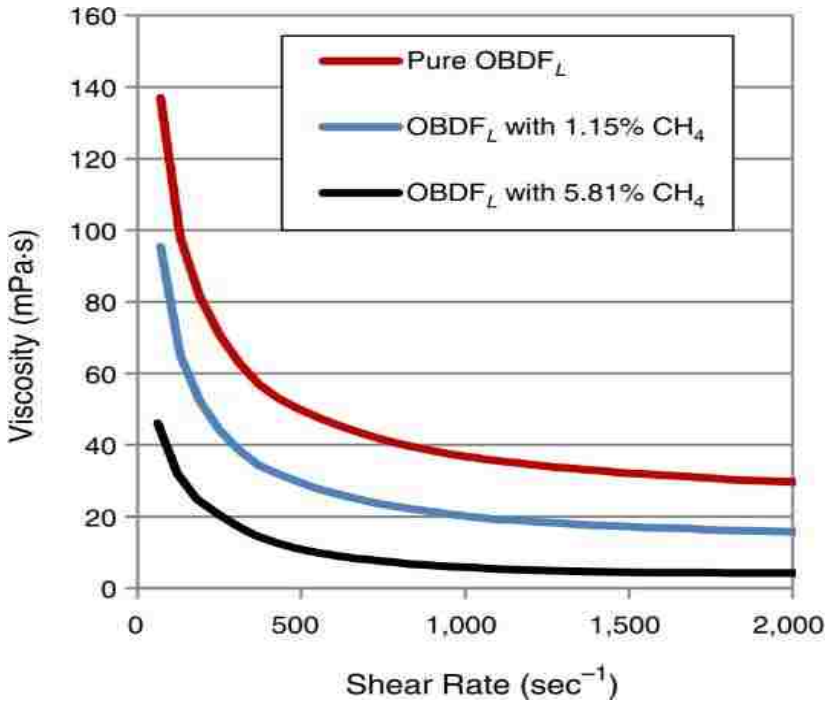

Figure 2.5. Viscosity profile of an oil-based drilling fluid for varying values of gas content.[74]

2.9.2. Effect of Bubble Size

Flatbo et al. (2015)[67] presented results from the Controlled Mud Pressure (CMP) field trial that encompassed well control on a rig equipped for dual gradient drilling. His paper focuses on the analysis of results to quantify the ability to detect influxes of gas and liquid, circulating out gas with both an open and closed annular preventer, and suppress migration of drilled gas into the evacuated part of the riser during drilling. The datasets produced during his experiments serve as an excellent basis for determining the migration velocity of the gas. The velocities reported are between 3 – 9 ft/sec based on the mass of gas injected during the experiments – Nitrogen and Methane used in WBM. Yuan et al. (2016)[75] conducted a study using a dynamic multiphase flow software to simulate a rapid unloading event and determined the gas fraction in the riser annulus. Data fed from a field observation conducted by Flatbo et al. (2015)[67] was used to verify the dynamic software model and simulation results. Conclusions which were drawn from the study state that higher liquid and gas flow rates can be seen on the surface in oil-based mud than water-based mud.

Lab-scale tests to experimentally examine gas migration rates in drilling fluids were performed by Johnson et al. in a large flow loop using air and xanthan gum.[72,73] Their findings suggested that gas bubbles are larger in the viscous mud than those in equivalent air/water flows. The difference in bubble size probably resulted from the stabilizing effect of the higher viscosity of the mud. The viscosity of the drilling fluid was shown to have hindered bubble break- up which resulted in the gas migrating as big bubbles, which in turn have the ability to migrate at faster velocities. The data showcased that a kick rises faster in viscous drilling fluids than in water due to the change in flow regime caused by large slug type bubbles forming at lower void fractions. Hovland and

Rommetveit (1992) analyzed data from full-scale experiments and made comparisons between high and low concentration kicks in WBM and OBM.[76]

2.9.3. Effect of Gas-Liquid Solubility

The most significant effect on riser gas migration is the gas-liquid solubility. The solubility of the gas within a liquid is highly dependent on the compatibility that exists due to intermolecular forces between the gas and the liquid. From this solubility, the concentration is then determined by the PVT properties of the gas and liquid at a given state.[62,70,76] Most gas influxes are comprised of methane with low concentrations of ethane. At 190 K and 4.6 MPa, methane reaches its critical point and beyond these values, methane enters its supercritical phase. It is at this point that methane is considered completely soluble within a nonaqueous fluid and the solubility will theoretically become infinite.[4,5,77] This relatively low critical point is why the behavior of a gas influx is very important when drilling while using nonaqueous drilling fluids in high-temperature and high-pressure wells. A study by Monteieo et al. (2008)[63] was carried out to understand the pressure/volume/temperature (PVT) behavior of the fluids by experimental determination and modeling of properties such as solubility, specific gravity, and formation volume factor of the fluid. The experimental work was conducted using mixtures of methane and n-paraffin-based emulsions. Tests were performed at a pressure of 7,500 psi and a temperature range of 158 - 302°F. Analytical expressions based on experimental data were developed to evaluate solubility and formation volume fraction of methane/n-paraffin-based fluids. The mathematical model developed by Moneteio allows for quick computation of essential parameters for kick detection in synthetic oil-based muds. Various models have been formulated from these to understand the expansion behavior and gas kick migration velocities better. Furthermore, it has been shown that even state

of the art PVT software requires the use of non-trivial tuning procedures to match measured results.[78]

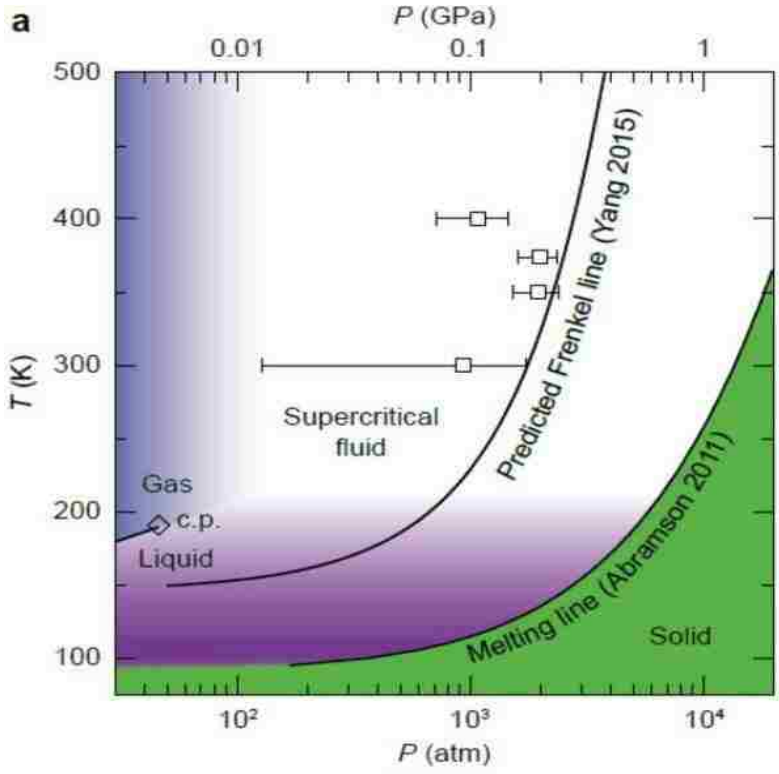

Figure 2.6. Methane phase diagram. The critical point is indicated at 190.55 K and 45.29 atm.[80]

The maximum gas absorption for both base oils and oil-based drilling fluids, follow a linear curve, corresponding to Henry's Law with little or no dependence until reaching the critical point.[79] At or near the critical point, the base oil starts deviating from the conventional trend where the saturation pressure levels off and decreases with increasing temperature conditions. Viscosity profiles of the drilling fluids with gas absorbed at 1,000 bar (14,500 psi) show that at high shear rates, gas content as low as 1.15% can considerably reduce the viscosity by almost 50% and higher amounts of gas absorbed at 5.81% decrease the viscosity in the region of 80%.[80]

CHAPTER 3. EXPERIMENTAL DEVELOPMENT

In this chapter, we will discuss the many experimental developments that were both discovered and necessary to be able to accomplish each of the objectives of this thesis. From developing the initial low-pressure apparatus, we identified how our assumptions for measuring the desorption of gas changed and new parameters were required and utilized for a more accurate representation of the desorption phenomena. Each stage of the experimental development brought new methods and processes which were required during each experimental run that allowed us to complete this study. We progressively upscaled and improved the equipment to allow for higher pressures to better replicate real downhole conditions to eventually develop a new high-pressure apparatus that has been built and will soon be used to conduct these same experiments at pressures up to 5,000 psia.

3.1. Initial Low-Pressure Apparatus Development

During the initial phases of development for this study, we wanted to develop an apparatus that gave us the capability of measuring the mass transfer for three separate processes: absorption, desorption, and convection. We found that there had been little to no previous research conducted to help guide us and provide a foundation to design an apparatus that could be used to measure two, let alone all three phenomena. There are many studies which describe apparatus' which can be used for each of these processes, however, we required one apparatus to be used for all three. The desorption kinetics that this thesis is focused on, is one of the three branches of a mass transfer project that my research group is currently working on. The other two processes are the absorption kinetics of methane in nonaqueous fluids, and the convection of dissolved methane in nonaqueous fluids.

Because the experimental apparatus would be used to study all three phenomena, the design was heavily dictated by the requirements of each investigation. We understood the various parameters which would affect the processes of absorption and desorption from previous literature that studied other fluids and gasses. We then designed the apparatus to measure these selected parameters but also allow for future upgrades to the apparatus so that new potential parameters could be investigated.

The following list was developed from a review paper by Ghandi et al. (2009) which includes many papers focusing on the many properties which affect both the absorption and desorption processes of gas-liquid mass transfer.[81]

Table 3.1. Properties affecting gas-liquid mass transfer.[81]

Properties Affecting Gas-Liquid Mass Transfer	
Column Dimensions	Diameter
	Height
Sparger Type	Hole Diameter
	Number of Holes
System Properties	Temperature
	Pressure
Superficial Velocity	Gas
	Liquid
Liquid Properties	Density
	Viscosity
	Surface Tension
Gas Properties	Density
	Viscosity

The experimental procedures used to study the processes of absorption and desorption require two test sections. One where the nonaqueous fluid could be saturated and an additional test section above, acting as a buffer section. The convection tests required at least three test sections so that two may contain the fluid and a top section to act as a buffer, similar to the one used in both the absorption and desorption experiments. The additional test section for the convection experiments

was required to be able to isolate a portion of the fluid in the column to measure the rate of convection due to the natural buoyancy of the gas-cut base fluid. The apparatus also required a way to regulate the inlet flow of gas to measure the mass transfer as a function of flow rate for the absorption process and required a method to measure the outlet flow of gas for the desorption process. All of these considerations from the experimental requirements were included in the final developed form on the low-pressure apparatus and the future high-pressure apparatus.

Figure 3.1. The first low-pressure prototype experimental apparatus used to develop the experimental procedures for each of the mass transfer processes and test initial concepts of future apparatus designs.

The initial prototype apparatus was constructed using all schedule 80 PVC components to provide a 2-inch cross-section within each test section and included clear PVC piping to allow for visual observation of the fluids inside. Initially, a vacuum tank was used to pull the fluids out from

each test section to allow for the gas to evolve and then measure the concentration of gas dissolved within the fluid. The prototype allowed us to test the mass transfer phenomenon of each process as a proof of concept using CO_2 in water before developing a more specialized apparatus.

3.2. Low-Pressure Proof of Concept Studies

After the prototype apparatus was replaced, early experimental runs to further develop the design of the experimental procedures were conducted using CO_2 and vegetable oil as a methane-diesel analog. During this stage of the study, we made significant improvements to our experimental procedure and progressed to using propane in oil and then propane in diesel as our analogs before beginning the methane in diesel and synthetic fluid tests. Our experimental study was focused on using one kinetic model of mass transfer by Linga 2013 which uses a mass transfer coefficient, K_D. This model is further described in Chapter 5. Through experimental measurements, the K_D value was found to drastically change based on the flow rate of gas exiting the column. When the flow rate of gas exiting the column is increased, the K_D values were observed to reach an asymptotic limit. Data that resulted in these conclusions is shown in Figure 5.1 under Chapter 5.4. Therefore, higher flowrate flowmeters were required to ensure accurate results following this model.

3.3. Final Low-Pressure Apparatus

The final low-pressure apparatus, shown in Figure 3.2, was used for all methane and nonaqueous fluid experiments performed for this thesis. It consisted of a similar design to the first prototype apparatus. PVC valves and components were exchanged for brass and stainless steel fittings and the cross-section of the apparatus was shrunk from the prototype's 2-inch ID down to a 1-inch ID to allow for a higher burst pressure tolerance of 320 psia, and therefore, expand the

possible pressure conditions for each test. Volumes of each test section were measured to be between 230 and 250 mL. All analog pressure gauges were replaced with digital gauges to allow for more accurate pressure measurements. From the new low-pressure apparatus, many modifications were made to the column to suit changing experimental procedures. Later, pressure transducers were installed and both the transducers and flow meters were utilized by a new data acquisition unit to measure and record each at 0.1-second time-steps.

The degassing tests were carried out by injecting methane into the lowest test section of the apparatus which had been filled with diesel and internal olefins. The experiments were performed at isothermal conditions at different internal pressures which were set by pressurizing the chamber during the saturation procedure using methane. Pressure conditions for this experiment were selected considering the total working pressure range of the column.

3.4. Major Early Findings and Experimental Considerations

The most important findings which we were able to experimentally determine during the early stages of this desorption study are as follows:

- The starting saturation pressure is the only function of pressure which was found to be an important factor that will affect the rate of mass transfer in the desorption process where higher starting saturation pressures yielded higher mass transfer coefficient K_D.
- The second most important factor has been designated as the peak exiting flow rate. This flow rate represents an instantaneous release of gas from the fluid in the column by dropping the starting pressure to atmospheric rapidly. If the exiting flow rate of the gas is restricted, the amount of time it takes for the gas to evolve is lengthened which will significantly shift the mass transfer coefficient.

- When changing the peak exiting flow rates, our results indicate that the mass transfer coefficient, when following Linga's model, will reach an asymptotic limit for any starting saturation pressure up to 200 psig when the peak exiting flowrate is maintained at 25 Ln/min.
- When applying Linga's model, using K_D as the mass transfer coefficient of desorption, we have a linear relationship for the desorption of gas at early time measurements in terms of concentration vs. time which represents the mechanism of bubble desorption.

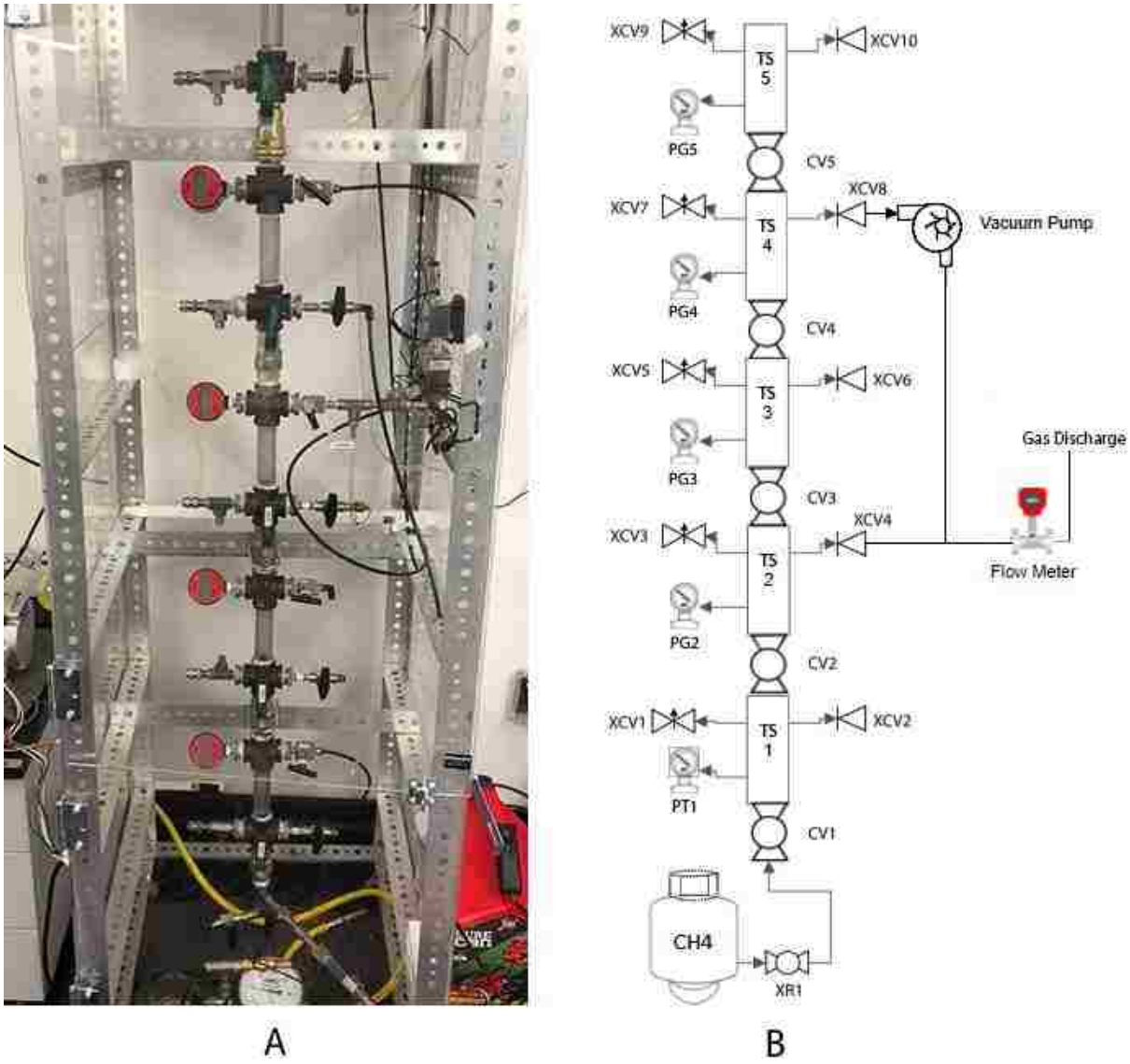

Figure 3.2. Final low-pressure apparatus desorption configuration. A) Picture of the updated apparatus. B) P&ID configuration of the apparatus.

Many more developments were made in regard to the absorption and convection experiments. Notable initial results from the absorption experiments identified that the absorption process is significantly faster than expected, reaching very high methane concentrations in diesel within the first minute of gas injection. Initial convection experiments using propane in diesel allowed us to visually observe natural convection of the gas-cut fluid rising into the uncut fluid through the clear PVC sections. The natural convection was very fast and appeared to have unique flow patterns. When convection tests were repeated using methane and diesel, no visual disturbances were observed but convection was detected after analyzing the fluids in each test section. We attribute the visual change in the fluid, when using propane, to the high concentrations achieved. In the low-pressure apparatus, we are limited by the apparatus' functional pressure range and cannot achieve as high of concentrations when dissolving methane as we can with propane. We expect to see the visual disturbance of dissolved methane in diesel while using the high-pressure apparatus. The results of these two mass transfer studies will be shown in future publications.

3.5. High-Pressure Apparatus Development

All of the design and procedural considerations that have been developed from the initial prototype and the final low-pressure apparatus have had a great impact on the next stage of this study. A high-pressure apparatus was designed and developed by myself and Syed Nahri to include all our prior knowledge to study these phenomena at pressures up to 5,000 psi. The high-pressure apparatus has four test sections providing a continuous 2-inch ID. Each test section has an optical sapphire glass port to allow us to visually observe the fluids within each of the sections during the upcoming experiments as we could through the clear PVC sections of the low-pressure apparatus.

Tests performed in the high-pressure apparatus will expand the possible pressure range from the low-pressure apparatus significantly. To be able to reach gas pressures of up to 5000 psi, a

buffer tank is used and charged using a methane pump when testing pressures above 1000 psia. This procedure is required due to standard 200 L methane cylinders only being charged with up to 1500 psia. After charging the buffer tank. The gas is directed through a variable inlet gas regulator which will allow us to set a specific inlet gas velocity. The gas will enter the bottom of the column, similarly as in the low-pressure apparatus, to saturate the fluid in the lowest test section for each of the three mass transfer studies. Depending on which experiment is being performed, the fluid within the column is directed to an external knock-out drum acting as a separation vessel to induce gas evolution. It has been custom-designed to contain a series of baffles to allow the gas to quickly evolve from the fluid. After the methane has evolved from the fluid, it is pumped through a methane flowmeter from the knock-out drum to measure the amount of evolved gas. From this point, all spent fluids and gas are pumped into liquid waste containers and empty gas cylinders.

Similar procedures followed on the low-pressure apparatus apply to the high-pressure apparatus, but now, all valve and operational controls are done through digital controllers to allow for automation and enhanced user safety. The apparatus has been constructed and was delivered to the LSU Petroleum Engineering Research & Technology Transfer Laboratory (PERTT Laboratory) in the Fall of 2019. It gives us the capabilities of investigating each of the three branches of our mass transfer experiments as we have done using the low-pressure apparatus. The high-pressure apparatus benefits us with expanded pressure and geometry conditions required to better replicate real downhole conditions. We expect very interesting results to come about from the high-pressure apparatus, especially during the convection experiments. Further tests in the absorption and desorption studies will help either confirm the observations we have seen over a greater pressure range or allow us to observe and measure new phenomena.

Figure 3.3. High-Pressure apparatus currently installed at the PERTT laboratory.

CHAPTER 4. EXPERIMENTAL STUDY

In this chapter, we will discuss the materials involving the two fluid types, the experimental procedures used in this study, and the results of each experiment.

4.1. Materials and Characterization of Fluids

The diesel used in this study was a standard blended diesel used for both oil-based drilling fluids and for automotive use, designated No. 2 Diesel Fuel. This fluid is subject to EPA regulations on the sulfur content of <15 ppm and consists of carbon numbers generally between C9-C23 in weight, as seen in Figure 4.1. The synthetic fluid was provided by Halliburton is entirely comprised of a blend of internal olefins. Internal olefin fluids are much more homogenous in chemical structure than diesel fuels and much safer for the environment due to their low toxicity to wildlife.[10]

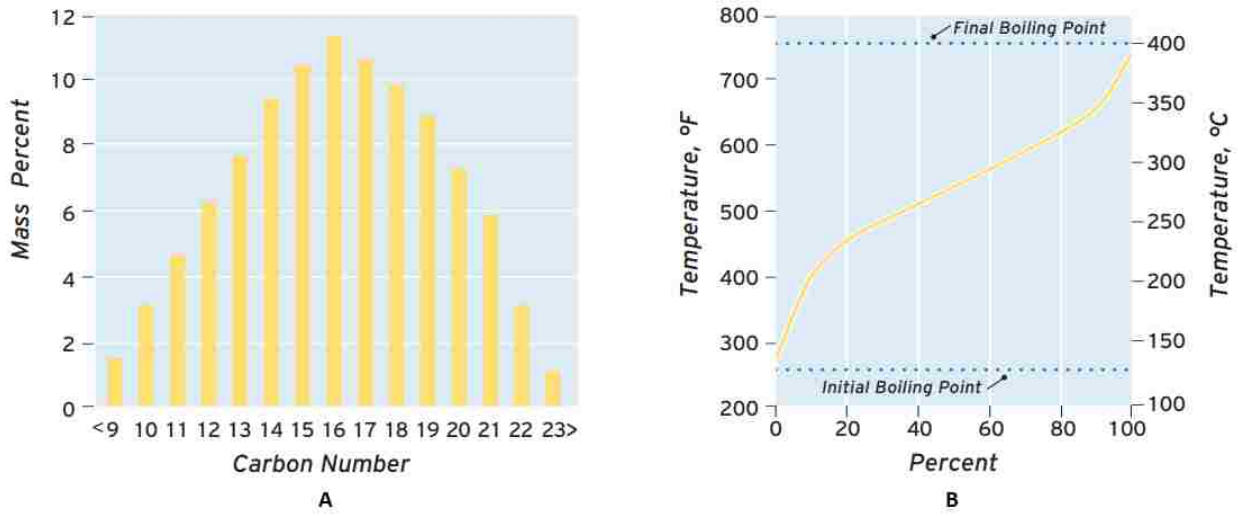

Figure 4.1. Typical carbon number distribution for No. 2-D diesel fuel (A). Typical distillation profile of diesel (B).[87]

Internal olefins are defined as organic long-chain carbon molecules that have at least one carbon-carbon double bond which is not on the C1 position, illustrated in Figure 4.2. When the double bond is on the C1 position, it is considered a linear alpha-olefin (LAO). LAO's are no

longer often used by the oil and gas industry when developing drilling fluids. The physical properties of each fluid used in this study are listed below in Table 4.1.

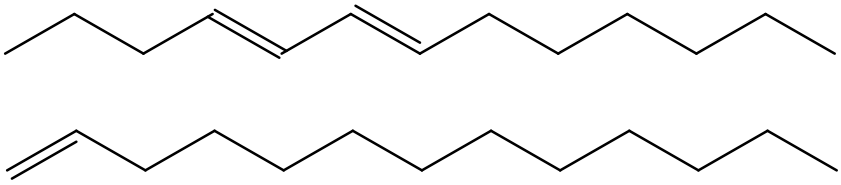

Figure 4.2. Illustration of 3,5-tridecene representing internal olefin in a double trans configuration (Top), and 1-tridecene representing a linear alpha-olefin (Bottom).

Table 4.1. Physical Properties of Diesel and the Synthetic Internal Olefin used in this study.

Fluid	Density (lb./gal)	Viscosity (40 °C, mm^2/s)	Aniline Point (°C)	Sulfur Content (ppm)	Color
Diesel	6.943	2.1	49	<500	Yellow
EDC 99-DW US Internal Olefin	6.809	2.4	79	<1	Clear

4.2. Internal Olefins Used in This Study

The internal olefins which were used in this study were characterized to determine the compositional makeup of the fluid. Nonaqueous-based drilling fluids are never composed of a pure chemical species, instead, they are composed of possibly hundreds of different compounds. Each of these compounds in their pure state each have a specific solubility and affinity to methane absorption and desorption, therefore it is crucial to understand the compounds that exist within a drilling fluid being tested. Slight alterations to the compositional makeup will have a significant effect on the mass transfer of methane to and from the drilling fluid.[82-86] Components of the diesel used in this study were found in literature knowing that it was a standard blend diesel fuel used for powering diesel vehicles and equipment. To characterize the internal olefins, GC-MS analysis was conducted on the fluid. The following GC-MS procedure was conducted to analyze the fluid. The

internal olefins were determined by gas chromatography, model GC-6890N coupled with a mass spectrometer, model MS-5973 MSD (mass selective detector). The separation was performed on a capillary column DB-5MS (30 m × 0.32 mm, 0.25 μm of film thickness). The carrier gas was helium with a flow rate of 1.5 mL/min. The column temperature was programmed from 80 to 300 °C at the rate of 5 °C/min. The temperature of both injector and detector was set at 250 °C. A sample volume of 20 μL IO's diluted with heptane was injected using a split mode, with the split ratio of 1:10. The mass spectrometer was set to scan in the range of m/z 50–550 with electron impact (EI) mode of ionization.

Table 4.2. GC-MS Analysis results of identifiable compounds within the internal olefin sample

Compound	Location of C=C bonds	Carbon Chain Length
Decane		10
Tridecane		13
Tridecene	1,	13
Tetradecane		14
Tetradecene	2, 3, 5, 6	14
Hexadecane		16
Hexadecene	7	16
Heptadecene	3, 8	17
Octadecene	3, 5	18
Nonadecene	1, 5	19

From the GC-MS analysis, we found that the internal olefins tested in this study ranged from C10-C19. The analysis showed that there were detectable levels of linear alpha olefins, 1-Tridecene and 1-Nonadecene, and saturated hydrocarbons Decane, Tridecane, Tetradecane, and Hexadecane. These results, although the samples were not analyzed for molar ratios, show how diverse in molecular composition the synthetic fluids are which will lead to changes in the calculated mass transfer coefficients when testing other fluids of different compositions.

4.3. Development of the Emulsion Fluids

In part three of this study, we investigated how emulsion fluids performed when compared to the pure diesel and internal olefins tested in parts one and two, respectively. To develop the emulsion fluids, a two-step blending process was utilized to ensure that the fluid remained homogenous during the subsequent desorption tests. Every test performed on a specific fluid would take on average 45-60 minutes including the saturation and vacuum degassing stages, therefore, a stable emulsion was required while performing each test. Table 4.2 below illustrates the three different emulsion oil/water ratios which were used in this study.

Table 4.3. Emulsion fluid ratios tested in this study. Both for diesel and internal olefins.

Emulsion #	Nonaqueous Fluid/Water Ratio
1	90/10
2	80/20
3	70/30

When developing an oil-water emulsion, it can be very difficult because the hydrocarbon-based fluids used in this study naturally do not mix well with water due to the nonpolar nature of the nonaqueous-based fluids. To help force diesel and internal olefins to form emulsions, both a standard mixing blender and an ultrasonicator were used in a two-step process to develop a stable emulsion. An ultrasonicator works by vibrating a solid metal probe at extremely high frequencies. When submerged within a fluid, the vibrating probe will induce cavitation bubbles to form which collapse very rapidly and causes the fluids surrounding the cavitation bubbles to disperse homogeneously. An ultrasonicator is the only means to produce a pure oil-water emulsion without the addition of surfactants and detergents that would help stabilize the emulsion between each fluid. To make the pure oil-water emulsion, a small volume of the nonaqueous fluids was added to a 50 mL beaker and water was titrated using a burette very slowly into the beaker while the

ultrasonicator was running. After producing an emulsion between the oil and water at this small volume, more of the nonaqueous fluids can be added slowly until the desired volume was achieved. This procedure, however, was not ideal for the volumes required for each test. TS1 holds exactly 250 mL of fluid and developing one sample of the emulsion fluid required between 2-4 hours of continuous sonicating to ensure that a strong and stable emulsion developed. While sonicating, the before mentioned cavitation bubbles produce an extremely large amount of heat which reduces the stability of the forming emulsion so constant cooling was required using either an ice bath within the ultrasonicator box or periodically transferring the samples to a refrigerated bath.

Figure 4.3. Q-Sonica Q500 Ultrasonicator used to generate each of the emulsion fluids.

To develop the emulsion fluids used in this study, a modified procedure was used to include an emulsifier. Commonly used emulsifiers and detergents, used to develop drilling fluids, have a

natural solubility for methane.[88] We previously discussed in Chapter 2.7 that when developing emulsion fluids which use common emulsifiers and detergents, the solubility factor must be accounted for when calculating the amount of dissolved gas. Therefore, we required an emulsifier that could be used which does not affect the desorption results. We identified through testing, that in low quantities, lecithin, a natural food product derivative from egg yolks and soybeans, produced a very stable emulsion. When tested against a pure oil-water emulsion, there were no significant differences observed between each test and the resulting mass transfer coefficients were within the measurable accuracy of the experiment. Therefore, we concluded that lecithin does not affect solubility and it became an ideal material to use for all our emulsion tests.

To produce each of the emulsions used in this study, the following procedure was followed. To a steel mixing cup, a specified volume of nonaqueous fluids was added to represent either a 90, 80, or 70% ratio of nonaqueous fluid to water in a final 250 mL sample. The water phase of the emulsion was measured out and added to a 100 mL beaker and placed on a stir plate with a stir bar. 1.5 grams of lecithin was measured using a scale and added to the beaker before turning on the stir-plate to dissolve the lecithin. The blender was then turned on and the water and lecithin solution was slowly added to the mixing diesel. The fluid was blended for five minutes before cooling in a refrigerated bath set to 0 °C for 10 minutes. After cooling, the fluid was transferred to a 400 mL beaker and then sonicated using a Q-Sonica Q500 Ultrasonicator at 50% amplitude pulsing for 5 minutes, 15 seconds on and 5 seconds off. After sonicating, the resulting emulsion was transferred into the apparatus to begin testing. The emulsions developed following this procedure were found to be extremely stable. Samples of the 70/30 emulsions were allowed to rest for 24 hours in 10 mL graduated cylinders and were observed to show approximately only 10-15% emulsion degradation. Emulsion degradation was measured using the volume of the water phase

that had completely separated from the emulsion. Using this volume we can calculate the relative percentage of water which had separated compared to the original volume of water suspended in the emulsion.

Figure 4.4. Picture of the 70/30 internal olefin water emulsion. Left, before mixing and sonication. Right, two-hours post mixing and sonication.

4.4. Experimental Design

The degassing tests were carried out by injecting methane into the lowest test section of the apparatus which had been filled with the specified fluid. The experiments were performed at isothermal conditions under different internal pressures which were set by pressurizing the chamber during the saturation procedure using methane. Pressure conditions for this experiment were selected considering the total working pressure range of the column. A complete test matrix describing the conditions of each test performed is listed in Appendix A.

The tests conducted were used to measure the degassing coefficient K_D after applying the calculated concentration changes to the Linga (2013) model. The concentrations were determined by saturating the fluid with methane at a specific pressure then allowing the chamber to depressurize and then vacuum pumped to find the concentration at all pressures used in this study. One of the objectives of this study was to determine how the starting saturation pressure affects

the mass transfer coefficient K_D in the Linga model. The second scenario was to consider the effect of fluid type in the form of testing two different base fluids and oil/water emulsions of each to determine the effect that water content and fluid type has on the K_D value.

4.5. Initial Saturation Procedure

The following procedure was followed to prepare the apparatus for methane injection. Test section 1 was first filled with the specified fluid. Methane was then injected from the bottom of the test section at a specific predesignated pressure. The methane was allowed to flow into the test section without consideration of flow rate or bubble size. The methane which bubbled through the fluid was allowed to exit the column through XCV4 on TS2. XCV4 comprised of a needle valve and a downstream ball valve. During the initial saturation procedure, the needle valve was adjusted so that when the ball valve was opened to release the methane in the degassing procedure, a specific peak exiting flow rate at the given starting pressure within TS1 and TS2 would flow through the flow meter. Setting the needle valve is crucial to ensure that the flowmeter was not overloaded by a flowrate above which the flowmeter could measure or too low of a flow rate to cause a large shift in the measured degassing coefficients. Methane was injected until the pressure decay method confirmed the saturation of methane within the nonaqueous fluid. Typical gas flow times for any pressure tested were between 20-25 minutes. Flow times of this duration are not required but were used to ensure that the fluid had been completely saturated.

4.5.1. Pressure Decay Method

To ensure that the fluid within TS1 had been saturated with methane, a technique known as the pressure decay method can be used to confirm saturation. The pressure decay method is a means to determine if a fluid can be further saturated with gas. The pressure decay method relies

on a significant amount of free gas to exist above the column of fluid in relation to the total volume of fluid. If the fluid has not yet been fully saturated with gas at a specific pressure, the free gas above the column of fluid will continue to diffuse into the liquid and the pressure within the chamber will decrease. If the fluid has been fully saturated, the mass transfer between the free gas phase and dissolved gas has reached an equilibrium between absorption and desorption.

4.5.2. Degassing and Measuring Procedures

To measure the amount of methane that had dissolved within the diesel, a mass flow meter/controller was used downstream of XCV4 to totalize the amount of methane that evolved from the diesel and exited the column. To measure the gas evolving from the fluid, cameras were used to record the change in pressure and flow meter readings. Later, a data acquisition unit was used to record the flow meter measurements every 0.1 seconds. Each test concluded when the pressure within TS1 and TS2 read 0 psig and the mass flow meter read 0.00 ln/min. At the end of each test, the column was mechanically degassed using a vacuum pump which directed all of the remaining dissolved gas in the fluid and pumped it through the flow meter to find the total dissolved gas which was in the fluid.

4.5.3. The Buffer Layer

During the experiment, we allowed TS2 to be filled with additional methane which was progressively subtracted from the totalized methane readings on the flow meter. This buffer layer, therefore, adds a significant amount of gas to the system and increases the possible error in our results. Our intention of using a gas buffer layer was to help prevent a surge of fluid which would generate bubbles as the pressure drops within TS1 and flows towards the flow meter. In the event that any fluids passed through the flow meter, we would lose calibration, and the flow meter would

require cleaning before being able to continue and generate accurate data. During our initial procedural development, it was found that the buffer layer was necessary to protect the flow meters used in this study. The calculations used to determine and subtract the volume of gas within TS2 from our totalized measurements at any given pressure is further described in Appendix B.

4.6. Saturation Results

It was important to first measure the solubility of methane in diesel so that it could be used in the Linga model to know the theoretical gas loading from the concentration at a given pressure and time during each test. The saturation curve seen in Figure 4.5 was found by performing a series of saturation experiments on a sample of diesel from 25 psig to 300 psig. Each experiment involved saturating the diesel with methane before mechanically degassing the fluid sample using the vacuum pump.

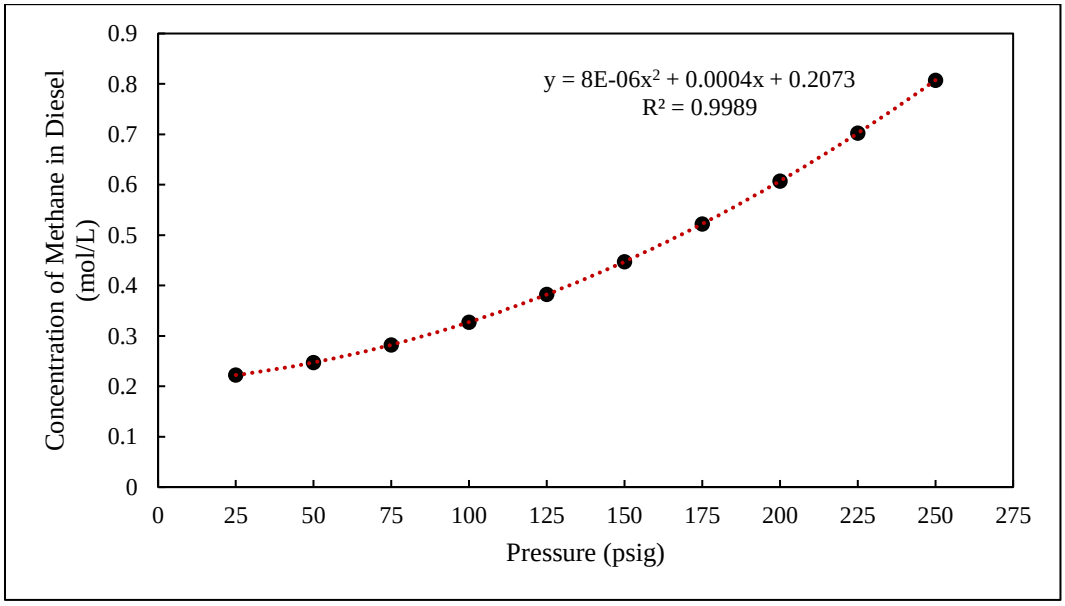

Figure 4.5. The concentration of methane in diesel at saturation for various pressures ranging from 25 psig to 300 psig.

A saturation curve for the Internal Olefin fluid was also required and the same procedures used for methane in diesel were followed as seen in section 4.6.1 to develop the following curve, Figure

4.8. The resulting saturation curves show a lower concentration at saturation at the same pressures for internal olefins compared to diesel for the same respective pressures the fluids were saturated at.

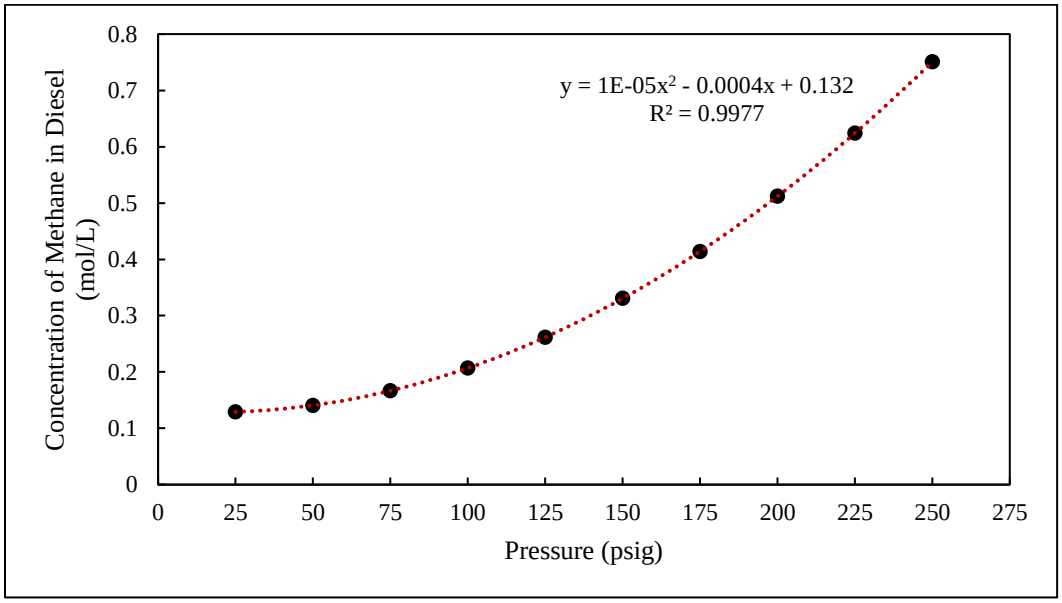

Figure 4.6. The concentration of methane in synthetic internal olefins at saturation for various pressures ranging from 25 psig to 300 psig.

The results of this series of saturation experiments show that our hypothesis was correct that the concentration at saturation for the internal olefins is, in fact, lower than those observed for diesel. It was predicted that this would be the case due to the relative chemical homogeneity of the internal olefin blend compared to diesel as discussed in section 4.2.1 where the internal olefins were characterized by GC-MS analysis.

4.7. Desorption Results

In this subsection of Chapter 4, we will discuss and analyze the raw data which was collected through experimental observation of the degassing phenomenon for various nonaqueous-based fluids with dissolved methane. In Chapter 5, we will use the data obtained in this part of the chapter to develop and calculate the mass transfer coefficients from each test. Each of the figures in the

following sections represent the data sets from 100, 150, and 200 psig for the flow rate, totalized volume of evolved gas, taking into account of the buffer layer of gas, and the decrease in pressure within the test section as the test was conducted, respectively. 125 and 175 psig data sets were left out of these figures for clarity.

It must be noted that in each of the tests performed, the starting pressures were not necessarily the exact pressures that were desired for the beginning of each experiment. The temperament of the apparatus made it difficult to set an exact starting pressure. Error in the starting saturation pressure was mainted at +/- 5 psig. This discrepancy, however, has little effect on the modeling portion of the data analysis in Chapter 5 because pressure data is only needed after $t = 1\ s$.

4.7.1. Methane in Diesel

Figures 4.7, 4.8, and 4.9 each represent the results from the methane in diesel tests.

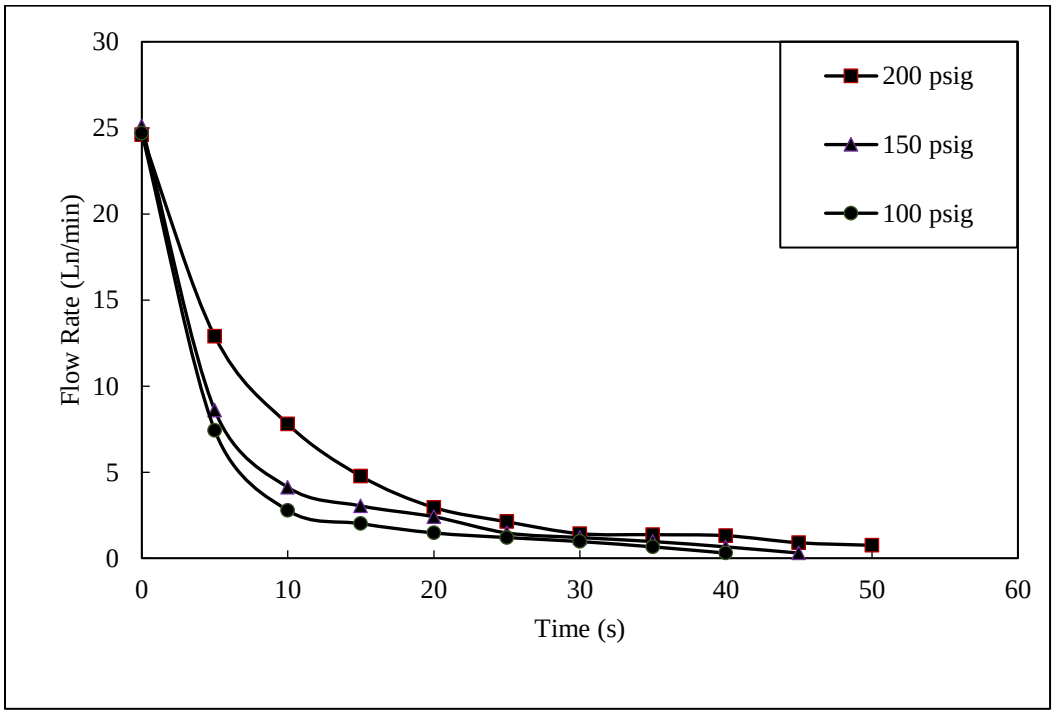

Figure 4.7. Measured flow rates of methane leaving the column through the mass flow meter for 100, 150, and 200 psig diesel tests.

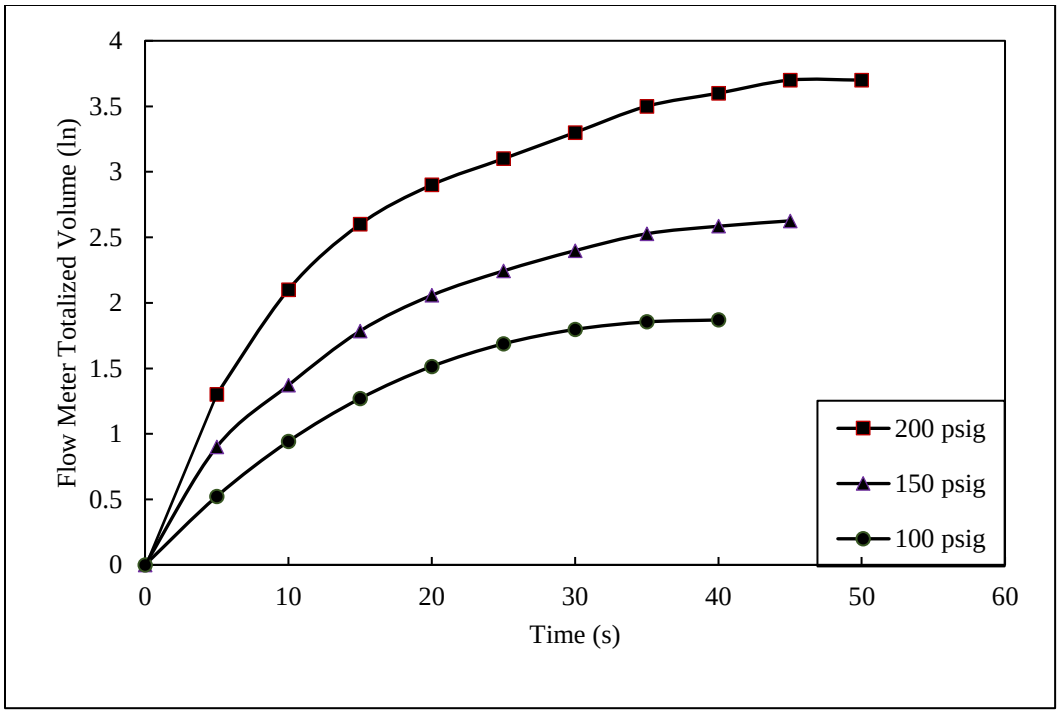

Figure 4.8. Totalized volume of gas which has evolved from the column over time for methane in diesel at 100, 150, and 200 psig.

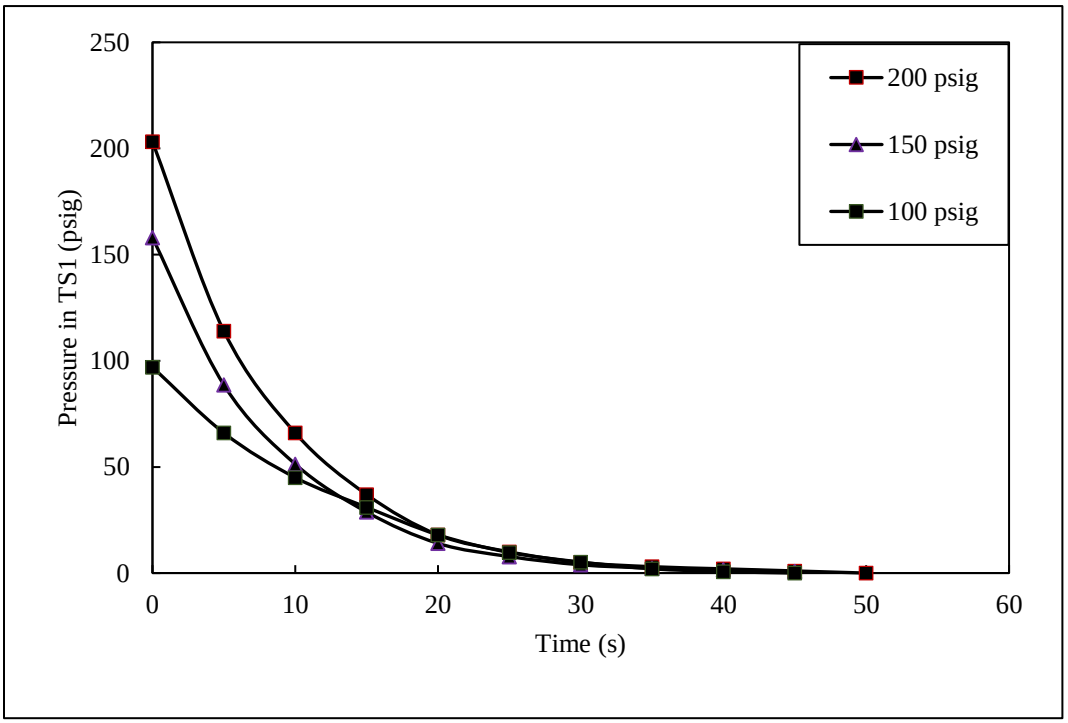

Figure 4.9. Pressure drop within test section 1 for methane in diesel at 100, 150, and 200 psig.

4.7.2. Methane in Internal Olefin

Figures 4.10, 4.11, and 4.12 each reflect the same tests conducted on diesel seen before. Each show the same general relationship and trend of raw data.

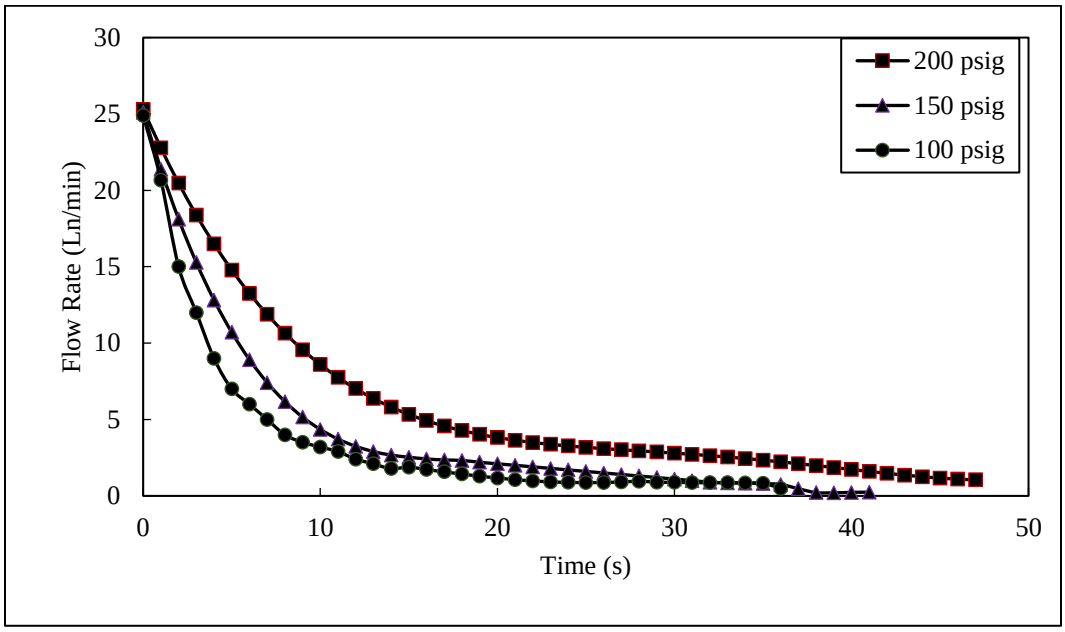

Figure 4.10. Measured flow rates of methane leaving the column through the mass flow meter for 100, 150, and 200 psig internal olefin tests.

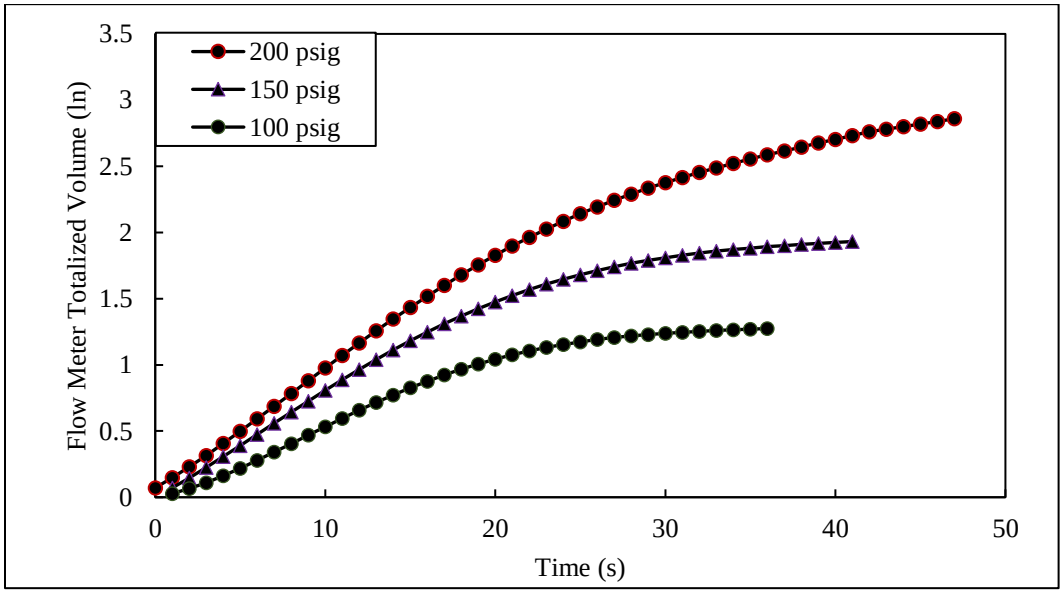

Figure 4.11. Totalized volume of methane that evolved from test section one for methane in internal olefin samples at 100, 150, and 200.

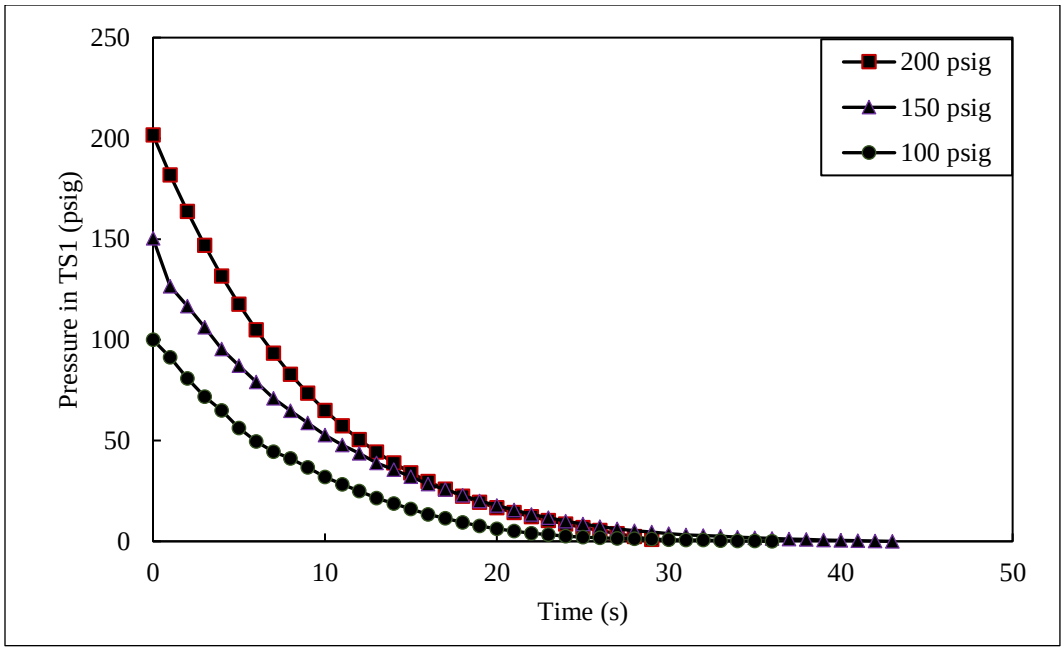

Figure 4.12. Pressure drop in test section 1 for methane in internal olefin samples at 100, 150, and 200 psig.

When comparing the diesel to internal olefin data sets, there are many more data points because we had shortened the timestep interval for each data point retrieved from the data acquisition unit when running the internal olefin results. These tests were completed after both the diesel and all emulsion results had been collected.

4.7.3. Methane in Emulsion Fluids

This section covers the emulsion fluids tested in this study. The oil/water ratios of nonaqueous fluids to water was previously listed in Table 4.2. The first round of experiments was conducted using diesel and water with increasing volumetric ratios of water. Each emulsion was tested to determine the concentration at saturation within each sample. The following two figures, Figures 4.13 and 4.14, illustrate the concentration at saturation for each of the three nonaqueous fluid/water ratios for each fluid.

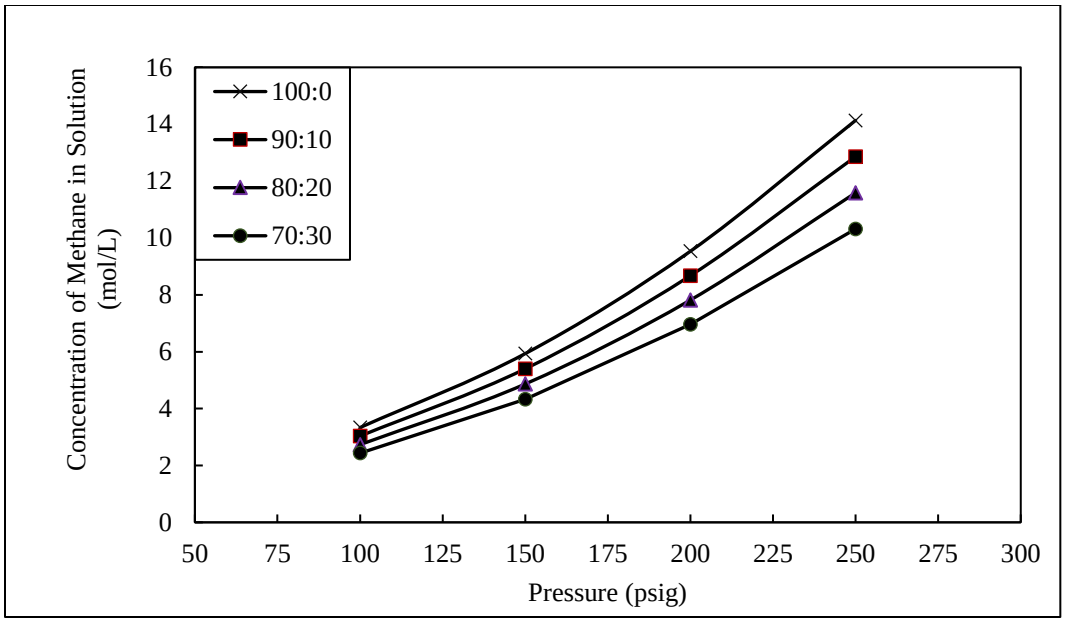

Figure 4.13. Concentrations at saturation for methane in diesel emulsion for pressures 100-250 psig with emulsion ratios 100/0, 90/10, 80/20, and 70/30.

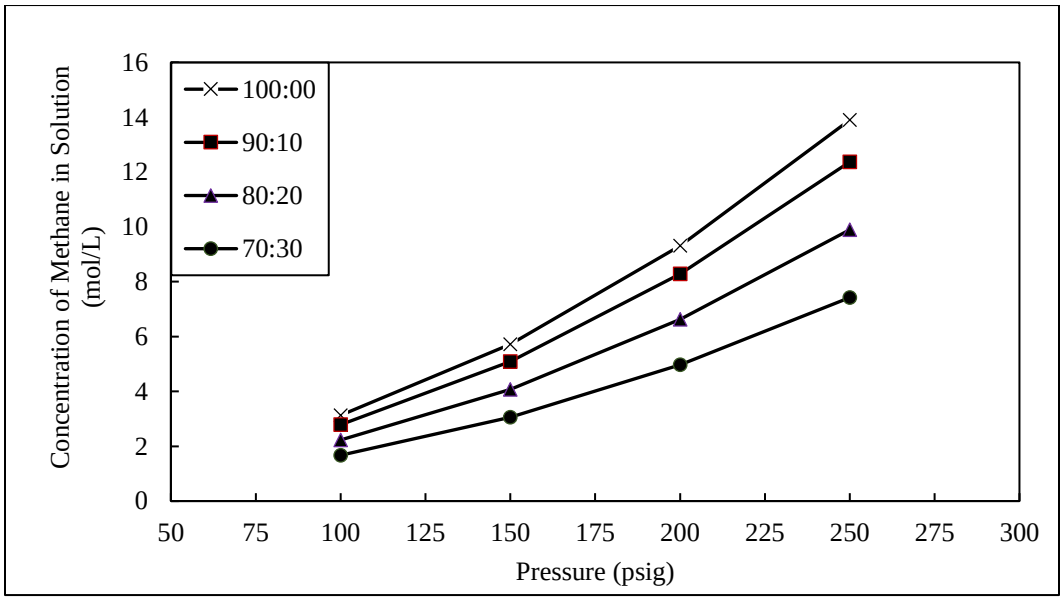

Figure 4.14. Concentrations at saturation for methane in internal olefin emulsions for pressures 100-250 psig with emulsion ratios 100/0, 90/10, 80/20, and 70/30.

4.7.3.1. Diesel Emulsions

The following results were obtained for the diesel/water emulsions which were developed using the low-pressure apparatus. In Figure 4.15, 4.16, and 4.17 below, the flow rate of methane

through the flow meter, the totalized volume of gas which evolved from solution and the pressure decrease, respectively. The results of both of these graphs were used in conjunction in determining the K_D mass transfer coefficient for each subsequent test. Only three starting saturation pressures, 100, 150, and 200 psig, were included in the following graphs for clarity.

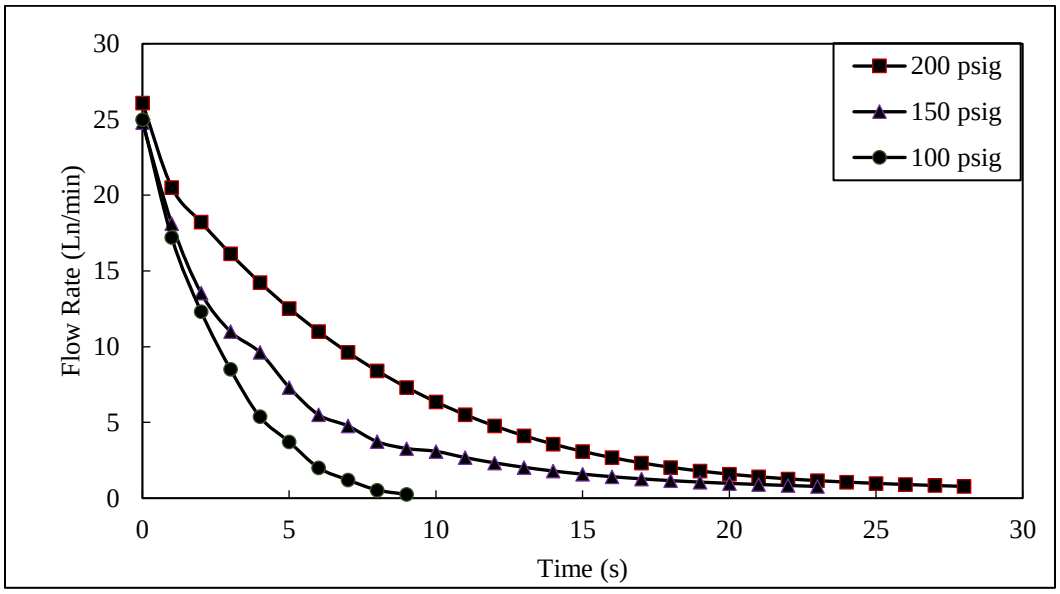

Figure 4.15. Measured flow rates of methane leaving the column through the mass flow meter for 100, 150, and 200 psig 90/10 diesel/water tests.

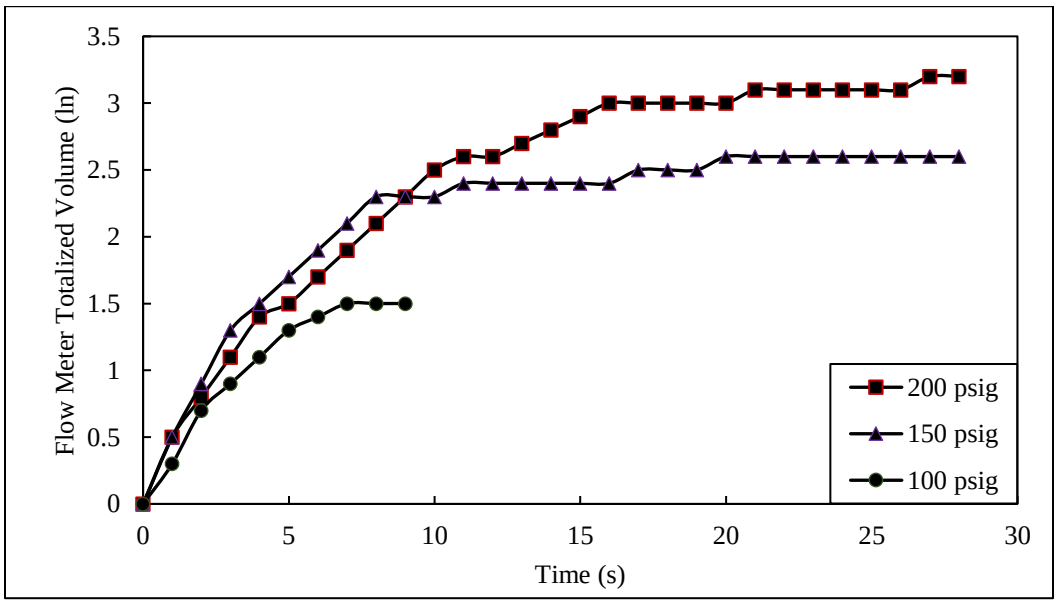

Figure 4.16. Flowmeter totalized volumes for the methane in diesel/water 90/10 emulsion results.

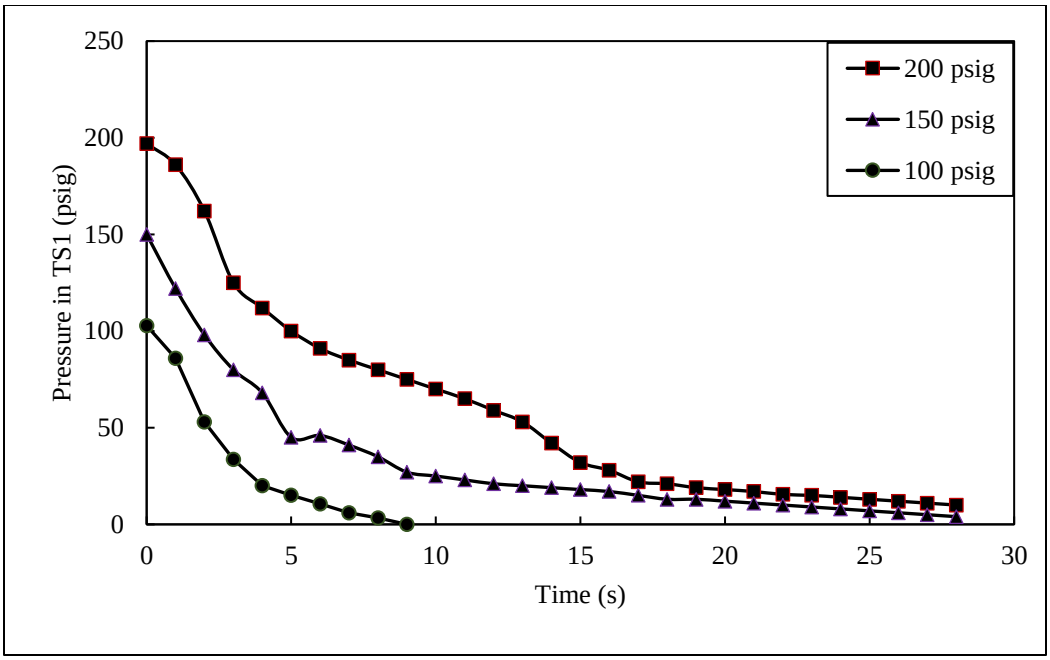

Figure 4.17. 90/10 Diesel emulsion data showing the change in pressure as the emulsion fluid degasses due to a decrease in pressure within the test section.

The tests conducted on the diesel/water emulsions were repeated multiple times testing pressures of 100, 125, 150, 175, and 200 psig at diesel/water ratios of 90/10, 80/20, and 70/30. The results of this part of the experiment show that increasing amounts of water in the emulsions produced fluids which more readily degassed themselves when the pressure above the fluid decreases rapidly.

4.7.3.2. Internal Olefin Emulsions

The internal olefin emulsion results in Figures 4.18, 4.19, and 4.20 were each very similar to the diesel emulsion results. It was observed during the internal olefin experiments, that there was significantly less methane dissolved into solution compared to the diesel fluids. We believe this is a product of the composition of the internal olefins and their solubility when compared to the composition of diesel and each chemical species solubility when dissolving methane into the fluid.

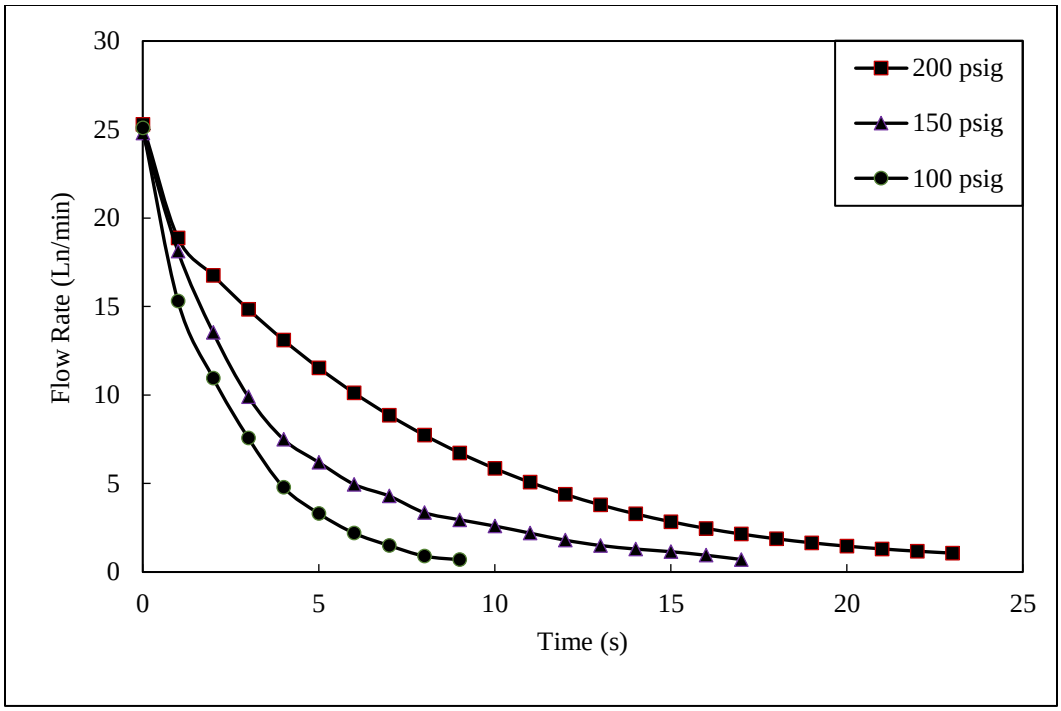

Figure 4.18. Measured flow rates of methane leaving the column through the mass flow meter for 100, 150, and 200 psig 90/10 internal olefin/water tests.

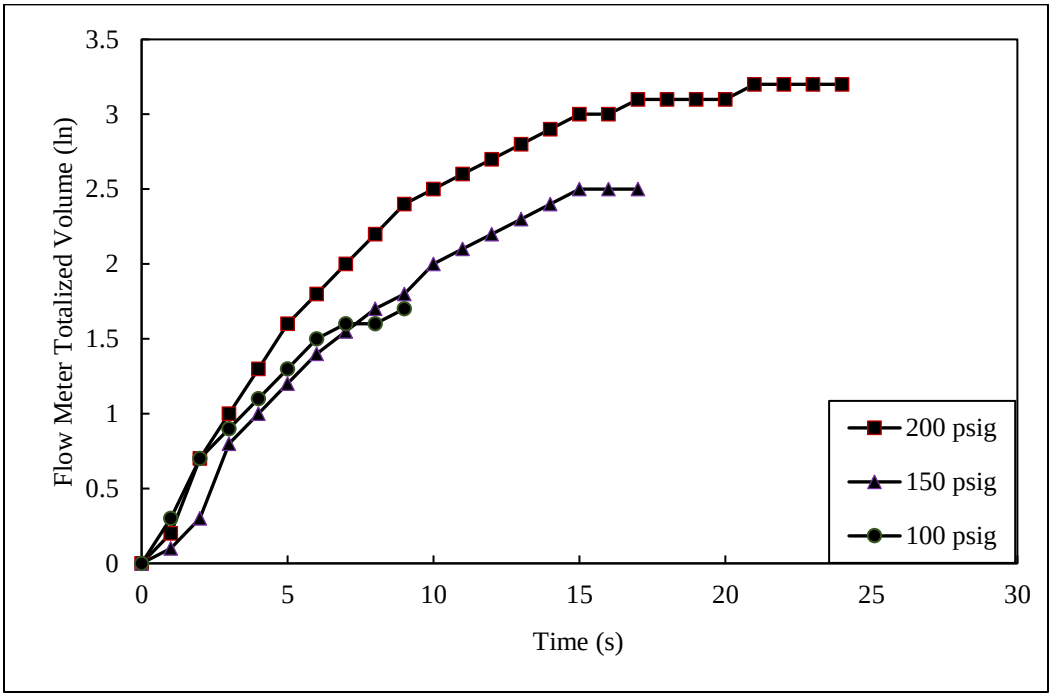

Figure 4.19. Flowmeter totalized volumes for the methane in internal olefin/water 90/10 emulsion results.

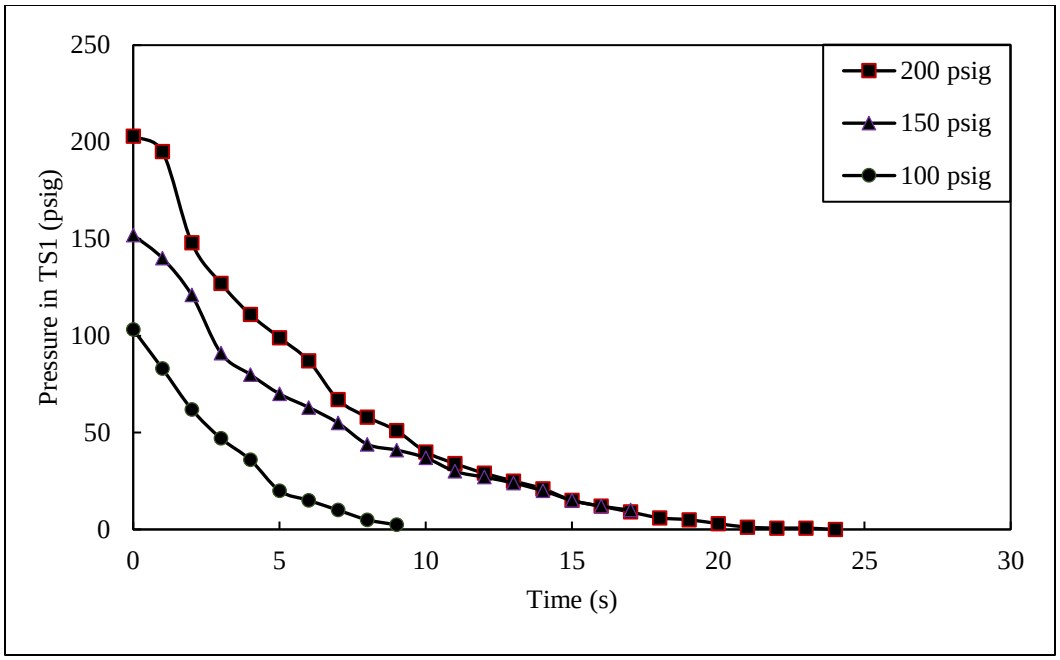

Figure 4.20. 90/10 Internal olefin emulsion data showing the change in pressure as the emulsion fluid degasses due to a decrease in pressure within the test section.

4.8. Summary of Experimental Results

In sub-sections 4.6 and 4.7, we show how each of the fluids performed during their respected desorption experiments. It was observed that the internal olefin fluids do not reach as high of a concentration of methane at saturation when compared to diesel. This can be attributed to the vast distribution of hundreds of compounds found in diesel and greater range of carbon chain lengths compared to the relative chemical homogeneity of the internal olefins. The data obtained from these results were utilized in further analysis to calculate mass transfer coefficients in Chapter 5.

CHAPTER 5. MODELING THE DESORPTION PHENOMENON

5.1. Modeling Desorption Kinetics

To select a model that will be used to analyze the experimental data we found in Chapter 4, we have two basic requirements of the model. 1) The model must be able to predict a mass transfer coefficient for desorption using the data that we have measured from our experimental apparatus. 2) It must also have the capability of determining a mass transfer coefficient as a function of pressure. The fundamental purpose of this study is to predict the behavior of dissolved gas as it evolves from a drilling fluid within a well where the depth of when the influx was taken and the rate at which the drilling fluid is circulating can both be used to determine the hydrostatic pressure above the fluid which will induce gas desorption. As previously described in Chapter 2, much of the literature that exists studying mass transfer for the process of desorption involves an active method of gas desorption which involves the use of stripping gasses to remove the dissolved gas from solution.[25]

Table 5.1. Selected desorption models with correlations for the corresponding mass transfer coefficient.

Authors	System	Water	Correlation for k_La
Sherwood et al.[50]	Packed column	Tap water	$k_La = b_1L^{0.88}$
Sherwood and Holloway[51]	Packed column	Tap water	$k_La = b_2\left(\frac{L}{\mu}\right)^{.75}\left(\frac{D_{CO_2}\mu}{\rho}\right)^{.5}$
Rixon[52]	Packed column	Tap water	$k_La = b_3L$
Hikita and Konishi[55]	Stirred vessel	DI water/ electrolyte solutions	$k_La = b_4\left(\frac{d_L^2n_{L_\rho}}{\mu}\right)^{.5}\sigma_{super}^{.78}$ $k_La = b_5\left(\frac{d_L^2n_{L_\rho}}{\mu}\right)^{.93}\sigma_{super}^{2.5}$
Tokumura et al.[95]	Bubble column	DI water and saltwater	$k_La = \left(\frac{D_{CO_2}}{D_{O_2}}\right)^{.5}(0.19u_G^{.44})$
Barrut et al.[96]	Vacuum air lift or cocurrent column	Fresh and saltwater	$k_La = (0.9 - 62d_b)Q_G$

Although many of these studies relied on this method of inducing a dissolved gas to evolve, they should be investigated to determine if they fulfill the first requirement and can be modified to incorporate pressure either directly or indirectly by considering a change in concentration or gas loading. Utilizing the review paper by Elhajj et al. 2013, Table 5.1 was generated to display multiple models that have been developed to measure the mass transfer coefficient for desorption.

Each of these six desorption studies utilizes the mass transfer coefficient k_La. The first two models from Table 5.1, Sherwood et al. (1937) and Sherwood and Holloway (1940) simplify the mass transfer coefficient to be a function of the mass flow rate with a variable constant to simplify calculations of k_La. Sherwood remarks in the first investigation that he was not able to relate the mass transfer coefficient to any specific variable to indicate a strong relationship that would affect the coefficient beyond the mass flow rate (L). In the second investigation which included Holloway, the two identified a relationship between the mass transfer coefficient and viscosity of the fluid and the diffusivity of the system but did not investigate other variables in the system. Using a similar system, Rixon could only confirm the results of the first study listed by Sherwood and reported in his study, where he investigated both processes of absorption and desorption, that desorption had significantly higher k_La values than what was measured in absorption. The general models proposed in these three studies rely on measuring the mass flow rate. We can easily measure this within the capabilities of our experimental apparatus, however, this model does not give us a way to predict a mass transfer coefficient that is based on a specific parameter such as pressure. The coefficients b in each of the correlations are based on the specific operating conditions in each study and cannot be simplified. The second study by Sherwood relates the coefficient to the viscosity and diffusivity but does not account for a means of considering changing pressure conditions which we require with our application.

The study performed by Hikita and Konishi found the volumetric liquid-phase mass transfer coefficients for the evolving bubbles by calculating the measured desorption rates and correlated each as functions of the relative supersaturation of the solution and the liquid-phase Reynolds number. Tokumura et al. performed an investigation into the neutralization of acidified seawater which had absorbed CO_2. His investigation incorporated a chemical reaction series included in his study but the model used to determine the mass transfer coefficients was based on the diffusivity of O_2 and SO_2/CO_2 in solution. Results of experimental trials show that the mass transfer coefficient k_La changed based on the gas holdup in solution but were strongly influenced by the chemical reaction series of CO_2 in water.

In 2013, Tunnat et al. performed a study detailing another model that can be used for modeling of desorption using CO_2 and water with aqueous amine solutions. The paper described the following equation that relates the flux of CO_2 to the Henrys constant and two mass transfer terms k_g and k_L using two-film theory.[92]

$$j_{CO_2} = \frac{1}{\frac{1}{k_g}+\frac{R*T}{H_{CO_2}}*\frac{1}{k_L}} * \left(\frac{p_{CO_2}}{k_{HCO_2}} - c_b\right) \quad [5.10]$$

Where c_b is the concentration of component b. This model for measuring the mass transfer of CO_2 from aqueous solutions was shown to be quite accurate according to Tunnat when comparing the experimental results to published literature of the two-film model for CO_2 desorption. Tunnat identifies that this model did not work well with fluids containing gas loadings above 0.5, therefore this model does not align itself well with the scope of our own experiments when we max out the gas loading in our solutions by reaching gas saturation at a specific starting pressure.

5.2. Linga's Kinetic Model of Gas Desorption

Another model that was developed by Linga et al. in 2003, uses the gas loading within a fluid to determine the mass transfer coefficient.[69] The initial study was done investigating how H_2S and natural gas evolves from oil. His investigation studied the desorption process by measuring when the gas loading exceeds the maximum capacity of the fluid, due to pressure reduction, and measuring both the volume and the rate at which the gas will evolve from the liquid phase and return to the gas phase. The model proposed by Linga et al. also allows for the prediction of the mass transfer coefficient based on this change in gas loading. We can easily calculate the gas loading of methane in our nonaqueous-based drilling fluids using our experimentally obtained data. One drawback of this model is that the mass transfer coefficient is considered to be constant during the desorption process. In previous literature, it was noted that this is not generally the case.[25] However, Linga gives us this simplified model that can later be expanded upon to account for the changing mass transfer coefficient. The model proposed by Linga fulfills both of the general requirements that we ask for in a model to analyze our experimental data. The simplifications inherent to Linga's desorption model allow us to determine the mass transfer coefficient more easily and predict the mass transfer coefficient based on experimentally correlated changes in gas loading determined through changes in pressure. Linga's model has been used in other studies involving gas desorption that have shown good results and conclusions even with the assumptions set forth in it.[90] The governing equations for Linga's model are as follows in Equations 5.1 and 5.2.

$$\frac{dl}{dt} = K_D(l_{max} - l) \qquad l \geq l_{max} \tag{5.1}$$

$$l = l_{max} + (l_0 - l_{max})e^{-K_D t} \tag{5.2}$$

Here K_D is the rate of desorption parameter described by a closure law depending on gas and liquid types and flow characteristics. l is the current gas loading in the liquid phase, l_{max} is the gas loading of the fluid at saturation for a specific pressure. l_0 is the initial gas loading in the liquid phase when saturated at a specific starting pressure. This study will focus on how the K_D will be affected by the starting conditions of determined using experimentally obtained desorption data which was described in Chapter 4. By graphing $\ln\left(\frac{l-l_{max}}{l_0-l_{max}}\right)$ vs t, we can determine the value of K_D from the absolute value of the slope of the graph.

5.3. The Drift Flux Model

The simplicity of the drift-flux model is beneficial in many petroleum engineering applications. The governing equations are two mass conservation equations and one momentum conservation equation. The system of differential equations in the drift-flux model can be written in a conservative vector form generally expressed as[91]:

$$\frac{\partial w}{\partial t} + \frac{\partial F(w)}{\partial x} = Q(w) \qquad [5.3]$$

Where:

$$w = \begin{bmatrix} \alpha_l \rho_l \\ \alpha_g \rho_g \\ \alpha_l \rho_l v_l + \alpha_g \rho_g v_g \end{bmatrix} \qquad [5.4]$$

$$F(w) = \begin{bmatrix} \alpha_l \rho_l v_l \\ \alpha_g \rho_g v_g \\ \alpha_l \rho_l v_l^2 + \alpha_g \rho_g v_g^2 + p \end{bmatrix} \qquad [5.5]$$

$$Q(w) = \begin{bmatrix} \Gamma_g \\ -\Gamma_g \\ -q \end{bmatrix} \qquad [5.6]$$

The system can then be expressed in the form:

$$\partial_t \begin{bmatrix} w_1 \\ w_2 \\ w_3 \end{bmatrix} + \partial_x \begin{bmatrix} v_l w_1 \\ v_g w_2 \\ v_l^2 w_1 + v_g^2 w_2 + p(w_1, w_2) \end{bmatrix} = \begin{bmatrix} \Gamma_g \\ -\Gamma_g \\ -q \end{bmatrix} \quad [5.7]$$

Linga et al. (2003)[69] formulated his kinetic sub-model for the rate of change of H_2S concentration in a solvent in the process of natural gas sweetening. The rate of degassing is a function of the amount of dissolved gas only. The rate of change of the gas loading capacity in mud (L) is given as:

$$\frac{\partial R_s}{\partial t} = K_d(l_{max} - l), \quad l \geq l_{max} \quad [5.8]$$

Thus, we will have:

$$\Gamma_g = \alpha_l \rho_l \frac{\partial l}{\partial t} \quad [5.9]$$

The value of l is obtained at every time step using Equation 5.8. l_{max} is a function of temperature and pressure and is thus initially obtained during a step using the available pressure and temperature for that step. The values used for l_{max} were obtained from saturation curves we developed and are shown in Chapter 4.6.

5.4. Application of Linga's Model to Experimental Results

As described previously in Section 5.1 using Equation 5.2 the mass transfer coefficient K_D was obtained through experimental results and plotting the $\ln\left(\frac{l-l_{max}}{l_0-l_{max}}\right)$ vs t to obtain a slope which equaled the $-K_D$. This mass transfer coefficient was compared between tests to develop a trend which could be equated to a mathematical equation to predict the mass transfer at any pressure for any fluid as long as the fluid has been previously tested to determine a solubility factor for methane.

As described in Chapter 3, it was very important to maintain as high of an initial exiting flow rate of the methane through the flow meter as possible. When the flow rate of gas is high, it

replicates a more true-to-world scenario where the desorption is considered instantaneous and not restricted by a low exiting flow rate. When the flow rate was restricted, the K_D values were suppressed significantly. This phenomenon can be seen in Figure 5.1 below.

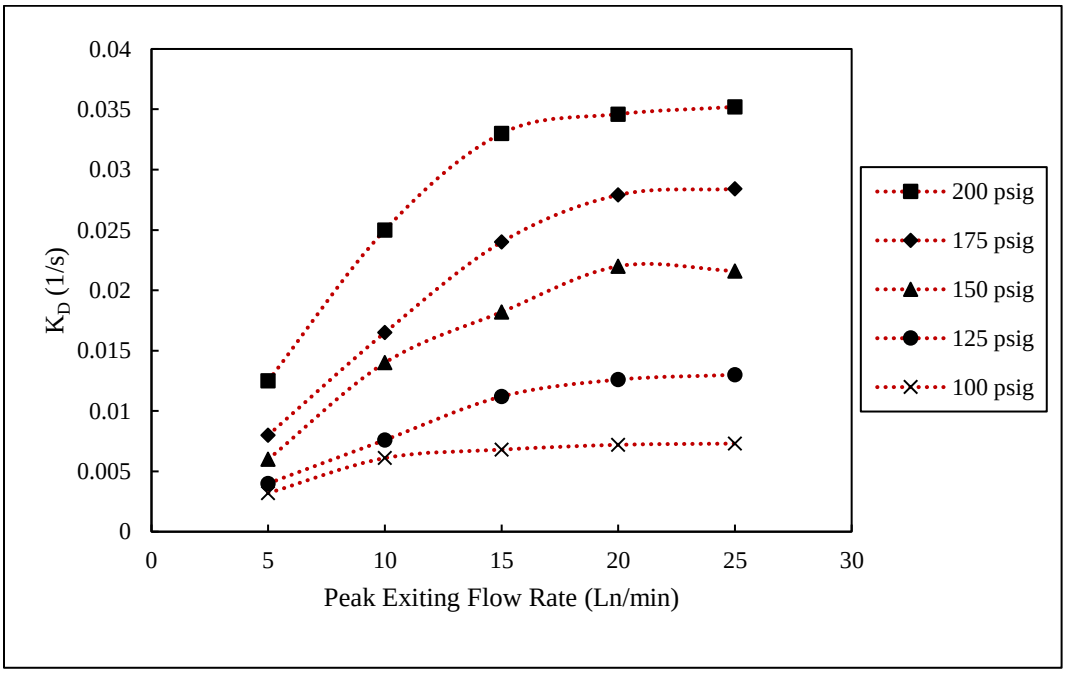

Figure 5.1. Mass transfer desorption coefficient K_D at changing peak exiting flow rates of methane through the flow meter from 5-25 ln/min at pressures of 100-200 psig.

By increasing the peak exiting flow rate from TS2 in the experiment, we can maximize the value of K_D which is obtained to better develop a relationship between this mass transfer term and the pressure at which the fluid was saturated.

5.4.1. Range of Selected Data Points

In Chapter 2 of this thesis, we noted from the research conducted by Weiland and Thuy (1977), that during the process of desorption, there are two identifiable mechanisms by which a gas will evolve from a liquid where the mechanism shifts from what was defined as bubble desorption to quiescent desorption.[26] During the analysis of our data, with regards to Weiland's model and fitting to Linga's model, we can identify two regions within each data set that represents the shift from

bubble desorption to quiescent desorption. Figure 5.2 represents our experimental data following Weiland's model outlined in Chapter 2.5.1, this results in a similar graph to Figure 2.3.

As in Weiland's research, the inflection point indicates a change in the mechanism governing gas desorption. The time period where Figure 5.2 shows bubble desorption, above a pressure reduction ratio of approximately 1.2, is reflected as the same time period during the experimental run in Figure 5.3 from the beginning of the test until a rapid shift in the slope of $\ln\left(\frac{l-l_{max}}{l_0-l_{max}}\right)$ vs t. In Figure 5.4, the data set used to develop Figure 5.3 was reduced to the time period of 0-9 seconds. Linear regression of this reduced dataset resulted in a line with the slope -0.03155. As per the model developed by Linga et al., the absolute value of this slope is the resulting mass transfer coefficient. Therefore, during each of the following subsections within this chapter, the data sets have been reduced with respect to time to the period where bubble desorption is dominant in order to provide results that are not affected by quiescent desorption.

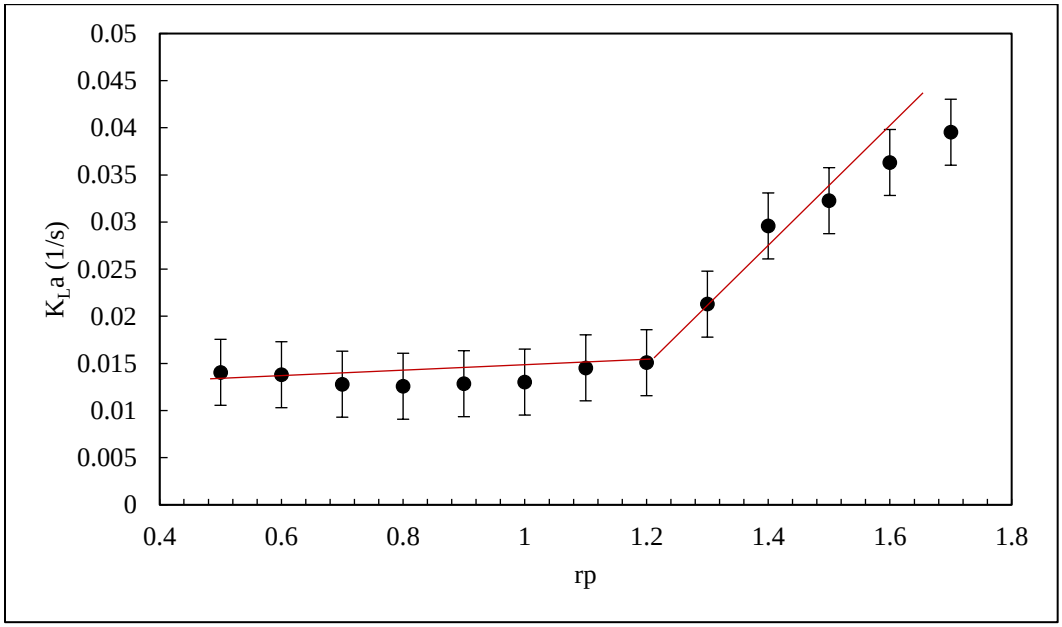

Figure 5.2. Weiland's model of desorption applied to the 80/20 diesel emulsion results showing two distinct periods of calculated mass transfer coefficients. Bubble desorption shifts to quiescent desorption at a pressure reduction ratio of approximately 1.2. Best fit lines for each region have been drawn showing the shift from bubble to quiescent desorption.

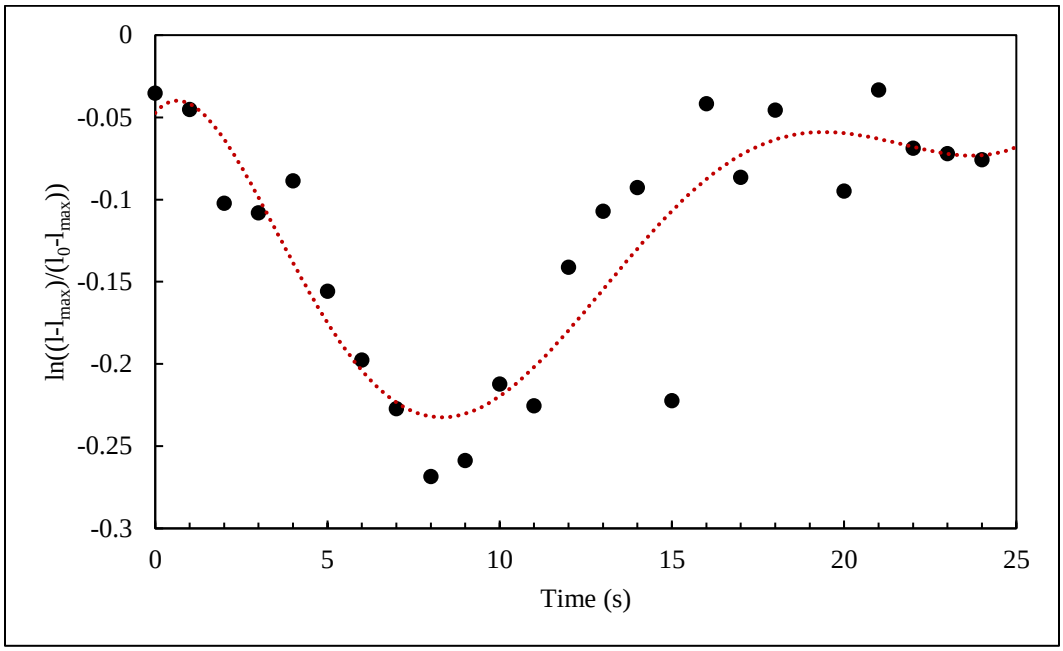

Figure 5.3. Graph showing the relationship of ln $\left(\frac{l-l_{max}}{l_0-l_{max}}\right)$ vs t for the 80/20 diesel emulsion result at 200 psig. From 1-8 seconds, the mechanism of bubble desorption is dominant before the sharp change in values at 9 seconds where quiescent desorption becomes dominant.

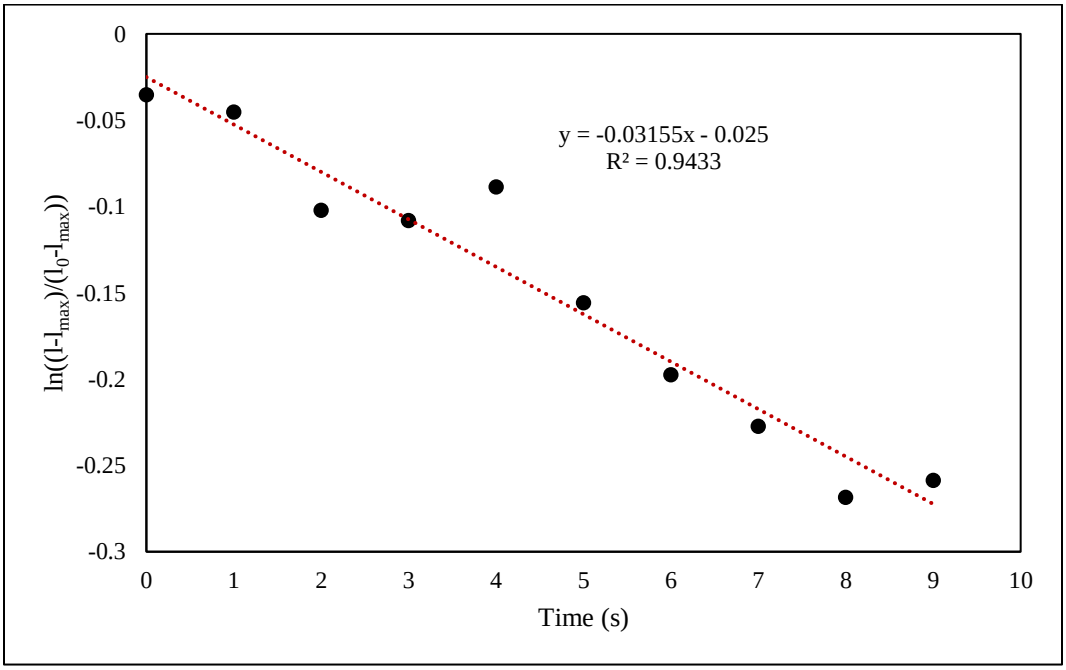

Figure 5.4. Reduced data set showing the ln $\left(\frac{l-l_{max}}{l_0-l_{max}}\right)$ vs t relationship for the 80/20 diesel emulsion result at 200 psig diesel and methane experiment. The mass transfer coefficient is indicated by the absolute value of the slope, 0.03155.

5.4.2. Methane in Diesel

The first data set analyzed using Linga's model was methane in diesel. Using the experimentally determined data which was used to generate Figures 4.6-4.15, we were able to develop the following relationship of K_D for each pressure tested. The relationship between the starting saturation pressure and K_D is indicated below in Figure 5.5 showing a relatively linear increase as pressure increases. We generated a second-degree polynomial equation fit to these results fitting the y-intercept to equal zero so that the K_D values extrapolated would be consistent with expected results. It is not reasonable to maintain a linear relationship among this data range because it would not be accurate to represent any pressure values above atmospheric as having a negative mass transfer coefficient.

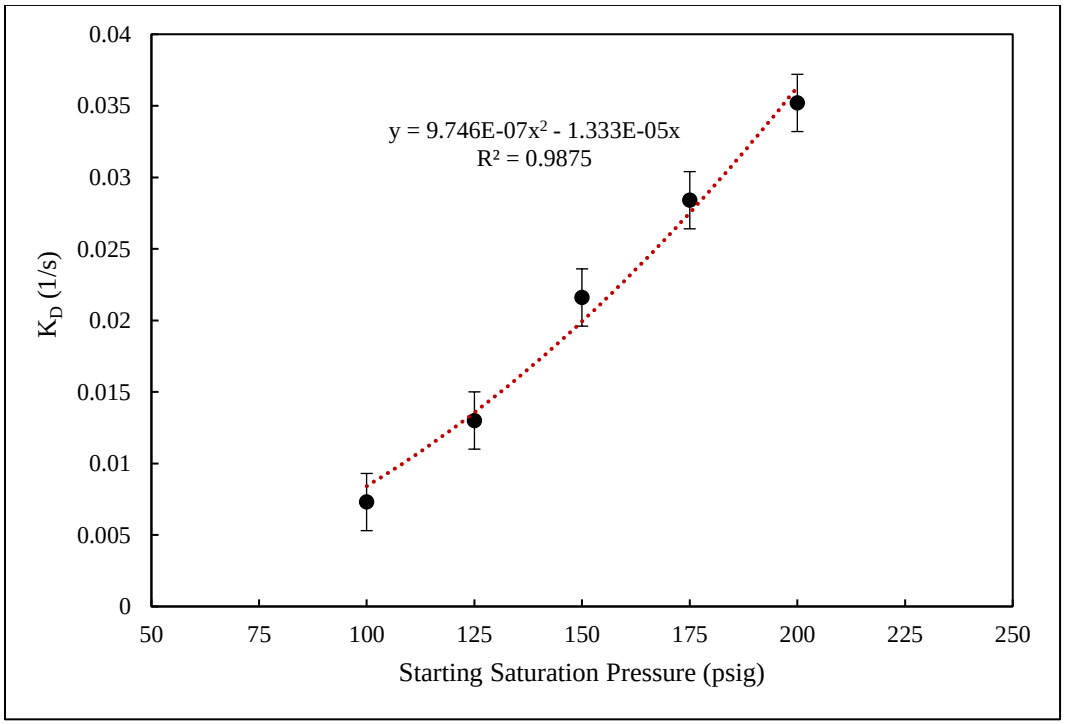

Figure 5.5. Calculated K_D values for methane in diesel for pressures 100 to 200 psig showing a sharp increase in K_D as the starting saturation pressure increases.

5.4.3. Methane in Internal Olefins

As shown in section 5.4.2, the same process used to calculate the mass transfer desorption coefficient K_D was used for the internal olefin data set The resulting values of K_D vs starting saturating pressure shown below in Figure 5.6 show a very similar relationship to the diesel results in Figure 5.5. The relationship is slightly greater compared to the diesel results. This was expected due to the amount of methane that was able to be absorbed in each fluid during the saturation phase and the gas/fluid solubility.

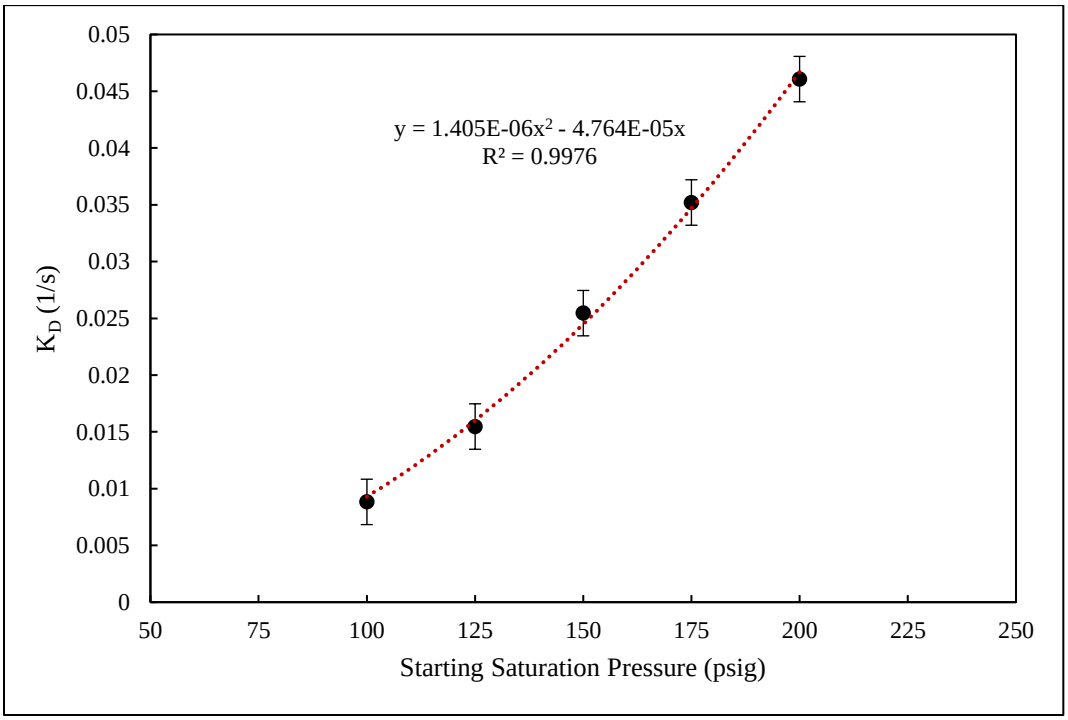

Figure 5.6. Calculated K_D values for methane in internal olefins for pressures between 100-200 psig, showing a sharp increase in K_D as the starting saturation pressure increases.

5.4.4. Methane in Emulsion Fluids

In this section, we will compare the methane in diesel emulsion results to the methane in internal olefin results when implementing Linga's model of mass transfer.

5.4.4.1. Diesel Emulsion Fluids

In Figure 5.7, shown below, the relationship between the K_D mass transfer coefficient for the methane in diesel emulsions can be seen. There was a very clear relationship between the mass transfer coefficients and the emulsion ratio with increasing K_D and decreasing nonaqueous fluid concentration within the fluid. This agrees well with our hypothesis that due to the decreased solubility of methane in the internal olefins, that we should see faster rates of desorption and therefore higher mass transfer coefficients because any addition of water will further reduce the solubility of the resulting fluid.

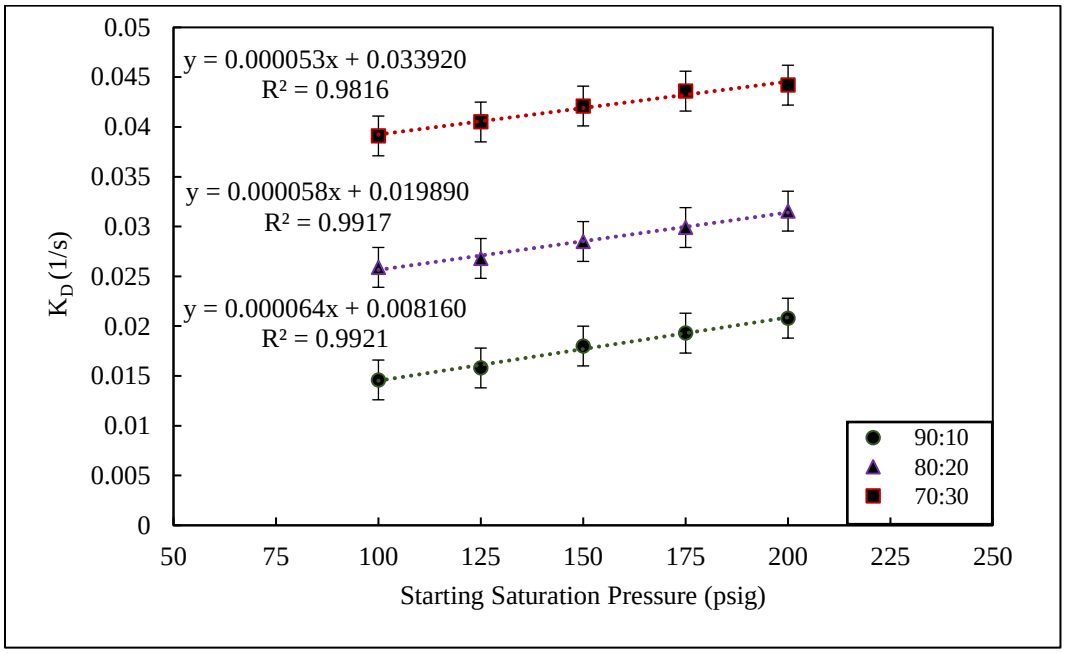

Figure 5.7. Methane in diesel emulsion results comparing the calculated K_D values to the starting saturation pressure for emulsion ratios 90/10, 80/20, and 70/30.

5.4.4.2. Internal Olefin Emulsion Fluids

The results for methane in the internal olefin emulsions were observed to align themselves well with the results from the methane in diesel emulsions. The same trends that appeared with the previous tests involving pure diesel or pure internal olefins were observed showing that the mass

transfer rates for the internal olefins were higher than those with diesel. In Figure 5.8, the trend between K_D and starting saturation pressure can be seen and the similarity to the methane in internal olefin results. It must be noted for each of these emulsion tests, that the change in the mass transfer coefficients for each starting saturation pressure was found to be significantly less than the change observed in the coefficients for each of the pure base fluids. This could be due to the change in solubility, or an additional property or interaction between the gas and liquid that develops within emulsion fluids that was not known before testing. Further analysis is required to characterize the emulsion fluids to help identify the cause of this observation.

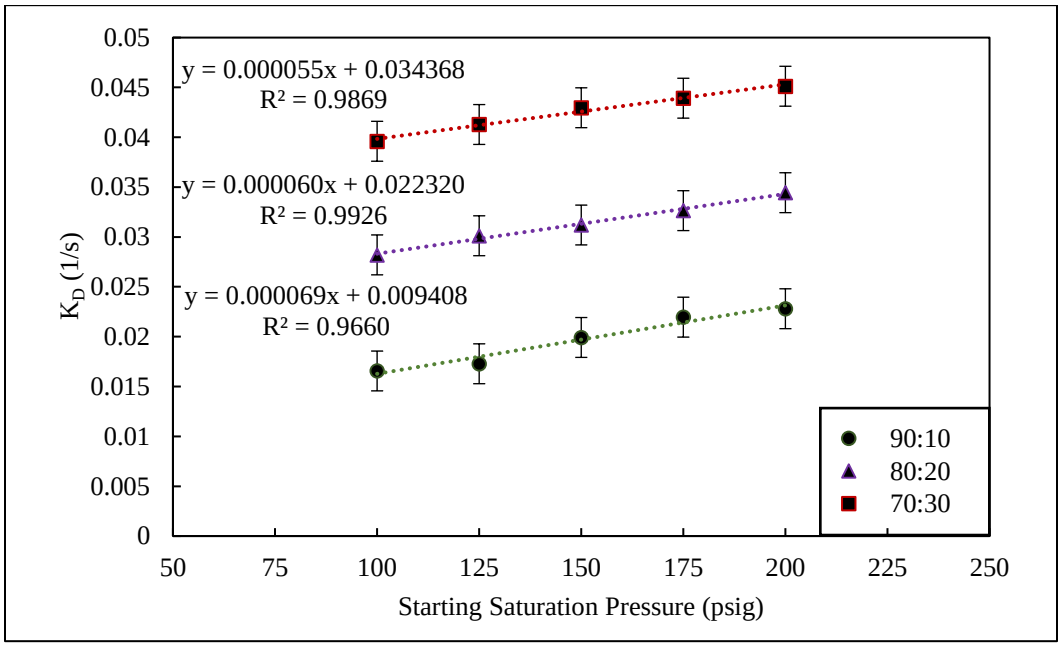

Figure 5.8. Methane in internal olefin emulsion results comparing the calculated K_D values to the starting saturation pressure for emulsion ratios of 90/10, 80/20, and 70/30.

In Figures 5.9 and 5.10, a direct comparison between the mass transfer coefficients are displayed for the diesel fluids and the internal olefin fluids. This trend was expected based on the previous results of the pure internal olefin having noticeably higher mass transfer coefficients compared to the pure diesel tests in the previous subsection 5.3.1 and 5.3.2. We believe this is a result due to the lower solubility of methane in internal olefins compared to diesel fuels and

therefore leads to a greater mass transfer coefficient of desorption. There is an unusual discrepancy between the pure nonaqueous fluids and the emulsions. Below 125 psig starting saturation pressure, decreasing the oil/water ratio of the fluid produces a consistent increase in the mass transfer coefficients. At 150 psig, the calculated mass transfer coefficients for the pure fluids are higher than those seen in the 90/10 emulsion fluids. This continues for each of the progressively decreasing oil/water ratios and increasing pressures. It appears as if there is an additional property within the emulsion fluids that is causing this discrepancy as we previously discussed when analyzing the emulsion results.

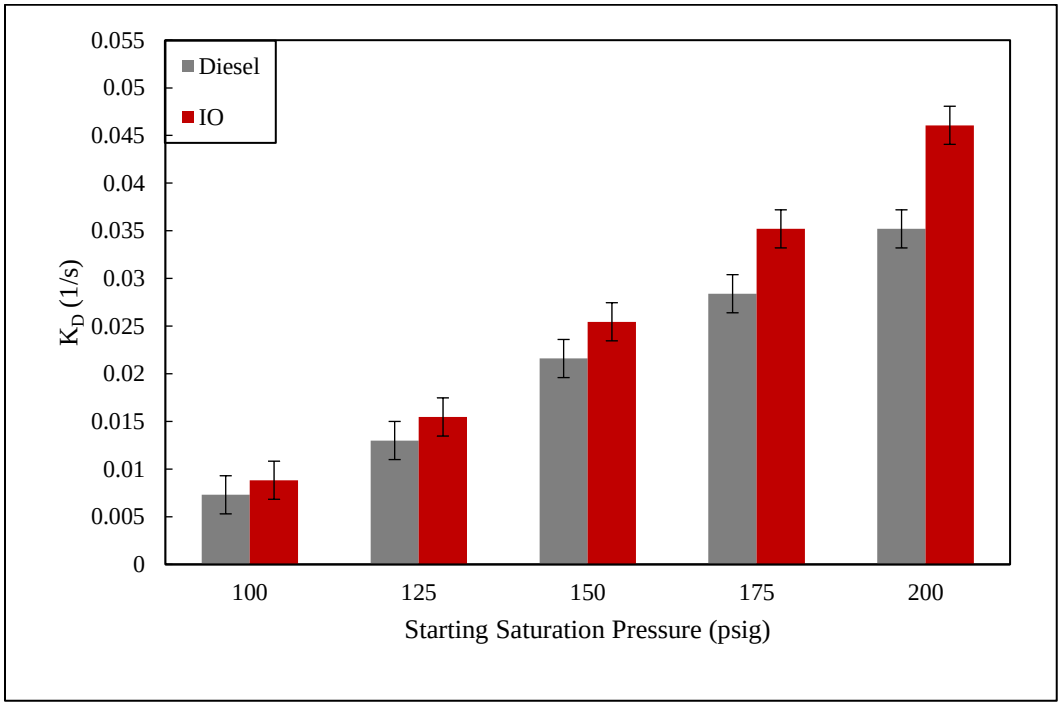

Figure 5.9. Comparison of K_D values for diesel and internal olefin 100/0 samples from 100 to 200 psig.

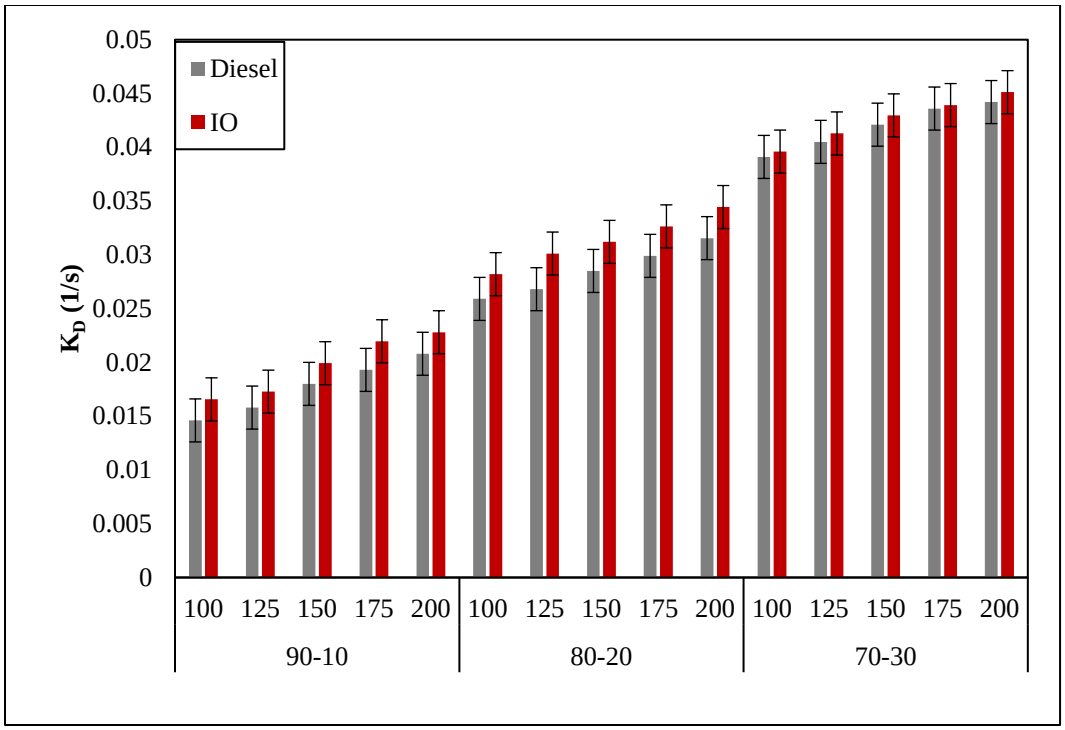

Figure 5.10. Comparison of K_D values for diesel and internal olefin emulsions at each pressure and emulsion ratio.

5.5. Summary of Mass Transfer Coefficients

Table 5.1, below, shows the quantified difference between the K_D values found for samples of diesel and internal olefins. The internal olefin base fluid was found to consistently have a higher mass transfer coefficient than diesel with an average percent increase of 22.4% when investigating the effect of increasing starting saturation pressure in this study. The same analysis for changes between each emulsion fluid was also determined and displayed below in Table 5.2.

Table 5.2. Quantified difference table showing the change in average K_D values between diesel and internal olefin base fluid samples at starting saturation pressures from 100-200 psig.

Pressure (psig)	Diesel K_D (1/s)	IO K_D (1/s)	Change	% Change
100	0.00730	0.00883	+0.00153	20.96%
125	0.01300	0.01547	+0.00247	19.00%
150	0.02160	0.02540	+0.00380	17.59%
175	0.02840	0.03520	+0.00680	23.94%
200	0.03520	0.04600	+0.01080	30.68%

Table 5.3. Quantified difference table showing the change in average K_D values between diesel and internal olefin emulsion samples at starting saturation pressures from 100-200 psig and O/W ratios of 90/10, 80/20, and 70/30.

O/W Ratio	Pressure (psig)	Diesel K_D (1/s)	IO K_D (1/s)	Change	% Change
90/10	100	0.01460	0.01656	0.00196	13.42%
	125	0.01580	0.01728	0.00148	9.37%
	150	0.01800	0.01992	0.00192	10.67%
	175	0.01930	0.02196	0.00266	13.78%
	200	0.02080	0.02280	0.00200	9.62%
80/20	100	0.02590	0.02820	0.00230	8.88%
	125	0.02680	0.03012	0.00332	12.39%
	150	0.02850	0.03120	0.00270	9.47%
	175	0.02990	0.03264	0.00274	9.16%
	200	0.03155	0.03444	0.00289	9.16%
70/30	100	0.03910	0.03960	0.00050	1.28%
	125	0.04050	0.04128	0.00078	1.93%
	150	0.04210	0.04296	0.00086	2.04%
	175	0.04360	0.04392	0.00032	0.73%
	200	0.04420	0.04512	0.00092	2.08%

In Table 5.2, the percent change between the mass transfer coefficients was observed to be lower than that of the changes in the base fluid results. There is not a significant decrease in this percent change from decreasing the oil/water ratio from 90/10 to 80/20 showing an average change from 11.37% down to 9.81% whereas the averages decrease for the 70/30 O/W ratios to 1.61% between the diesel and internal olefin emulsions.

5.6. Statistical Analysis of Modeling Results

To analyze the mass transfer coefficients which were determined following Linga's model in this chapter, statistical analysis was required to determine if any of the variables which were tested in this study proved significant. The type of statistical analysis which was performed in this study was regression analysis. Regression analysis has been widely used as a powerful statistical method that allows us to examine the relationship between multiple variables investigated within a study.[97] We performed the analysis on each of the properties which were tested during each experimental

trial, starting saturation pressure and oil/water ratio for the emulsion fluids. With the number of variables tested and the resulting data set of mass transfer coefficients for each, regression analysis was the ideal statistical means of determining the influence of each. Statistical analysis of the results in this study was performed using SAS University Edition statistical software. Expanded tables of all regression analyses can be found in Appendix C.

5.6.1. Starting Saturation Pressure

The starting saturation pressure was observed in the previous subsection to have a significant impact on the resulting K_D value of each test. As the starting saturation pressure increases, the K_D value will also increase. To determine the influence of the starting saturation pressure on the mass transfer coefficients of each experiment, regression was conducted and the results are indicated below in Table 5.3. The 100/0 oil/water ratio results show a negative intercept value when fit to a linear regression model. It is not reasonable to assume that there could be a negative mass transfer coefficient value, therefore when fitting to a quadratic linear regression model and setting the intercept at 0, a stronger relationship was determined and is indicated in Figures 5.5 and 5.6.

Table 5.4. Regression results indicating the influence of the starting saturation pressure on the mass transfer coefficients.

Diesel			
O/W Ratio	Intercept	X-Variable	P-Value
100/0	-0.02162	2.85E-05	0.00054
90/10	0.00816	6.36E-05	0.00051
80/20	0.01989	5.76E-05	2.84E-05
70/30	0.03392	5.32E-05	1.53E-05
IO			
O/W Ratio	Intercept	X-Variable	P-Value
100/0	-0.03026	3.76E-05	0.00147
90/10	0.00941	6.86E-05	0.00378
80/20	0.02232	6.00E-05	1.90E-05
70/30	0.03437	5.47E-05	9.54E-06

5.6.2. O/W Ratio

The results of the regression analysis conducted to determine the observed relationship between the oil/water ratio for each type of fluids is listed below in Table 5.5. The resulting P-values for each test show a progressively increasing P-value for each pressure tested. At 150 psig, the results of the analysis may be considered inconclusive because the P-value is around 0.05. For analysis above 150 psig, the regression results indicate no relationship between the oil/water ratio and the mass transfer coefficient for each given pressure tested.

Table 5.5. Regression analysis probability values of the oil/water ratio having an influence on the mass transfer coefficient found each tested pressure.

P-Values		
Pressure (psig)	Diesel	IO
100	0.0051	0.0024
125	0.0207	0.0202
150	0.0672	0.0799
175	0.1382	0.2149
200	0.2396	0.4713

It was observed in the previous subsection, illustrated in Figures 5.7 and 5.8, that the mass transfer coefficients do have a very good linear relationship with decreasing oil/water ratio when tested at each given pressure. This inconsistency is due to the results of the 100/0 base fluid desorption tests. At pressures above 150 psig, the mass transfer coefficients for each of the base fluids increases beyond the results of each of the emulsion fluid results. We believe that there is a physical change in the resulting fluids when an emulsion is developed that is not yet understood. Regression analysis, when removing the base fluid results, indicates a much stronger relationship between the oil/water ratio and the mass transfer coefficients for each tested pressure. Table 5.6 indicates the new regression results that do not consider the 100/0 base fluid tests.

Table 5.6. Regression analysis probability values of the oil/water ratio having an influence on the mass transfer coefficient found each tested pressure without including 100/0 O/W ratio results.

P-Values		
Pressure (psig)	Diesel	IO
100	0.0225	0.0029
125	0.0315	0.0197
150	0.0363	0.0057
175	0.0357	0.0073
200	0.0223	0.0114

5.7. Summary of Modeling

Using Linga's model, we were able to successfully develop a relationship between the fluids used in this study under these conditions and the mass transfer coefficient K_D. There are quantifiable differences that were discovered that affect the mass transfer coefficient when the starting saturation pressure and fluid type are changed. There was an unusual relationship found with the emulsion fluids when comparing the individual base fluids to their respected emulsion counterparts, we predict that this may be due to additional unforeseen variables affecting the fluid properties. A change in the intermolecular forces after emulsifying the oils with water may be the cause of this unusual discrepancy. We tested pure base fluids that had been subjected to the emulsification procedures but those results did not show any change in the resulting mass transfer coefficients that were observed when emulsifying them with water.

Statistical analysis was performed on the resulting data sets of each calculated mass transfer coefficient values to determine the influence of each variable. After conducting regression analysis, we found that the starting saturation pressure produces a second power quadratic relationship between the starting saturation pressure and the resulting mass transfer coefficient K_D. Within the range of tests performed in this study, the oil/water ratio did not indicate a strong relationship when considering the full range of oil/water ratios when including the 100/0 pure base

fluid results. When only investigating the emulsion results, regression analysis indicated a linear relationship, albeit a very shallow increase in calculated K_D values with decreasing O/W ratios.

Further analysis is required so that we will be able to relate the now predictable mass transfer coefficient K_D to real-world well data by using the drift flux model to predict the behavior of an influx.

CHAPTER 6. CONCLUSIONS AND RECOMMENDATIONS

We have developed a foundation where there was previously very little published research on the evolution of methane from nonaqueous fluids and can accurately replicate results using the equipment which we have designed and developed. During the progression of this study, we made great progress in understanding the desorption phenomenon as it relates to methane evolving from nonaqueous-based fluids. We identified the importance of the peak exiting flow rate and how it affects Linga's mass transfer coefficient and potentially many other desorption models. While performing the experiments in this study, we developed progressively more advanced apparatus' that are better equipped to provide more accurate and reproducible results. All of the combined knowledge and skills used to develop the low-pressure apparatus' allowed us to develop a high-pressure apparatus that will soon be used to investigate and perform mass transfer studies on the processes of absorption, desorption, and convection of methane in nonaqueous-based fluids. The new high-pressure apparatus which has been developed allows us to perform experiments under significantly higher pressures and under new geometry conditions to either confirm the results we have from the low-pressure apparatus or observe new phenomena as we enter supercritical conditions.

We predict that the peak exiting flow rate will significantly affect results when using other desorption models and other experimental apparatus designs. While investigating mass transfer and performing experiments related to this field of research, the time required to absorb or desorb a gas from any fluid is extremely important when determining the mass transfer coefficient. Any restriction in the flow rate out of the apparatus will affect the resulting mass transfer coefficient of desorption. For our study, increasing the peak exiting flow rate was found to be crucial and increasing it allows us to more accurately replicate real-world conditions where an influx will not

be restricted and will rapidly begin to evolve from solution based on the change in hydrostatic pressure within a well.

We identified, under the experimental conditions in this study, that as the starting saturation pressure increases, the mass transfer coefficients will also increase. Statistical analysis showed that the starting saturation pressure affects the mass transfer coefficient and can be predicted using linear or polynomial relationships. It was also found that the oil/water ratio of the fluid affects the mass transfer coefficient. As the oil/water ratio decreases, the mass transfer coefficient increases. We proved that there is a significant difference in the mass transfer of methane from diesel when compared to internal olefin synthetic fluids. In our study, the calculated mass transfer coefficients for internal olefins were consistently higher than those observed with diesel.

The results of this study can be used by industry to be able to better develop software used for predicting the behavior of a gas influx in nonaqueous-based fluids by using these mass transfer coefficients to calculate the volume of gas released when the influx begins to evolve from the drilling fluid. By predicting accurate volumes of gas evolving out of solution, more precautions may be implemented at the surface to ensure worker and equipment safety. A gas kick event should always be taken seriously, especially when using nonaqueous-based fluids due to their inherent ability to hide the presence of a natural gas influx.

The future work of this research is to better parse the many variables which are involved with the process of gas desorption from a nonaqueous-based fluid. Of the variables listed in Table 3.1, many are difficult to isolate and therefore measure the importance of each in regards to this phenomenon. We have been able to successfully develop a relationship based on the starting saturation pressure along with identifying differences based on fluid type and oil/water ratio. Many of the variables which impact the evolution of gas from a fluid may be further identified along

with their significance using the high-pressure apparatus. Emulsion fluids should be further investigated to determine the cause of the phenomena observed showing changes in the trends for the calculated mass transfer coefficients when compared to pure base fluids when testing above 150 psig.

The experimental procedures used in this study require more adjustment to increase the accuracy of the results generated from each experimental trial. There are many steps throughout the current experimental procedure, such as using the buffer gas, where an additional degree of error is incorporated into our results. For this study, the procedures that brought about this error were set forth resulting from the current phase of our apparatus' setup. Advancements in the experimental procedures and alterations to the design of the low-pressure apparatus have already begun and the newly obtained results are promising.

APPENDIX A. TEST MATRICES FOR EXPERIMENTAL TRIALS

Table A.1. Nonaqueous Base Fluid Test.

Test	Fluid Type	O/W Ratio	Starting Saturation Pressure (psig)
1	Diesel	100/0	100
2			125
3			150
4			175
5			200
6	Internal Olefin	100/0	100
7			125
8			150
9			175
10			200

Table A.2. Test Matrix for Diesel and Internal Olefin Emulsion Fluid Tests.

Test	Fluid Type	O/W Ratio	Starting Saturation Pressure
11	Diesel/Water	90/10	100
12			125
13			150
14			175
15			200
16		80/20	100
17			125
18			150
19			175
20			200
21		70/30	100
22			125
23			150
24			175
25			200
26	Internal Olefin/Water	90/10	100
27			125
28			150
29			175
30			200
31		80/20	100
32			125
33			150
34			175
35			200
36		70/30	100
37			125
38			150
39			175
40			200

APPENDIX B. CALCULATIONS GOVERNING THE BUFFER LAYER

Test section 2 (TS2) in the low-pressure apparatus was measured to be 0.25 L in volume. The pressurized gas within this test section was considered an ideal gas for the simplification of the calculations. At each time step, the pressure which was read on TS2 was used to calculate the equivalent volume of gas at normal conditions. The flow meter used on our apparatus measures the mass rates and total volume at normal conditions (1 atmosphere 0 °C) so it was convenient to do the calculations to quickly determine the volume. The change in volume from the calculated blanket gas was subtracted from the flowmeter measurements to calculate the volume of gas from TS1 which had evolved from solution and exited the column through the flowmeter.

$$PV = nRT \qquad [B.1]$$

The total volume of gas in test section II at a given time and pressure condition is equal to the total volume of voids in the test section:

$$V_I' + (V_B' - V_{II}') = V \qquad [B.2]$$

V_I' is given by ideal gas law

$$V_I' = \frac{14.7 V_1 T_1}{P_1 T_0} \qquad [B.3]$$

Substitute A.3, and A.4 in A.2

$$V_1 = \frac{V - (V_B - V_{II})\frac{14.7 T_1}{P_1 T_0}}{\frac{14.7 T_1}{P_1 T_0}} \qquad [B.4]$$

$$V_I = V_T - V_B + \frac{V P T_0}{14.7 T_1} \qquad [B.5]$$

$P = P_1$ when $V_T = V_B$

APPENDIX C. REGRESSION ANALYSIS TABLES

Tables C.1-C.8 shows the regression analysis which was used to determine the influence that the starting saturation pressure has on the mass transfer coefficient K_D when maintaining a set oil/water ratio.

Table C.1. Regression table for the 100/0 O/W ratio of diesel to determine the influence on the mass transfer coefficient when increasing pressure.

100/0 - O/W Ratio - Diesel Regression Statistics						
		Multiple R	0.998567			
		R Square	0.997136			
		Adjusted R Square	0.996181			
		Standard Error	0.000697			
		Observations	5			
	df	SS	MS	F	Significance F	
Regression	1	0.000507	0.000507	1044.527	6.51023E-05	
Residual	3	1.46E-06	4.85E-07			
Total	4	0.000508				
	Coefficients	Standard Error	t Stat	P-value	Lower 95%	Upper 95%
Intercept	-0.02162	0.001358	-15.92	0.000539	-0.02594	-0.0173
X Variable 1	0.000285	8.81E-06	32.31915	6.51E-05	0.000257	0.000313

Table C.2. Regression table for the 90/10 O/W ratio of diesel to determine the influence on the mass transfer coefficient when increasing pressure.

90/10 - O/W Ratio - Diesel Regression Statistics						
		Multiple R	0.996087			
		R Square	0.99219			
		Adjusted R Square	0.989587			
		Standard Error	0.000258			
		Observations	5			
	df	SS	MS	F	Significance F	
Regression	1	2.53E-05	2.53E-05	381.1206	0.000293623	
Residual	3	1.99E-07	6.63E-08			
Total	4	2.55E-05				
	Coefficients	Standard Error	t Stat	P-value	Lower 95%	Upper 95%
Intercept	0.00816	0.000502	16.25296	0.000507	0.006562	0.009758
X Variable 1	6.36E-05	3.26E-06	19.52231	0.000294	5.32E-05	7.4E-05

Table C.3. Regression table for the 80/20 O/W ratio of diesel to determine the influence on the mass transfer coefficient when increasing pressure.

80/20 - O/W Ratio - Diesel Regression Statistics						
		Multiple R	0.995878			
		R Square	0.991773			
		Adjusted R Square	0.989031			
		Standard Error	0.000239			
		Observations	5			
	df	SS	MS	F	Significance F	
Regression	1	2.07E-05	2.07E-05	361.6744	0.000317459	
Residual	3	1.72E-07	5.73E-08			
Total	4	2.09E-05				
	Coefficients	Standard Error	t Stat	P-value	Lower 95%	Upper 95%
Intercept	0.01989	0.000467	42.61273	2.84E-05	0.018405	0.021375
X Variable 1	5.76E-05	3.03E-06	19.01774	0.000317	4.8E-05	6.72E-05

Table C.4. Regression table for the 70/30 O/W ratio of diesel to determine the influence on the mass transfer coefficient when increasing pressure.

70/30 - O/W Ratio - Diesel Regression Statistics						
		Multiple R	0.990773			
		R Square	0.981632			
		Adjusted R Square	0.975509			
		Standard Error	0.000332			
		Observations	5			
	df	SS	MS	F	Significance F	
Regression	1	1.77E-05	1.77E-05	160.3233	0.001062451	
Residual	3	3.31E-07	1.1E-07			
Total	4	1.8E-05				
	Coefficients	Standard Error	t Stat	P-value	Lower 95%	Upper 95%
Intercept	0.03392	0.000648	52.38545	1.53E-05	0.031859	0.035981
X Variable 1	5.32E-05	4.2E-06	12.66188	0.001062	3.98E-05	6.66E-05

Table C.5. Regression table for the 100/0 O/W ratio of internal olefins to determine the influence on the mass transfer coefficient when increasing pressure.

100/0 - O/W Ratio - IO Regression Statistics						
		Multiple R	0.996844			
		R Square	0.993699			
		Adjusted R Square	0.991599			
		Standard Error	0.001368			
		Observations	5			
	df	SS	MS	F	Significance F	
Regression	1	0.000885	0.000885	473.1069	0.000212685	
Residual	3	5.61E-06	1.87E-06			
Total	4	0.000891				
	Coefficients	Standard Error	t Stat	P-value	Lower 95%	Upper 95%
Intercept	-0.03026	0.002666	-11.351	0.001467	-0.03875	-0.02178
X Variable 1	0.000376	1.73E-05	21.75102	0.000213	0.000321	0.000431

Table C.6. Regression table for the 90/10 O/W ratio of internal olefins to determine the influence on the mass transfer coefficient when increasing pressure.

90/10 - O/W Ratio - IO Regression Statistics						
		Multiple R	0.98287			
		R Square	0.966034			
		Adjusted R Square	0.954712			
		Standard Error	0.000587			
		Observations	5			
	df	SS	MS	F	Significance F	
Regression	1	2.94E-05	2.94E-05	85.32267	0.002684399	
Residual	3	1.04E-06	3.45E-07			
Total	4	3.05E-05				
	Coefficients	Standard Error	t Stat	P-value	Lower 95%	Upper 95%
Intercept	0.009408	0.001145	8.215244	0.003775	0.005764	0.013052
X Variable 1	6.86E-05	7.43E-06	9.237027	0.002684	4.5E-05	9.23E-05

Table C.7. Regression table for the 80/20 O/W ratio of internal olefins to determine the influence on the mass transfer coefficient when increasing pressure.

80/20 - O/W Ratio - IO Regression Statistics						
		Multiple R	0.99634			
		R Square	0.992694			
		Adjusted R Square	0.990258			
		Standard Error	0.000235			
		Observations	5			
	df	SS	MS	F	Significance F	
Regression	1	2.25E-05	2.25E-05	407.6087	0.000265634	
Residual	3	1.66E-07	5.52E-08			
Total	4	2.27E-05				
	Coefficients	Standard Error	t Stat	P-value	Lower 95%	Upper 95%
Intercept	0.02232	0.000458	48.73409	1.9E-05	0.020862	0.023778
X Variable 1	0.00006	2.97E-06	20.18932	0.000266	5.05E-05	6.95E-05

Table C.8. Regression table for the 70/30 O/W ratio of internal olefins to determine the influence on the mass transfer coefficient when increasing pressure.

70-30 - O/W Ratio - IO Regression Statistics						
		Multiple R	0.993448			
		R Square	0.986938			
		Adjusted R Square	0.982584			
		Standard Error	0.000287			
		Observations	5			
	df	SS	MS	F	Significance F	
Regression	1	1.87E-05	1.87E-05	226.6744	0.000636081	
Residual	3	2.48E-07	8.26E-08			
Total	4	1.9E-05				
	Coefficients	Standard Error	t Stat	P-value	Lower 95%	Upper 95%
Intercept	0.034368	0.00056	61.35891	9.54E-06	0.032585	0.036151
X Variable 1	5.47E-05	3.63E-06	15.05571	0.000636	4.32E-05	6.63E-05

The following series of tables record the influence that a decreasing oil/water ratio has on the mass transfer coefficient at a set starting saturation pressure. Tables C.9 through C.18 include the pure base fluids in the data set. Tables C.19 through C.28 only include the emulsion fluids.

Table C.9. Regression table for the 100 psig tests using diesel to determine the influence on the mass transfer coefficient when decreasing the O/W ratio.

100 psig - Diesel Regression Statistics						
		Multiple R	0.992253			
		R Square	0.984567			
		Adjusted R Square	0.97685			
		Standard Error	0.002112			
		Observations	4			
	df	SS	MS	F	Significance F	
Regression	1	0.000569	0.000569	127.5904	0.007746627	
Residual	2	8.92E-06	4.46E-06			
Total	3	0.000578				
	Coefficients	Standard Error	t Stat	P-value	Lower 95%	Upper 95%
Intercept	0.11242	0.008098	13.88176	0.005149	0.077575	0.147265
X Variable 1	-0.00107	9.45E-05	-11.2956	0.007747	-0.00147	-0.00066

Table C.10. Regression table for the 125 psig tests using diesel to determine the influence on the mass transfer coefficient when decreasing the O/W ratio.

125 psig - Diesel Regression Statistics						
		Multiple R	0.966099			
		R Square	0.933348			
		Adjusted R Square	0.900022			
		Standard Error	0.003951			
		Observations	4			
	df	SS	MS	F	Significance F	
Regression	1	0.000437	0.000437	28.00657	0.033900665	
Residual	2	3.12E-05	1.56E-05			
Total	3	0.000468				
	Coefficients	Standard Error	t Stat	P-value	Lower 95%	Upper 95%
Intercept	0.1035	0.015147	6.833056	0.020753	0.038328	0.168672
X Variable 1	-0.00094	0.000177	-5.29212	0.033901	-0.0017	-0.00017

Table C.11. Regression table for the 150 psig tests using diesel to determine the influence on the mass transfer coefficient when decreasing the O/W ratio.

150 psig - Diesel Regression Statistics						
		Multiple R	0.874144			
		R Square	0.764128			
		Adjusted R Square	0.646193			
		Standard Error	0.006325			
		Observations	4			
	df	SS	MS	F	Significance F	
Regression	1	0.000259	0.000259	6.47919	0.125855609	
Residual	2	8E-05	4E-05			
Total	3	0.000339				
	Coefficients	Standard Error	t Stat	P-value	Lower 95%	Upper 95%
Intercept	0.08875	0.02425	3.65976	0.06722	-0.01559	0.19309
X Variable 1	-0.00072	0.000283	-2.54543	0.125856	-0.00194	0.000497

Table C.12. Regression table for the 175 psig tests using diesel to determine the influence on the mass transfer coefficient when decreasing the O/W ratio.

175 psig - Diesel Regression Statistics						
		Multiple R	0.72354			
		R Square	0.52351			
		Adjusted R Square	0.285265			
		Standard Error	0.008478			
		Observations	4			
	df	SS	MS	F	Significance F	
Regression	1	0.000158	0.000158	2.197359	0.276460152	
Residual	2	0.000144	7.19E-05			
Total	3	0.000302				
	Coefficients	Standard Error	t Stat	P-value	Lower 95%	Upper 95%
Intercept	0.07807	0.032503	2.401899	0.138275	-0.06178	0.217921
X Variable 1	-0.00056	0.000379	-1.48235	0.27646	-0.00219	0.001069

Table C.13. Regression table for the 200 psig tests using diesel to determine the influence on the mass transfer coefficient when decreasing the O/W ratio.

200 psig - Diesel Regression Statistics						
		Multiple R	0.503372			
		R Square	0.253383			
		Adjusted R Square	-0.11993			
		Standard Error	0.010246			
		Observations	4			
	df	SS	MS	F	Significance F	
Regression	1	7.13E-05	7.13E-05	0.678751	0.496628073	
Residual	2	0.00021	0.000105			
Total	3	0.000281				
	Coefficients	Standard Error	t Stat	P-value	Lower 95%	Upper 95%
Intercept	0.065025	0.039283	1.655293	0.239698	-0.104	0.234046
X Variable 1	-0.00038	0.000458	-0.82386	0.496628	-0.00235	0.001594

Table C.14. Regression table for the 100 psig tests using internal olefins to determine the influence on the mass transfer coefficient when decreasing the O/W ratio.

100 psig - IO Regression Statistics						
		Multiple R	0.99611			
		R Square	0.992235			
		Adjusted R Square	0.988352			
		Standard Error	0.001454			
		Observations	4			
	df	SS	MS	F	Significance F	
Regression	1	0.00054	0.00054	255.5513	0.003890289	
Residual	2	4.23E-06	2.11E-06			
Total	3	0.000545				
	Coefficients	Standard Error	t Stat	P-value	Lower 95%	Upper 95%
Intercept	0.111655	0.005575	20.02853	0.002484	0.087669	0.135641
X Variable 1	-0.00104	6.5E-05	-15.986	0.00389	-0.00132	-0.00076

Table C.15. Regression table for the 125 psig tests using internal olefins to determine the influence on the mass transfer coefficient when decreasing the O/W ratio.

125 psig - IO Regression Statistics						
		Multiple R	0.965174			
		R Square	0.931561			
		Adjusted R Square	0.897342			
		Standard Error	0.003869			
		Observations	4			
	df	SS	MS	F	Significance F	
Regression	1	0.000407	0.000407	27.2232	0.034825811	
Residual	2	2.99E-05	1.5E-05			
Total	3	0.000437				
	Coefficients	Standard Error	t Stat	P-value	Lower 95%	Upper 95%
Intercept	0.102767	0.014833	6.928451	0.020203	0.038947	0.166587
X Variable 1	-0.0009	0.000173	-5.21759	0.034826	-0.00165	-0.00016

Table C.16. Regression table for the 150 psig tests using internal olefins to determine the influence on the mass transfer coefficient when decreasing the O/W ratio.

150 psig - IO Regression Statistics						
		Multiple R	0.836811			
		R Square	0.700253			
		Adjusted R Square	0.550379			
		Standard Error	0.006617			
		Observations	4			
	df	SS	MS	F	Significance F	
Regression	1	0.000205	0.000205	4.672286	0.163188998	
Residual	2	8.76E-05	4.38E-05			
Total	3	0.000292				
	Coefficients	Standard Error	t Stat	P-value	Lower 95%	Upper 95%
Intercept	0.084236	0.025368	3.320552	0.079966	-0.02491	0.193386
X Variable 1	-0.00064	0.000296	-2.16155	0.163189	-0.00191	0.000634

Table C.17. Regression table for the 175 psig tests using internal olefins to determine the influence on the mass transfer coefficient when decreasing the O/W ratio.

175 psig - IO Regression Statistics						
		Multiple R	0.525902			
		R Square	0.276573			
		Adjusted R Square	-0.08514			
		Standard Error	0.009421			
		Observations	4			
	df	SS	MS	F	Significance F	
Regression	1	6.79E-05	6.79E-05	0.764617	0.474098376	
Residual	2	0.000177	8.87E-05			
Total	3	0.000245				
	Coefficients	Standard Error	t Stat	P-value	Lower 95%	Upper 95%
Intercept	0.064744	0.036119	1.792496	0.214922	-0.09067	0.220154
X Variable 1	-0.00037	0.000421	-0.87442	0.474098	-0.00218	0.001444

Table C.18. Regression table for the 200 psig tests using internal olefins to determine the influence on the mass transfer coefficient when decreasing the O/W ratio.

200 psig - IO Regression Statistics						
		Multiple R	0.106796			
		R Square	0.011405			
		Adjusted R Square	-0.48289			
		Standard Error	0.013249			
		Observations	4			
	df	SS	MS	F	Significance F	
Regression	1	4.05E-06	4.05E-06	0.023074	0.89320403	
Residual	2	0.000351	0.000176			
Total	3	0.000355				
	Coefficients	Standard Error	t Stat	P-value	Lower 95%	Upper 95%
Intercept	0.04474	0.050796	0.880786	0.471339	-0.17382	0.263295
X Variable 1	-9E-05	0.000592	-0.1519	0.893204	-0.00264	0.002459

The following tables represent the regression analysis that was performed on the mass transfer data sets where the 100/0 O/W ratio results were removed due to the discrepancy in the trend observed above 150 psig.

Table C.19. Regression table for the 100 psig tests using diesel to determine the influence on the mass transfer coefficient when decreasing the O/W ratio without the 100/0 sample.

100 psig - Diesel Regression Statistics						
		Multiple R	0.998999			
		R Square	0.997999			
		Adjusted R Square	0.995999			
		Standard Error	0.000776			
		Observations	3			
	df	SS	MS	F	Significance F	
Regression	1	0.0003	0.0003	498.8227	0.028485054	
Residual	1	6.02E-07	6.02E-07			
Total	2	0.000301				
	Coefficients	Standard Error	t Stat	P-value	Lower 95%	Upper 95%
Intercept	0.124533	0.004411	28.23465	0.022538	0.068491	0.180576
X Variable 1	-0.00123	5.48E-05	-22.3343	0.028485	-0.00192	-0.00053

Table C.20. Regression table for the 125 psig tests using diesel to determine the influence on the mass transfer coefficient when decreasing the O/W ratio without the 100/0 sample.

125 psig - Diesel Regression Statistics						
		Multiple R	0.998014			
		R Square	0.996033			
		Adjusted R Square	0.992066			
		Standard Error	0.001102			
		Observations	3			
	df	SS	MS	F	Significance F	
Regression	1	0.000305	0.000305	251.0658	0.040124598	
Residual	1	1.22E-06	1.22E-06			
Total	2	0.000306				
	Coefficients	Standard Error	t Stat	P-value	Lower 95%	Upper 95%
Intercept	0.1265	0.006268	20.1826	0.031517	0.04686	0.20614
X Variable 1	-0.00124	7.79E-05	-15.8451	0.040125	-0.00223	-0.00024

Table C.21. Regression table for the 150 psig tests using diesel to determine the influence on the mass transfer coefficient when decreasing the O/W ratio without the 100/0 sample.

150 psig - Diesel Regression Statistics						
		Multiple R	0.997254			
		R Square	0.994515			
		Adjusted R Square	0.98903			
		Standard Error	0.001266			
		Observations	3			
	df	SS	MS	F	Significance F	
Regression	1	0.00029	0.00029	181.3143	0.047191918	
Residual	1	1.6E-06	1.6E-06			
Total	2	0.000292				
	Coefficients	Standard Error	t Stat	P-value	Lower 95%	Upper 95%
Intercept	0.125933	0.007196	17.49965	0.036339	0.034495	0.217371
X Variable 1	-0.00121	8.95E-05	-13.4653	0.047192	-0.00234	-6.8E-05

Table C.22. Regression table for the 175 psig tests using diesel to determine the influence on the mass transfer coefficient when decreasing the O/W ratio without the 100/0 sample.

175 psig - Diesel Regression Statistics						
		Multiple R	0.997299			
		R Square	0.994604			
		Adjusted R Square	0.989209			
		Standard Error	0.001266			
		Observations	3			
	df	SS	MS	F	Significance F	
Regression	1	0.000295	0.000295	184.3361	0.046804911	
Residual	1	1.6E-06	1.6E-06			
Total	2	0.000297				
	Coefficients	Standard Error	t Stat	P-value	Lower 95%	Upper 95%
Intercept	0.128133	0.007196	17.80536	0.035717	0.036695	0.219571
X Variable 1	-0.00122	8.95E-05	-13.577	0.046805	-0.00235	-7.8E-05

Table C.23. Regression table for the 200 psig tests using diesel to determine the influence on the mass transfer coefficient when decreasing the O/W ratio without the 100/0 sample.

200 psig - Diesel Regression Statistics						
		Multiple R	0.998903			
		R Square	0.997807			
		Adjusted R Square	0.995614			
		Standard Error	0.000776			
		Observations	3			
	df	SS	MS	F	Significance F	
Regression	1	0.000274	0.000274	455.036	0.029822181	
Residual	1	6.02E-07	6.02E-07			
Total	2	0.000274				
	Coefficients	Standard Error	t Stat	P-value	Lower 95%	Upper 95%
Intercept	0.125783	0.004411	28.51805	0.022314	0.069741	0.181826
X Variable 1	-0.00117	5.48E-05	-21.3316	0.029822	-0.00187	-0.00047

Table C.24. Regression table for the 100 psig tests using internal olefins to determine the influence on the mass transfer coefficient when decreasing the O/W ratio without the 100/0 sample.

100 psig – IO Regression Statistics						
		Multiple R	0.999982			
		R Square	0.999964			
		Adjusted R Square	0.999928			
		Standard Error	9.8E-05			
		Observations	3			
	df	SS	MS	F	Significance F	
Regression	1	0.000265	0.000265	27648	0.003828627	
Residual	1	9.6E-09	9.6E-09			
Total	2	0.000265				
	Coefficients	Standard Error	t Stat	P-value	Lower 95%	Upper 95%
Intercept	0.12028	0.000557	215.89	0.002949	0.113201	0.127359
X Variable 1	-0.00115	6.93E-06	-166.277	0.003829	-0.00124	-0.00106

Table C.25. Regression table for the 125 psig tests using internal olefins to determine the influence on the mass transfer coefficient when decreasing the O/W ratio without the 100/0 sample.

125 psig - IO Regression Statistics						
		Multiple R	0.999184			
		R Square	0.998369			
		Adjusted R Square	0.996739			
		Standard Error	0.000686			
		Observations	3			
	df	SS	MS	F	Significance F	
Regression	1	0.000288	0.000288	612.2449	0.025714688	
Residual	1	4.7E-07	4.7E-07			
Total	2	0.000288				
	Coefficients	Standard Error	t Stat	P-value	Lower 95%	Upper 95%
Intercept	0.12556	0.0039	32.1953	0.019767	0.076006	0.175114
X Variable 1	-0.0012	4.85E-05	-24.7436	0.025715	-0.00182	-0.00058

Table C.26. Regression table for the 150 psig tests using internal olefins to determine the influence on the mass transfer coefficient when decreasing the O/W ratio without the 100/0 sample.

150 psig - IO Regression Statistics						
		Multiple R	0.999928			
		R Square	0.999855			
		Adjusted R Square	0.999711			
		Standard Error	0.000196			
		Observations	3			
	df	SS	MS	F	Significance F	
Regression	1	0.000265	0.000265	6912	0.007656977	
Residual	1	3.84E-08	3.84E-08			
Total	2	0.000265				
	Coefficients	Standard Error	t Stat	P-value	Lower 95%	Upper 95%
Intercept	0.12352	0.001114	110.8527	0.005743	0.109362	0.137678
X Variable 1	-0.00115	1.39E-05	-83.1384	0.007657	-0.00133	-0.00098

Table C.27. Regression table for the 175 psig tests using internal olefins to determine the influence on the mass transfer coefficient when decreasing the O/W ratio without the 100/0 sample.

175 psig - IO Regression Statistics						
		Multiple R	0.999876			
		R Square	0.999751			
		Adjusted R Square	0.999502			
		Standard Error	0.000245			
		Observations	3			
	df	SS	MS	F	Significance F	
Regression	1	0.000241	0.000241	4018.68	0.010041588	
Residual	1	6E-08	6E-08			
Total	2	0.000241				
	Coefficients	Standard Error	t Stat	P-value	Lower 95%	Upper 95%
Intercept	0.12068	0.001393	86.64319	0.007347	0.102982	0.138378
X Variable 1	-0.0011	1.73E-05	-63.3931	0.010042	-0.00132	-0.00088

Table C.28. Regression table for the 200 psig tests using internal olefins to determine the influence on the mass transfer coefficient when decreasing the O/W ratio without the 100/0 sample.

200 psig - IO Regression Statistics						
		Multiple R	0.999692			
		R Square	0.999384			
		Adjusted R Square	0.998767			
		Standard Error	0.000392			
		Observations	3			
	df	SS	MS	F	Significance F	
Regression	1	0.000249	0.000249	1621.688	0.015805466	
Residual	1	1.54E-07	1.54E-07			
Total	2	0.000249				
	Coefficients	Standard Error	t Stat	P-value	Lower 95%	Upper 95%
Intercept	0.1234	0.002229	55.37252	0.011496	0.095084	0.151716
X Variable 1	-0.00112	2.77E-05	-40.2702	0.015805	-0.00147	-0.00076

LIST OF REFERENCES

1. O'bryan, Patrick Leon, "Well Control Problems Associated With Gas Solubility in Oil-Based Drilling Fluids.". LSU Historical Dissertations and Theses. 1988.

2. Selley, R. C.; Sonnenberg, S. A. Elements of Petroleum Geology; Academic Press: Amsterdam, 2016.

3. Al-Areeq, N. M. Recent Insights in Petroleum Science and Engineering - Petroleum Source Rocks Characterization and Hydrocarbon Generation; InTechOpen: London, 2018.

4. O'bryan, Patrick Leon, "The Experimental and Theoretical Study of Methane Solubility in an Oil-Base Drilling Fluid.". LSU Historical Dissertations and Theses. 1983.

5. National Academy of Engineering and National Research Council. Macondo Well Deepwater Horizon Blowout: Lessons for Improving Offshore Drilling Safety. Washington, DC: The National Academies Press. 2012. https://doi.org/10.17226/13273.

6. Neff, J. M.; McKelvie, S.; Ayers, R. C. Environmental Impacts of Synthetic Based Drilling Fluids; U.S. Dept. of the Interior, Minerals Management Service, Gulf of Mexico OCS Region: New Orleans, 2000.

7. Fakhr, S. Faman Chemie Strang Co. Ltd., 2016.

8. Torsvik, A., Myrseth, V. & Linga, H."Drilling fluid rheology at challenging drilling conditions – an experimental study using a 1000 bar pressure cell". In Nordic Rheology Conference. 2015.

9. Demirdal, B. and Cunha, J.C. Olefin-Based Synthetic-Drilling-Fluids Volumetric Behavior Under Downhole Conditions. SPE Drilling & Completion: 239–248. SPE-108159-PA. http://dx.doi.org/10.2118/108159-PA. 2009.

10. Norwegian Oil Industry Association Working Group. Criteria for selection and approval of drilling fluids: with respect to effects on human workers and marine ecological systems. Norwegian Oil Industry Association, Stavanger, Norway. 1996. 70 pp.

11. Veil, J.A., C.J. Burke and D.O. Moses. Synthetic-based muds can improve drilling efficiency without polluting. Oil & Gas Journal. 1996. 94(10):49-54.

12. Hamarhaug, Marianne, "Well Control and Training Scenarios". University of Stavanger. 2011.

13. Grace, R. and Cudd, B. Advanced blowout & well control. 1st ed. Houston: Gulf Publishing Company. 1994.

14. IADC, "UBO & MPD Glossary," 2011.

15. K. P. Malloy et al., "Managed-Pressure Drilling: What It Is and What It Is Not," in IADC/SPE Managed Pressure Drilling and Underbalanced Operations Conference and Exhibition, Texas, 2009: IADC/SPE 122281.

16. Oxtoby, D. W.; Gillis, H. P.; Butler, L. J. Principles of Modern Chemistry; Cengage Learning: Boston, MA, 2016.

17. Velmurugan, N., Godhavn, J.-M., & Hauge, E. Dynamic Simulation of Gas Migration in Marine Risers. Society of Petroleum Engineers. 2016. doi:10.2118/180022-MS.

18. Lloyd, L. W., Andrea, M. D., and Kozicz, J. R. New Considerations for Handling Gas in a Deepwater Riser. Presented at the IADC/SPE Drilling Conference, New Orleans, USA, 23– 35 February. SPE- 59183-MS. 2000. https://doi.org/10.2118/59183-MS.

19. R.B. Bird , W.E. Stewart , and E.N. Lightfoot , Transport Phenomena, 2nd edition, John Wiley & Sons, Inc., 2007.

20. Nighswander, J. A.; Kalogerakis, N.; Mehrotra, A. K. Solubilities of carbon dioxide in water and 1 wt % NaCl solution at pressures up to 10 MPa and temperatures from 80 to 200 °C. J. Chem. Eng. Data 1989, 34, 355−360.

21. Yan, W.; Huang, S.; Stenby, E. H. Measurement and modeling of CO2 solubility in NaCl brine and CO2-saturated NaCl brine density. Int. J. Greenhouse Gas Control 2011, 5, 1460−1477.

22. Michael Matthies. Handbook of chemical mass transport in the environment, edited by Louis J. Thibodeaux and Donald Mackay, Toxicological & Environmental Chemistry, 93:6, 1274-1275, 2011. DOI: 10.1080/02772248.2011.585777.

23. Astarita, G. Mass transfer with chemical reaction. Amsterdam: Elsevier. 1967.

24. Azizi, F.; Al Taweel, A. M. Inter-phase mass transfer in turbulent liquid−liquid dispersions: A comparative analysis of models. Chem. Eng. J. 2012, 179, 231−241.

25. Jessy Elhajj, Mahmoud Al-Hindi, Fouad Azizi. A Review of the Absorption and Desorption Processes of Carbon Dioxide in Water Systems. ACS Industrial and Engineering Chemistry Research. Vol 53, pg. 2-22. 2014.

26. Weiland, Ralph H. Thuy, Lam T. Liveris, Andrew N. Transition from Bubbling to Quiescent Desorption of Dissolved Gases. Industrial Engineering Chemistry Fundamentals, ACS. Vol. 16, No. 3, 1977.

27. Cyr, David Robert, "Bubble growth behavior in supersaturated liquid solutions". University of Maine Electronic Theses and Dissertations. 2001.

28. Harvey, E.N., Barnes, D.K., McElroy, W.D., Whiteley, A.H., Pease, D.C., and Cooper, K.W. Bubble Formation in Animals, I. Physical Factors. Journal of Cellular and Comparative Physiology. August. 1944. 24(1): 1-22.

29. Harvey, E.N., Barnes, D.K., McElroy, W.D., and Whiteley, A.H. On Cavity Formation in Water. Journal of Applied Physics. February. 1947. 18: 162-172.

30. Harvey, E.N., Whiteley, A.H., McElroy, W.D., Pease, D.C., and Barnes, D.K. Bubble Formation in Animals, 11. Gas Nuclei and Their Distribution in Blood and Tissues. Journal of Cellular and Comparative Physiology. August. 1944. 24(1): 23-34.

31. Kenrick, F.B., Wismer, K.L., and Wyatt, K.S. Supersaturation of Gases in Liquids. Journal of Physical Chemistry. 1924. 28: 1308-13 15.

32. Dean, R.B. The Formation of Bubbles. Journal of Applied Physics. May. 1944. 15:446-451.

34. Wilt, P.M. Nucleation Rates and Bubble Stability in Water-Carbon Dioxide Solutions. Journal of Colloid and Interface Science. 1986. 112(2): 530-538.

33. Tucker, A.S. and Ward, C.A. Critical State of Bubbles in Liquid-Gas Solutions. Journal of Applied Physics. November. 1975. 46(11): 4801-4808.

35. Eddington, R.I. and Kenning, D.B.R. The Effect of Contact Angle on Bubble Nucleation. International Journal of Heat and Mass Transfer. 1979. 22: 123 1-1236.

36. Jackson, M.L. Energy Effects in Bubble Nucleation. Industrial Engineering Chemistry and Research. 1994. 33(4): 929-933.

37. Taylor, R., & Krishna, R. Multicomponent mass transfer. New York: Wiley. 1993.

38. Li, Shaobai, Chunying Zhu, Taotao Fu, and Youguang Ma. "Study on the mass transfer of bubble swarms in three different rheological fluids." International Journal of Heat and Mass Transfer 55, no. 21-22. 2012. 6010-6016.

39. Hill, G. A. Measurement of overall volumetric mass transfer coefficients for carbon dioxide in a well-mixed reactor using a pH probe. Ind. Eng. Chem. Res. 2006, 45, 5796−5800.

40. Watten, B. J.; Boyd, C. E.; Schwartz, M. F.; Summerfelt, S. T.; Brazil, B. L. Feasibility of measuring dissolved carbon dioxide based on head space partial pressures. Aquacult. Eng. 2004, 30, 83−101. 131.

41. Pfeiffer, T. J.; Summerfelt, S. T.; Watten, B. J. Comparative performance of CO2 measuring methods: Marine aquaculture recirculation system application. Aquacult. Eng. 2011, 44, 1−9. 132.

42. Colt, J.; Watten, B.; Pfeiffer, T. Carbon dioxide stripping in aquaculture. Part 1: Terminology and reporting. Aquacult. Eng. 2012, 47, 27−37.

43. Bird, R.B., W.E. Stewart, and E.N. Lightfoot, “Transport Phenomena”, Second Edition, Wiley, New York, 2007.

44. A. Kayode Coker, Petroleum, Complex-Mixture Fractionation, Gas Processing, Dehydration, Hydrocarbon Absorption and Stripping Ludwig's Applied Process Design for Chemical and Petrochemical Plants (Fourth Edition), Volume 2, 2010.

45. Nighswander, J. A.; Kalogerakis, N.; Mehrotra, A. K. Solubilities of carbon dioxide in water and 1 wt % NaCl solution at pressures up to 10 MPa and temperatures from 80 to 200 °C. J. Chem. Eng. Data. 1989. 34, 355−360.

46. Tokumura, M.; Baba, M.; Kawase, Y. Dynamic modeling and simulation of absorption of carbon dioxide into seawater. Chem. Eng. Sci. 2007. 62, 7305−7311.

47. Shah, Y.; Sharma, M. Desorption with or without chemical reaction. Trans. Inst. Chem. Eng. 1976. 54, 1−41.

48. Panja, N. C.; Phaneswara Rao, D. Experimental studies on kLa in a mechanically agitated contactor from transient electrical conductivity response data. Chem. Eng. Res. Des. 1991. 69, 302−307.

49. Kordač, M.; Linek, V. Dynamic measurement of carbon dioxide volumetric mass transfer coefficient in a well-mixed reactor using a pH probe: Analysis of the salt and supersaturation effects. Ind. Eng. Chem. Res. 2008. 47, 1310−1317.

50. Sherwood, T.; Draemel, F.; Ruckman, N. Desorption of carbon dioxide from water in a packed tower. Ind. Eng. Chem. 1937. 29, 282−285.

51. Sherwood, T. K.; Holloway, F. L. Performance of packed towers-liquid film data for several packings. Trans. Am. Inst. Chem. Eng. 1940. 36, 39−70.

52. Rixon, F. The absorption of carbon dioxide in and desorption from water using packed towers. Trans. Inst. Chem. Eng. 1948. 26, 119.

53. MW Kellogg Company. Desorption of Carbon Dioxide and Oxygen from Sea Water; Research and Development Center; U.S. Office of Saline Water; 1965.

54. Cooper, C.; Christl, R.; Perry, L. Packed tower performance at high liquor rates. Trans. Am. Inst. Chem. Eng. 1941. 37, 979.

55. Hikita, H.; Konishi, Y. Desorption of carbon dioxide from supersaturated water in an agitated vessel. AIChE J. 1984. 30, 945−951.

56. J. Szekely, S.-D. Fang, Non-equilibrium effects in the growth of spherical gas bubbles due to solute diffusion—II: The combined effects of viscosity, liquid inertia, surface tension and surface kinetics, Chemical Engineering Science, Volume 28, Issue 12, 1973. Pages 2127-2140. ISSN 0009-2509, https://doi.org/10.1016/0009-2509(73)85003-1.

57. Hamam, S.E.M., Hamoda, M.F., Shaban, H.I., and Kikain, A.S. 1988. “Crude oil dissolution in saline water. Air, Water and Soil Pollution.” 37, 55-64.

58. Bjorkevoll, K.S., Skogestad, J.O., Froyen, J., and Linga, H. “Well control simulator: Enhancing models with compositional PVT models and kinetics.” IADC/SOE-189651-MS. Drilling conference and exhibition. 2018. 1-10.

59. O'Bryan, Patrick L., Adam T. Bourgoyne Jr, Teresa G. Monger, and Debra P. Kopcso. "An experimental study of gas solubility in oil-based drilling fluids." SPE drilling engineering 3, no. 01: 33-42. Industrial & engineering chemistry research 45, no. 16. 2006. 5796-5800.

60. Feng J, Fu J, Chen P, Xu L. Investigation of methane/drilling mud phase behavior and its influence to hydrocarbon drilling activity. Energy Sci Eng. 2019. 7:1280–1291. https://doi.org/10.1002/ ese3.345.

61. Bodwadkar, S. V., & Chenevert, M. E. Diffusion of Gas in Oil Based Drilling Fluids. Society of Petroleum Engineers. 1997. doi:10.2118/37475-MS.

62. Velmurugan, N., Godhavn, J.-M., & Hauge, E. Dynamic Simulation of Gas Migration in Marine Risers. Society of Petroleum Engineers. 2016. doi:10.2118/180022-MS.

63. Monteiro, E. N., Ribeiro, P. R., and Lomba, R. F. T. Study of the PVT Properties of Gas-Synthetic-Drilling-Fluid Mixtures Applied to Well Con- trol. SPE Drill & Compl 25 (1): 45–52. SPE-116013-PA. 2010. https://doi.org/10.2118/116013-PA.

64. Kim, N. R., Ribeiro, P. R., and Pessoˆa-Filho, P. A. PVT Behavior of Methane and Ester-Based Drilling Emulsion. J. Pet Sci. Eng. 135 (November): 360–366. 2015. https://doi.org/10.1016/j.petrol.2015.08.018.

65. O’Bryan, P.L., Bourgoyne, Jr., A.T., Monger, T.G., and Kopcso, D.P. “An experimental study of gas solubility in oil-based drilling fluids.” SPE Drilling Engineering, March, 1988. p. 33-42.

66. Feng, Jian; Fu, Jianhong; Chen, Ping: Du, Zheng and Qin, Lilan. “Experimental study and molecular simulation of gas dissolution and diffusion behavior in drilling fluid.” Journal Natural Gas Science and Engineering, 2016. 36, 424-433.

67. Flatabø, G. Ø., Torsvik, A., Oltedal, V. M. et al. “Experimental Gas Absorption in Petroleum Fluids at HPHT Conditions.” Presented at SPE Bergen One Day Seminar, Bergen, Norway, 22 April. SPE-173865-MS. 2015. https://doi.org/10.2118/173865-MS.

68. Skogestad, J. O., Linga, H., Bjørkevoll, K.S. et al., Predicting Gas Loading Capability in Oil-Based Drilling Fluids Gas Influx in Oil-Based Drilling Fluids. SPE/IADC Drilling Conference and Exhibition. The Hague, Netherlands. 2017.

69. Linga, H., Nilsen, F.P. and Kundsen, B.L. “Prediction model optimizes H2S Scavenging infection strategy.” Sulfur 2003, November 2003, Banff, CA. 2003. p. 1-16.

70. Lloyd, L. W., Andrea, M. D., and Kozicz, J. R. New Considerations for Handling Gas in a Deepwater Riser. Presented at the IADC/SPE Drilling Conference, New Orleans, USA, 23– 35 February. SPE- 59183-MS. 2000. https://doi.org/10.2118/59183-MS.

71. Gucuyener, I. A Rheological Model for Drilling Fluids and Cement Slurries. Middle East Oil Technical Conference and Exhibition. 1983.

72. Johnson, A. B., & Cooper, S. Gas Migration Velocities During Gas Kicks in Deviated Wells. Society of Petroleum Engineers. 1993 doi:10.2118/26331-MS.

73. Johnson, Ashley, Ian Rezmer-Cooper, Tim Bailey, and Dominic McCann. "Gas migration: Fast, slow or stopped." In SPE/IADC Drilling Conference. Society of Petroleum Engineers, 1995.

74. Torsvik, A.; Skogestad, J. O.; Linga, H. “An experimental study of gas influx in oil-based drilling fluids for improved modeling of high pressure, high-temperature wells.” SPE Drilling & Completion, December. 2017. 245-254.

75. Li, Shaobai, Chunying Zhu, Taotao Fu, and Youguang Ma. "Study on the mass transfer of bubble swarms in three different rheological fluids." International Journal of Heat and Mass Transfer 55, no. 21-22. 2012. 6010-6016.

76. Yuan, Z.; Morrell, D.; Sonnemann, P.; Leach, C. Mitigating Gas in Riser Rapid Unloading for Deepwater Dual Gradient Well Control. Offshore Technology Conference. 2016.

77. Sengers JML. Solubility near the solvent's critical point. J Supercrit. Fluids. 1991. 4(4):215-222.

78. Hovland, F. and Rommetveit, R., January. Analysis of gas-rise velocities from full-scale kick experiments. In SPE Annual Technical Conference and Exhibition. Society of Petroleum Engineers. 1992.

79. Fjelde, K. K., Frøyen, J., & Ghauri, A. A. A Numerical Study of Gas Kick Migration Velocities and Uncertainty. Society of Petroleum Engineers. 2016. doi:10.2118/180053-MS.

80. Fomin, Yu D., Ryzhov V. N., Tsiok, Elena. Dynamics, thermodynamics and structure of liquids and supercritical fluids: Crossover at the Frenkel line. Journal of Condensed Matter 30(13). February. 2018. DOI: 10.1088/1361-648X/aaaf39.

81. Gandhi, Ankit B., Prashant P. Gupta, Jyeshtharaj B. Joshi, Valadi K. Jayaraman, and Bhaskar D. Kulkarni. "Development of Unified Correlations for Volumetric Mass-Transfer Coefficient and Effective Interfacial Area in Bubble Column Reactors for Various Gas-Liquid Systems Using Support Vector Regression." Industrial & Engineering Chemistry Research 48, no. 9. 2009. 4216-4236.

82. Silva, C.T., Mariolani, J.R.L., Bonet, E.J. et al. Gas Solubility in Synthetic Fluids: A Well Control Issue. Presented at the SPE Annual Technical Conference and Exhibition, Houston, Texas, 26-29 September. 2004. SPE-91009-MS http://dx.doi.org/10.2118/91009-MS.

83. Berthezene, N., de Hemptinne, J.-C., Audibert, A., and Argillier, J.-F. “Methane solubility in synthetic oil-based drilling muds.” J. Petroleum Sci. & Eng. (23) 71-81. 1999. http://dx.doi.org/10.1016/S0920-4105(99)00008-X.

84. Darwish NA, Fathikalajahi J, Gasem KA, Robinson RL Jr. Solubility of methane in heavy normal paraffins at temperatures from 323 to 423 K and pressures to 10.7 MPa. J Chem. Eng. Data. 1993. 38(1):44-48.

85. Srivastan S, Darwish NA, Gasem KA, Robinson RL Jr. Solubility of methane in hexane, decane, and dodecane at temperatures from 311 to 423 K and pressures to 10.4 MPa. J. Chem. Eng. Data 1992. 37, 4, 516-520.

86. Thomas DC, Lea JF Jr, Turek EA. Gas solubility in oil-based drilling fluids: Effects on kick detection. J Petro Technol. 1984. 36(6):959-968.

87. Diesel Fuels Technical Review. Chevron. 2007.

88. Vázquez, G., M. A. Cancela, R. Varela, E. Alvarez, and J. M. Navaza. "Influence of surfactants on the absorption of CO2 in a stirred tank with and without bubbling." Chemical Engineering Journal 67, no. 2. 1997. 131-137.

89. Ribeiro, P.R., Pessoa-Filho, P.A., Lomba, F.T. and Bonet, E.J. 2006. “Measurement and modeling of methane dissolution in synthetic liquids applied to drilling fluid formulation for deep and ultradeep water wells.”. J. Petroleum Sci. & Eng. (51) 37-44. 2006.

90. Linga, H., Bjørkevoll, K.S., Skogestad, J.O., et al., Gas Influx into Drilling Fluids during Flow Check Operations as Affected by Gas Absorption Characteristics of the Drilling Fluid. SPE/IADC Drilling Conference and Exhibition. The Hague, Netherlands. 2017.

91. Evje, S. & Fjelde, K. K. Hybrid Flux-Splitting Schemes for a Two-Phase Flow Model. Journal of Computational Physics 175, 674-701. 2002.

92. Tunnat, A. Behr, P. Gorner, K. Desorption Kinetics of CO2 from water and aqueous amine solutions. Energy Procedia 51. 2014. 197-206.

93. Ma, Z., Vajargah, A. K., Chen, D., van Oort, E., May, R., MacPherson, J.D., Becker, G., and Curry.D.l-based drilling fluids. “Gas kicks in nonaqueous drilling fluids: A well control challenge.” IADC/SPE-189606-MS. Drilling conference and exhibition. 2018. p. 1-24.

94. Colt, J.; Watten, B.; Pfeiffer, T. Carbon dioxide stripping in aquaculture. Part 1: Terminology and reporting. Aquacult. Eng. 2012. 47, 27−37.

95. Tokumura, M.; Baba, M.; Znad, H. T.; Kawase, Y.; Yongsiri, C.; Takeda, K. Neutralization of the acidified seawater effluent from the flue gas desulfurization process: Experimental investigation, dynamic modeling, and simulation. Ind. Eng. Chem. Res. 2006. 45, 6339−6348.

96. Barrut, B.; Blancheton, J.; Champagne, J.; Grasmick, A. Mass transfer efficiency of a vacuum airlift, application to water recycling in aquaculture systems. Aquacult. Eng. 2012, 46, 18−26.

97. Crawley, Michael J. Statistics: an Introduction Using R. Wiley-Blackwell, 2015.

VITA

James L. Nielsen Jr., son of Jim and Stephanie Nielsen, was born in North Carolina. He started his undergraduate studies at Duquesne University in Pittsburgh, Pennsylvania to earn a Bachelor of Science in May of 2016, majoring in Chemistry and minoring in Mathematics. He attended the University of Pittsburgh while studying chemistry at Duquesne to begin his engineering studies. Before graduating from Duquesne University, James applied to, and then that coming August, began his education at Louisiana State University to earn a Master of Science degree in the Craft and Hawkins Department of Petroleum Engineering. James is planning on earning his degree in May 2020. James is passionate about photography, astronomy, cooking, golf, and offshore sportfishing, adventures with his dog Hershey, along with occasional spur of the moment travels abroad.